2018

NUMERICAL AND EXPERIMENTAL TECHNIQUES FOR ASSESSING THE ACOUSTIC PERFORMANCE OF DUCT SYSTEMS ABOVE THE PLANE WAVE CUTOFF FREQUENCY

Kangping Ruan
University of Kentucky, kangpingruan@uky.edu
Digital Object Identifier: https://doi.org/10.13023/etd.2018.320

STUDENT AGREEMENT:

I represent that my thesis or dissertation and abstract are my original work. Proper attribution has been given to all outside sources. I understand that I am solely responsible for obtaining any needed copyright permissions. I have obtained needed written permission statement(s) from the owner(s) of each third-party copyrighted matter to be included in my work, allowing electronic distribution (if such use is not permitted by the fair use doctrine) which will be submitted to UKnowledge as Additional File.

I hereby grant to The University of Kentucky and its agents the irrevocable, non-exclusive, and royalty-free license to archive and make accessible my work in whole or in part in all forms of media, now or hereafter known. I agree that the document mentioned above may be made available immediately for worldwide access unless an embargo applies.

I retain all other ownership rights to the copyright of my work. I also retain the right to use in future works (such as articles or books) all or part of my work. I understand that I am free to register the copyright to my work.

REVIEW, APPROVAL AND ACCEPTANCE

The document mentioned above has been reviewed and accepted by the student's advisor, on behalf of the advisory committee, and by the Director of Graduate Studies (DGS), on behalf of the program; we verify that this is the final, approved version of the student's thesis including all changes required by the advisory committee. The undersigned agree to abide by the statements above.

Kangping Ruan, Student

Dr. David W. Herrin, Major Professor

Dr. Alexandre Martin, Director of Graduate Studies

NUMERICAL AND EXPERIMENTAL TECHNIQUES FOR ASSESSING THE ACOUSTIC PERFORMANCE OF DUCT SYSTEMS ABOVE THE PLANE WAVE CUTOFF FREQUENCY

DISSERTATION

A dissertation submitted in partial fulfillment of the
requirements for the degree of Doctor of Philosophy in the
College of Engineering
at the University of Kentucky

By

Kangping Ruan

Lexington, Kentucky

Director: Dr. David W. Herrin, Professor of Mechanical Engineering

Lexington, Kentucky

2018

ABSTRACT OF DISSERTATION

NUMERICAL AND EXPERIMENTAL TECHNIQUES FOR ASSESSING THE ACOUSTIC PERFORMANCE OF DUCT SYSTEMS ABOVE THE PLANE WAVE CUTOFF FREQUENCY

This research deals with determining the acoustic attenuation of heating, ventilation, and air conditioning (HVAC) ductwork. A finite element approach was developed for calculating insertion loss and breakout transmission loss. Procedures for simulating the source and receiving rooms were developed and the effect of structureborne flanking was included. Simulation results have been compared with measurements from the literature and the agreement is very good. With a good model in place, the work was extended in three ways. 1) Since measurements on full-scale equipment are difficult, scale modeling rules were developed and validated. 2) Two different numerical approaches were developed for evaluating the transmission loss of silencers taking into account the effect of higher order modes. 3) A power transfer matrix approach was developed to assess the acoustic performance of several duct components connected in series.

KEYWORDS: Large Silencer, HVAC Duct, Scale Modeling, High-order Modes, Power Transfer Matrix

Kangping Ruan
Student's Signature

25th July, 2018
Date

NUMERICAL AND EXPERIMENTAL TECHNIQUES FOR ASSESSING THE ACOUSTIC PERFORMANCE OF DUCT SYSTEMS ABOVE THE PLANE WAVE CUTOFF FREQUENCY

By

Kangping Ruan

Dr. David W. Herrin
Director of Dissertation

Dr. Alexandre Martin
Director of Graduate Studies

25th July, 2018
Date

ACKNOWLEDGEMENTS

First and foremost, I would like to express my sincere and deep sense of gratitude to my academic advisor, Professor David W. Herrin, for his creative suggestions, enthusiastic encouragement and patient guidance throughout the course of my Ph.D. study. What I have learned from him includes not only scientific knowledge and skills, but also correct attitude towards research. I cannot offer enough thanks to Professor Herrin for providing me the learning opportunities.

I would also like to offer my special thanks to Professor Tingwen Wu. This dissertation would not have been possible without his academic guidance and comments. I would also like to extend my sincere thanks to my committee members: Professor Kozo Saito and Professor Qiang Ye, for their invaluable suggestions which helped me improve the research work.

I want to thank all my former and current colleagues, Connor Campbell, Huangxing Chen, Jonathan Chen, Keyu Chen, Gong Cheng, Rui He, Shujian He, Xin Hua, Quentin Hunsucker, Caoyang Li, Jiazhu Li, Jundong Li, Wanlu Li, Weiyun Liu, Shishuo Sun, Peng Wang, Weichen Wang, Ruimeng Wu, Xin Yan, Nan Zhang, Yitian Zhang, Hao Zhou, Limin Zhou, who all have made my stay in Kentucky so enjoyable.

Most importantly, I dedicate this dissertation to my parents, wife and elder sister for their love and support, and to my lovely daughter, for bringing so much joy laughter and happiness into my life.

TABLE OF CONTENTS

LIST OF TABLES

LIST OF FIGURES

Chapter 1 INTRODUCTION

1.1 Introduction

Large duct systems are universal in the heating, ventilation, and air conditioning (HVAC) systems that provide thermal comfort and maintain indoor air quality in buildings. Air handlers use large fans to move the cooled or heated air through the building. Not surprisingly, considerable noise is generated at the air handler and is transmitted through the HVAC ductwork to the occupants. This noise is tonal at low frequencies and is broadband at higher frequencies and must be dealt with. This may be accomplished by adding sound absorptive linings to ductwork or by inserting plenums into the duct systems.

There are three main paths for the flow of vibrational and acoustical energy through the HVAC ductwork. These paths are illustrated in Figure 1.1. One path (indicated by the red line) is a direct airborne path through the ductwork into the room. This path is most effectively treated by adding a sound absorptive fiber lining on the inside periphery of a duct. Sound absorptive treatments are especially effective at elbows or bends. At low frequencies, adding area changes into the ductwork reflects sound towards the source and produces a cancellation effect.

A second path is an airborne indirect or breakout path shown in green in Figure 1.1. Sound impinges on the inner surface of the ductwork which then vibrates and radiates sound into the environment. This path is especially important if rectangular ductwork is used. Breakout noise is most easily mitigated by using spiral wound ductwork which is much stiffer than rectangular. Additionally, lining ductwork on the inside or adding lagging on the outside can be very effective.

The third primary path is a structureborne path shown in blue in Figure 1.1. Vibrational energy travels, usually from the source, through the ductwork. Since structureborne vibrations can travel large distances, structureborne vibration can travel from the source, through the ductwork which may be extensive, where it is then radiated as sound near the termination. This path, though normally less

important, can be treated by adding discontinuities to the HVAC ductwork via plenums.

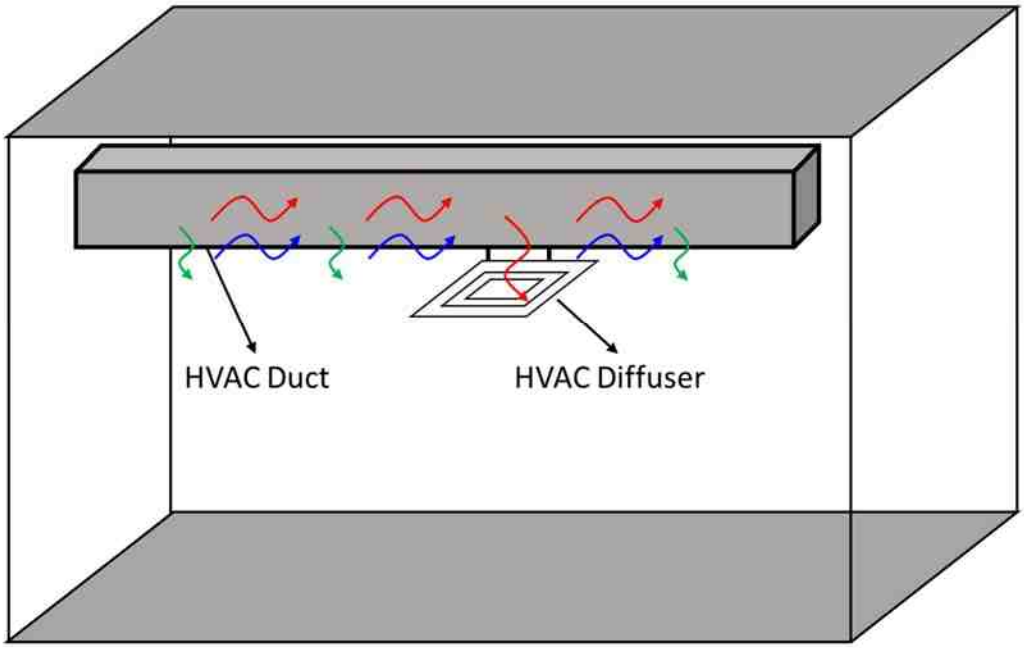

Figure 1.1 Illustration of HVAC noise transmission paths

Much of the past work looking at noise attenuation through HVAC duct systems has been performed experimentally in studies sponsored by the American Society of Heating, Refrigerating, and Air Conditioning Engineering (ASHRAE). These measurements require a source room and a receiving room connected by ductwork (ASTM E477, 2006). Loudspeakers are positioned in the source room with an aim to insure that a diffuse sound field is present at the duct entrance. The receiving room is most commonly a reverberation room (a room with hard surfaces). In theory, the sound pressure level should be the same at any position in the room. Normally, a microphone is traversed on a carousel in order to obtain an accurate average sound pressure level. The ductwork connecting the source and receiving rooms normally consists of two relatively rigid sections which should attenuate very little noise. A test duct or plenum section is placed between the

rigid sections. The attenuation or insertion loss is defined as the difference without and with the test section in place.

A few observations can be made. First, the method described is a well-defined standard but requires special facilities (i.e., a source and reverberation room) and expensive measurement equipment (i.e., microphones, loudspeakers, microphone traverse, and data acquisition). Secondly, the procedure deals primarily with the direct airborne path. The indirect airborne or breakout path can only be measured if the space between source and receiving rooms has low background noise. Moreover, the procedure has no way to differentiate in between airborne direct and structureborne flanking paths. Thirdly, the testing procedure takes a great deal of time to properly install ducts and perform measurements.

Though it is recognized that numerical simulation can supplement and reduce the number of tests, measurement studies are still essential. With that in mind, a simple scale modeling approach is recommended, tested, and validated. The suggested procedure can be used to determine insertion loss (i.e., airborne direct path) and breakout transmission loss (i.e., airborne indirect path). The procedure can partially include structureborne effects but scaling laws are not rigorous. Nevertheless, the testing procedure should be sufficient for confirming simulation and should reduce the necessity of more expensive full-scale testing.

To supplement the above research, first principle work is performed to determine the transmission loss of large ducts. Transmission loss is defined as the difference between incident and transmitted power in dB assuming an anechoic or non-reflecting termination. Transmission loss is a function of the attenuating element alone whereas insertion loss is a function of the element and system it is inserted in. Hence, insertion loss depends on the source, termination, and the lengths upstream and downstream of the test element. Transmission loss is trivial to determine if plane waves (i.e., the sound pressure is constant across the duct cross-section) can be assumed. However, the plane wave cutoff frequency is exceeded at relatively low frequencies in HVAC ducts since the cross-sectional

dimensions of the ducts are large. In that case, transmission loss calculation is complicated due to cross modes. Two numerical methods are proposed and compared to one another to assess the transmission loss of large duct elements.

The last section of the dissertation introduces a simplified procedure for determining the insertion loss of built-up duct systems consisting of a number of elements. A 2X2 power transfer matrix is developed which relates the incident and reflected energies on both sides of an attenuating element. After a power transfer matrix is determined for an attenuating element, matrices can be multiplied together in order to determine the attenuation of a series of elements. If power transfer matrices can be calculated and cataloged for a number of standard elements, calculation times can be reduced by orders of magnitude.

1.2 Organization

This dissertation is organized as.

Chapter 1 introduces the need for developing procedures for HVAC ductwork simulation and simplified measurement approaches.

Chapter 2 reviews prior measurement campaigns on determining insertion loss and breakout transmission loss of HVAC ductwork. Prior work on plenums is also reviewed. In addition, past work on simulation is also summarized.

Chapter 3 suggests and validates a finite element approach which can be used to determine the attenuation of ducts of any length and dimension. The approach detailed simulates the standard measurement approaches for assessing duct attenuation. The duct air space, including the source and termination, is modeled using acoustic finite elements. Poroelastic finite elements are used to simulate the fiber lining, and the metal ductwork is modeled using structural finite elements. The model is used to determine the insertion and transmission loss of unlined and lined ducts. Predicted results are compared to measurement with good agreement.

In Chapter 4, finite element analysis is used to predict the attenuation of elbows and side branches. Results for elbows and branches are compared to the ASHRAE Handbook with good agreement. In addition, an important secondary noise transmission path is through duct walls into rooms. This path, which is often termed breakout noise, is also investigated using the finite element approach and results are correlated with an analytical solution and the ASHRAE Handbook with good agreement. Of note, it is demonstrated that the breakout transmission loss is much less than the insertion loss through lined rectangular ducts at some frequencies. This suggests that breakout noise is the dominant noise path at these frequencies.

In Chapter 5, a scale modeling method is applied to assess the attenuation of heating, ventilation, and air conditioning ducts. Scaling rules for sound absorption and breakout noise transmission are reviewed. The scaling approach is first tested virtually via finite element analysis to validate the concept. This is followed by validation where a small expansion chamber, similar to a plenum, and its corresponding scale model are measured. Scale model results agree with full scale measurements of transmission loss, insertion loss, and breakout transmission loss.

Chapter 6 details two different numerical methods to compute the transmission loss of large silencers. The first method is a reciprocal work identity method when used in conjunction with the direct mixed-body boundary element method (BEM). The second is a finite element method (FEM) with a special non-reflecting boundary condition called a perfectly matched layer at the termination to determine the transmission loss. Results from both methods are compared to each other on multiple test cases including circular and rectangular cross-section ducts.

Chapter 7 proposes a power method to evaluate the acoustic performance for HVAC systems. The power transfer matrices can be multiplied together and then the insertion loss of a system consisting of several components can be predicted. The developed approach greatly reduces the computational cost. Results from the

power transfer matrix method are compared to the scattering matrix method with good agreement.

Chapter 8 summarizes the research and gives suggestions for future work.

Chapter 2 BACKGROUND

(Note: Most of the research in this chapter has been previously documented in Ruan and Herrin (2017a) and Herrin and Ruan (2018).)

Over the last several decades, ASHRAE sponsored several research efforts in an effort to better understand noise propagation in heating, ventilation, and air conditioning (HVAC) ductwork. Much of this work is the basis for the duct insertion loss and breakout noise information in the ASHRAE Handbook. Though this information is widely used in the building industry, the handbook provides little information about the basis for the equations and potential limitations. This chapter reviews the past work supported by ASHRAE, provides some context for the information in the ASHRAE Handbook, and looks at shortcomings that designers should be aware of.

2.1 Introduction

HVAC equipment noise is the primary noise concern in buildings and has an important effect on the acoustic acceptability of an architectural space. Indeed, noise control engineers routinely make noise measurements in rooms with the HVAC system running and compare measurements to established noise criterion (NC) and room criterion (RC) rating curves to assess acoustic acceptability (Long, 2014; ASHRAE Handbook, 2015). Appropriate criteria have been established for different categories of building spaces based on experience. As an example, criteria are stricter for conference rooms than office building lobbies.

Building noise arises primarily as a result of the air handling system. Though noise levels at the source are unacceptably high, noise is reduced via the path from the air handler to the room. Noise reductions are minimal in unlined ductwork, but the attenuation can be supplemented by adding sound absorption typically in the form of glass fiber linings to ducts and plenums. Moreover, plenums cancel out or reflect sound back towards the source as a result of an abrupt change in acoustic impedance at the inlet and outlet. ASHRAE has sponsored a great deal of

research to establish the amount of noise reduction along the duct stream. While noise should be reduced in the air handling equipment as much as possible, building designers rely on attenuating elements in the duct paths themselves to reduce the noise to acceptable levels. The ASHRAE Handbook incorporates a number of tables that are trusted by acoustical consultants and engineers for assessing this noise attenuation. That information is a consolidation of over 5 decades of accumulated research and consulting experience.

Acoustical engineers in the HVAC industry regularly use the tables in the handbook for design calculations, but are also aware that the tabulated information is by no means exhaustive. For example, many common duct cross-sections are not included, elbows and bends are limited to 90 degree angles, and the variety of sound absorptive lining materials and thicknesses is barely considered. In addition, handbook data is presented in octave instead of one-third octave bands. While perhaps sufficient for straight ducts, acoustical engineers recognize that octave band resolution is insufficient for plenums and lined ducts where attenuation may be quite high in narrower frequency bands. Furthermore, the uncertainty of the handbook predictions is not indicated. As a result, acoustical consultants err on the side of caution and overdesign for noise.

Acoustical engineers are less likely to be aware that the empirical equations for plenums are based on a very limited number of cases measured as part of RP-1026 (Mouratidis and Becker, 2003); attenuation predictions that are particularly suspect at low frequencies where acoustic modes dominate the response. Moreover, lined duct (with rectangular cross-section) results are based on measurement studies that were limited to duct lengths of 3.05 m (10 ft.) in length. Suitability for longer ducts is suspect.

These weaknesses are in no way due to lack of attentiveness on the part of the Sound and Vibration Technical Committee (TC 2.6). While additional measurement studies are desirable, it should be understood that such studies are difficult, expensive, and require specialized facilities. Only a few laboratories in

the USA are suitably equipped to make these measurements. In the author's opinion, TC 2.6 has rightly recognized that numerical simulation should be the preferred approach going forward. Consequently, ASHRAE has sponsored two projects (Herrin et al., 2007; Herrin and Seybert, 2006; Ruan and Herrin, 2016a; Ruan and Herrin, 2016b; Herrin, Ruan and Wu, 2016) to validate numerical simulation of HVAC components.

This chapter reviews prior ASHRAE project work and summarizes how it dovetails with the handbook. In the process, several equations that are not included in the handbook will be reviewed and the assumptions in the equations will be examined. The limitations of the handbook information will be discussed as well.

2.2 Measurement of HVAC Duct Insertion Loss

The terms insertion loss, transmission loss, noise reduction, and attenuation are often used interchangeably for HVAC duct systems. Though there are important differences between these metrics for smaller mufflers, the metrics are nearly the same for HVAC ducts at higher frequencies due to the large size of the systems. Insertion loss is the difference between the sound power at the termination without and with the attenuating element in place. Though it depends mostly on the attenuating element itself, there will be some effect due to the sound source, lengths of straight ductwork on each side of the attenuating element, and the outlet or termination. Transmission loss is the difference between the incident and transmitted power assuming an anechoic termination (i.e. infinitely long duct). It is solely a function of the attenuating component, but is very difficult to measure. Noise reduction is simply the difference between sound pressure levels on each side of the attenuating element but measurements must be made in duct.

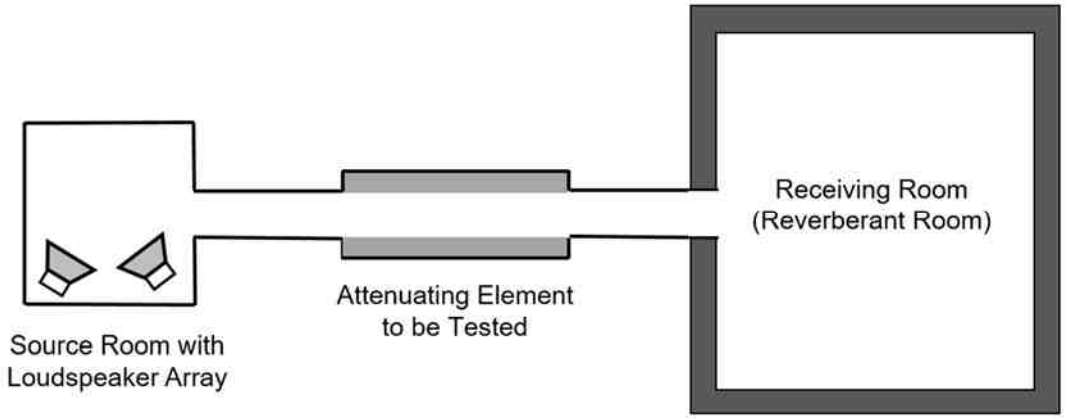

Figure 2.1 Schematic showing test setup for measurement of insertion loss.

Insertion loss has been preferred since all measurements are made at the outlet of the duct. The measurement procedure is described for HVAC applications in ASTM E477 (2006), and is shown in Figure 2.1. The attenuating element is positioned with straight ductwork on either side. A source room consisting of several loudspeakers is situated at the start of the duct. The source room should produce a diffuse field which implies that sound waves having all angles of incidence impinge at the inlet. The ductwork outlets into a reverberation room that is normally a much larger room than the source room. Most reverberation rooms have smooth concrete walls with rotating diffusers to break up low frequency acoustic modes. The average sound pressure is measured in the room using multiple microphones or with a single microphone on a rotating boom. In theory, the sound pressure should be relatively constant inside a reverberation room. Measurements are made in the reverberation room first without the attenuating element and then with the attenuating element inserted into the duct. Insertion loss is the difference between the two measurements.

For practical reasons, duct transitions must be constructed between the test duct and ductwork on both sides. These transitions will reflect some sound and have some effect on insertion loss especially at low frequencies. Furthermore, the

ductwork on each side of the test duct should be relatively rigid. Tests are normally restricted to ductwork with inlet and outlet in line with one another.

It should be appreciated that these experiments require specialized equipment including powerful loudspeakers, measurement grade microphones, and expensive data acquisition systems. Moreover, specialized facilities are required. Reverberation rooms are expensive and are not trivial to qualify. Measurements can also be compromised because background noise bleeds into the ducts. Hence, sound sources should be minimal outside the ductwork.

Subsequent sections examine the prior work and equations for ducts and plenums. Concerns examined include insertion loss and breakout noise. The basis for the *ASHRAE Handbook* tables and associated limitations are discussed.

2.3 Insertion Loss of Unlined Ducts

Unlined rectangular cross-section ducts provide several dB of noise attenuation at low frequencies, but are ineffective at higher frequencies. As part of ASHRAE RP-196 (Vér, 1978, 1977), Vér reviewed several prior measurement campaigns from the late 1950's and early 1960's which looked at unlined duct attenuation. Interestingly, Vér concluded that the peak attenuation at low frequency did not correspond to the fundamental vibrational resonances of the duct panels. Rather, it occurs at the resonance where the limp panel mass interacts with the stiffness of the air cavity. Vér suggested an approximate formula to identify the resonance frequency (f_{res}) for a straight unlined duct

$$f_{res} = \frac{c}{2\pi}\sqrt{\frac{\rho}{\rho_s}\frac{P}{A}} \tag{2.1}$$

where c is the speed of sound in air (m/s), ρ is the density of air in the duct (kg/m^3), ρ_s is the surface density of the duct wall (kg/m^2), P is cross-sectional perimeter (m) and A is cross-sectional area (m^2). The equation is based on the assumption that the wavelength of the sound in air is much larger than the cross-sectional

dimensions of the duct and that the response of the duct walls to the interior sound field is mass controlled.

As part of ASHRAE RP-556, Reynolds and Bledsoe (1989a, 1989b, 1990) helpfully tabulated the sound attenuation results for unlined ducts from the prior measurement campaigns. Reynolds and Bledsoe then performed a regression analysis for 6 commonly used duct cross-sections based on the legacy data. Air flow was not considered in the prior research, but should be unimportant. The insertion loss (IL) for octave band center frequencies spanning from 63 Hz to 250 Hz can be expressed as

$$IL = 1.7(P/A)^{-0.25} f^{-0.85} L \qquad \text{for } P/A \geq 3 \tag{2.2}$$

and

$$IL = 1.64(P/A)^{0.73} f^{-0.58} L \qquad \text{for } P/A < 3 \tag{2.3}$$

where P/A is the ratio of the perimeter (P) to the cross-sectional area (A) of the duct (in 1/ft or 1/0.3 m), f is the frequency (Hz) and L is the length of unlined duct (in ft or multiples of 0.3 m). Above 250 Hz, the insertion loss can be expressed as

$$IL = 0.02(P/A)^{0.8} L \tag{2.4}$$

and it is observed that the insertion loss increases linearly with length. These regression equations are the basis for the tables that are currently in the *ASHRAE Handbook*. TC 2.6 has elected to included tables in the handbook since equations are sometimes miscoded.

Compared to unlined rectangular ducts, circular ducts are stiffer and provide minimal attenuation even at low frequencies. Circular ducts only provide about one-tenth the sound attenuation at low frequencies as rectangular ducts. Kuntz and Hoover (1987) and Woods Fan Division (1973) performed measurements on unlined circular ducts. Their research appears to form the basis for the unlined

circular duct insertion loss data in the *ASHRAE Handbook – HVAC Applications* (2011).

2.4 Insertion Loss of Lined Ducts

Ducts lined with sound absorbing material provide far greater noise reduction than unlined ducts of similar length. Perforated plating is often used to encase the fiber lining but the perforation rate of the metal is large enough to have negligible acoustic effect. Sound absorptive lining is more effective at higher frequencies for a few reasons. Liners attenuate sound primarily due to viscous friction between the air and fiber. Friction and the accompanying dissipation is higher due to increasing particle velocity at higher frequencies. Effectiveness at higher frequencies is also related to the acoustic wavelength (λ) expressed as

$$\lambda = c/f \tag{2.5}$$

where c is the speed of sound (in m/s or ft/s) and f is the frequency in Hz. Liners are more effective if their thickness is ample compared to an acoustic wavelength. Data is provided for 1 in (2.5 cm) and 2 in (5 cm) fiber lining in the *ASHRAE Handbook*. The handbook is merely adequate since thicker lining is sometimes used in practice and the type of liner is not considered though it can greatly influence the degree of sound absorption.

Early work on lined ducts was performed by Morse (1939) and Scott (1946) who developed models for lined ducts which were suitable below the cutoff frequency. Following that, Vér (1978, 1977) developed a semi-empirical estimation procedure based on measurements provided by Owens-Corning Fiberglass Corporation. From the experimental data, Vér noted the insertion loss increases linearly with the length of the lined duct section at low frequencies, while it starts to level off when the length of the lined section exceeds 10 ft. Consequently, Vér capped the attenuation at 40 dB even if the predicted attenuation exceeded 40 dB. Vér correctly suggested that the reason for the plateauing in insertion loss was likely

due to flanking through the structure. This has been confirmed by finite element simulation in this dissertation. The experimental data for sound absorption was limited to four fiber duct liners, and the maximum thickness considered was 2 inches.

About a decade later, Kuntz and Hoover (1987) performed a measurement campaign on lined ducts as part of ASHRAE RP-478 (Kuntz, 1987). Fifteen 10 ft long ducts were measured having a variety of different cross-sectional areas and densities of sound absorbing lining. Kuntz and Hoover (1987) compared measurement results to the attenuation prediction method developed by Vér, and concluded that the procedure overestimates attenuation at low and high frequencies while underestimating the attenuation at the middle frequencies. Consequently, Kuntz and Hoover proposed modifications to the previous prediction method for lined HVAC ducts.

In ASHRAE RP-556 summarized in the ASHRAE publication *Algorithms for HVAC Acoustics*, Reynolds and Bledsoe (1990) analyzed the measured insertion loss data for lined rectangular ducts procured in measurement campaigns by Kuntz (1987), Kuntz and Hoover (1987), and Machen and Haines (1983) and developed a regression equation for each octave band center frequency from 63 Hz to 8000 Hz. The insertion loss (dB) can be expressed as

$$IL = B \cdot (P/A)^C \cdot t^D \cdot L \tag{2.6}$$

where P/A is the perimeter divided by the cross-sectional area of the free area inside the duct (1/ft or 1/0.3 m), t is the lining thickness (in inch or 2.5 cm), L is the duct length (in ft or 0.3 m), and B, C and D are regression constants that are dependent on frequency. The values for B, C and D are reproduced in Table 2.1. The aforementioned measurement campaigns and the regression equations developed by Reynolds and Bledsoe appear to form the basis for the rectangular duct insertion loss data in the *ASHRAE Handbook – HVAC Applications* (2011).

Table 2.1 Regression Constants for Use in Equation (2.6)

Octave Band Center Frequency (Hz)	B	C	D
63	0.013	1.959	0.917
125	0.057	1.410	0.941
250	0.271	0.824	1.079
500	1.015	0.500	1.087
1000	1.770	0.695	0.0
2000	1.392	0.802	0.0
4000	1.518	0.451	0.0
8000	1.581	0.219	0.0

Likewise, Bodely (1988) performed insertion loss measurements for lined circular ducts with 6 different diameters from 6 to 48 inch (15.2 to 122 cm), and with lining thicknesses of 1, 2, and 3 inch (2.5, 5.1, and 7.6 cm). Spiral dual-wall duct was used. The lining used was a 0.75 lb/ft^3 (12 kg/m^3) density fiber blanket covered with an internal liner of perforated galvanized steel which will have little acoustical effect. The length of the measured lined ducts was unclear though Reynolds and Bledsoe (1989b) conjectured that 20 ft (6.1 m) ducts were likely used for the measurement. Using the Bodely data, Reynolds and Bledsoe developed the regression equation

$$IL = (A + B \cdot t + C \cdot t^2 + D \cdot d + E \cdot d^2 + F \cdot d^3) \cdot L \qquad (2.7)$$

where t is the lining thickness (in inches or multiples of 2.5 cm), d is the duct diameter (in inches or multiples of 2.5 cm), and L is the duct length (in ft or multiples of 0.3 m). The coefficients for Equation (2.7) are provided in Table 2.2. Reynolds and Bledsoe noted that sound attenuation of lined circular ducts usually does not exceed 40 dB. The ASHRAE Handbook (2011) provides 2 data tables for the insertion loss of lined circular ducts with 1 inch (2.5 cm) and 2 inch (5.1 cm) thick sound absorptive linings. Those tables arise from Equation (2.7).

Table 2.2 Regression Constants for Use in Equation (2.7)

Octave Band Center Frequency (Hz)	A	B	C	D	E	F
63	0.283	0.345	-5.25E-2	-3.84E-2	9.13E-4	-8.29E-6
125	0.524	0.223	-4.94E-3	-2.72E-2	3.38E-4	-2.47E-6
250	0.365	0.790	-0.116	-1.83E-2	-1.21E-4	2.68E-6
500	0.133	1.845	-0.374	-1.29E-2	8.62E-5	-4.99E-6
1000	1.933	0	0	6.14E-2	-3.89E-3	3.93E-5
2000	2.730	0	0	-7.34E-2	4.43E-4	1.01E-6
4000	2.800	0	0	-0.15E-2	3.40E-3	-2.85E-5
8000	1.545	0	0	-5.45E-2	1.29E-3	-1.32E-5

The recent RP-1408 (Reynolds, 2015) is the most extensive experimental study to date on duct attenuation. A wide range of rectangular and circular ducts (unlined and lined) were measured and results are in 1/3-octave bands instead of octave bands. That higher resolution should prove quite useful at lower frequencies. Revised empirical equations have been generated and will be documented in an upcoming publication.

2.5 Insertion Loss of Unlined and Lined Plenums

The most effective means to attenuate noise between the source and room is to add a plenum. Plenums introduce abrupt area changes at their inlet and outlet. Sound reflects back towards the source and a cancellation effect is produced at the plenum entrance. When lined, sound is effectively absorbed in the plenum. Hence, plenums reduce sound at both low and high frequencies.

Wells (1958) measured single and double plenum chambers of two different sizes and varied the opening sizes. Wells developed equations, used in the handbook for decades, based on room acoustics theory which is appropriate at higher frequencies where the plenum cross-sectional dimension is several acoustic

wavelengths. Unfortunately, the equations developed were not suitable for low frequencies. The insertion loss for a plenum was expressed as

$$IL = 10\log_{10}\left(S_{out}\left(\frac{\cos\theta}{2\pi d^2}+\frac{1}{R}\right)\right)^{-1} \tag{2.8}$$

where d is the slant distance from the entrance to the exit (i.e., $d=\sqrt{(L-l)^2+H^2}$), R is the plenum room constant (i.e., $R=S\alpha/(1-\alpha)$), and $\cos\theta = H/d$. The geometric parameters are illustrated in Figure 2.2. S_{out} is the area of the slit (i.e., $S_{out}=lD$).

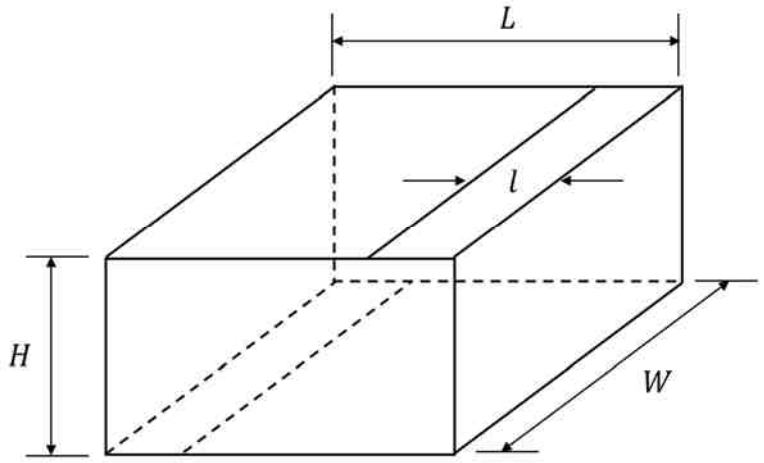

Figure 2.2 Schematic showing plenum geometric parameters (Wells, 1958).

In ASHRAE RP-1026, Mouratidis and Becker (2003) measured the insertion loss of 8 different sized plenums using ASTM E477 (2006). To our knowledge, this remains the most extensive measurement study on plenums. Inlet and outlet locations, wall construction, and lining was varied as well. Empirical equations were developed that are currently in the handbook. For frequencies below the cutoff frequency,

$$IL = A_f S + W_e + E_{oa} \tag{2.9}$$

where A_f, S, W_e, and E_{oa} are an empirically defined surface area coefficient (dB/ft^2 or dB/0.09 m^2), total inside surface area of plenum less the inlet and outlet areas (ft^2 or multiples of 0.09 m^2), wall effect (dB) and offset angle effect (dB) respectively that are tabulated in Mouratidis and Becker (2003). At frequencies above the cutoff, insertion loss can be expressed, using a variant of Wells equation, as

$$IL = b\left(\frac{S_{out}Q}{4\pi r^2} + \frac{S_{out}(1-\alpha_a)}{S\alpha_a}\right)^n + E_{oa} \qquad (2.10)$$

where S_{out} and S are the respective outlet cross-sectional and surface areas of the plenum, r is the distance between the centers of the inlet and outlet sections, Q is a directivity factor, and α_a is the average absorption coefficient in the plenum. The constants b and n are empirically determined and are 3.505 and -0.359 respectively.

Though 8 different plenum sizes were considered, the dataset is nonetheless small compared to the range of cases encountered in the building industry. The empirically based equations have not been validated on sizes other than the limited number in the measurement study, and the plenum empirical equations are particularly suspect at low frequencies. For a system consisting of ducts and plenums, predictions made using the handbook are likely to be several dB in error.

2.6 Breakout Noise

Though the air path from source to room is the most important, there is a secondary noise path commonly referred to as breakout noise. Breakout noise occurs when sound inside the duct vibrates the peripheral walls which in turn radiate noise to their surroundings. It is normally a greater concern at low frequencies for rectangular ductwork and is most effectively reduced by using the now ubiquitous spiral wound circular ductwork which is much stiffer.

Vér (1983b) and Cummings (1985) researched breakout noise in ASHRAE supported efforts and the work by Cummings is particularly exemplary. At low

frequencies, Cummings (1985) measured the breakout transmission loss in the following way. A test duct originating from a source room was capped with a sound absorptive wedge and a large mass so that sound transmission through the end of the duct is minimal. The test duct passed into a reverberation room and the sound power radiating from the periphery of the test duct was measured inside the reverberation room. A microphone was traversed inside the duct to determine the sound power incident on the duct sides. Breakout transmission loss was defined as the difference between the radiated and incident sound powers. This approach is illustrated in Figure 2.3.

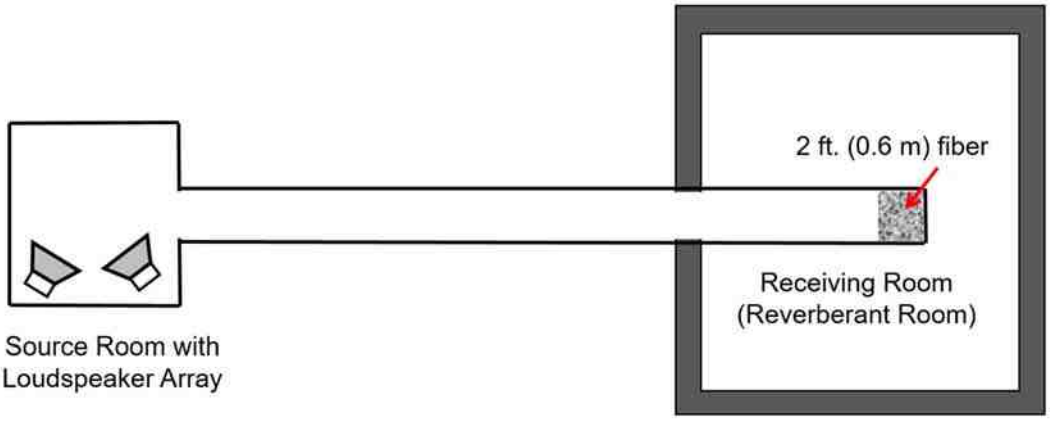

Figure 2.3 Schematic showing Cummings (1985) measurement setup for measurement of breakout transmission loss.

At higher frequencies, Cummings (1985) measured the breakout transmission loss using a two-step process. In the first step, the radiated sound power was measured as before. Then the cap was removed and replaced with a horn at the end of the duct so that the termination was approximately reflection free (Figure 2.4). Cummings measured the sound power using the reverberation room and determined the breakout transmission loss from the difference in measured sound powers.

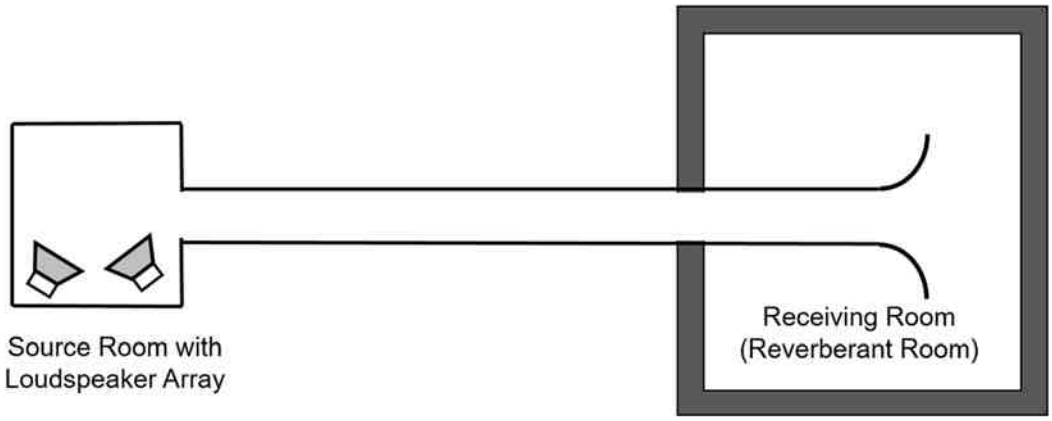

Figure 2.4 Schematic showing alternate approach for determining incident sound power.

Cummings (2001) summarized the two decades of work in a recommended comprehensive review paper. The ASHRAE Handbook relies mostly on the work by Cummings (1985) with some additional information provided by Lilly (1987).

The normalized breakout transmission loss for unlined ducts is defined in the *ASHRAE Handbook – HVAC Applications* (2015) as

$$TL_{out} = L_{W(in)} - L_{W(out)} + 10\log(S_{rad}/S) \tag{2.11}$$

where $L_{W(in)}$ is the incident sound power, $L_{W(out)}$ is the radiated sound power from the duct work, S_{rad} is the surface area of the outside radiating duct, and S is the cross-sectional area inside the duct. Though other definitions could be considered, Cummings (1985) pointed out that both incident ($L_{W(in)}$) and radiated ($L_{W(out)}$) sound power are directly measurable and useful in engineering calculations.

Equation (2.11) is valid for short lengths of duct where noise attenuation inside the duct versus distance is minimal. The equation is modified for lined ducts and takes into account the attenuation of the sound as it travels along the duct. In that case,

$$TL_{out} = L_{W(in)} - L_{Wout} + 10\log(S^{*}_{rad}/S) \tag{2.12}$$

with

$$S_{rad}^{*} = PL^{*} \tag{2.13}$$

where P is the duct perimeter and L^{*} is the effective length of the duct. The effective length is expressed as

$$L^{*} = \frac{\gamma^{L} - 1}{\ln \gamma} \tag{2.14}$$

with

$$\gamma = 10^{-\frac{\alpha}{10}} \tag{2.15}$$

where α is the duct attenuation rate in dB/ft (dB/0.3m).

Cummings (1983, 1985) developed expressions for the breakout transmission loss of unlined rectangular and circular ducts. For rectangular ducts, the breakout transmission loss (TL_{out}) can be expressed as

$$TL_{out} = 10 \log\left(\frac{4\omega\rho_s^2}{\rho^2 c(a+b)}\right) \tag{2.16}$$

and

$$TL_{out} = 10 \log\left(\frac{4\omega^2\rho_s^2}{7.5\rho^2 c}\right) \tag{2.17}$$

for frequencies below and above $24{,}134/\sqrt{ab}$ Hz ($613/\sqrt{ab}$ in meters) where a and b are the cross-sectional dimensions in inches. ρ_s and ω are the panel surface density (units of mass per unit area) and angular frequency (in rad/s) respectively. Equation (2.16) gives good results up to the frequency of the 10th acoustic cross mode in the duct and predicts a 3 dB increase per doubling of frequency while Equation (2.17) predicts 6 dB per doubling. One would anticipate

6 dB per doubling based on mass law but Equation (2.16) also accounts for the increasing radiation efficiency of the duct walls at low frequencies.

Below the cutoff frequency the breakout transmission loss for a circular duct can be predicted as

$$TL_{out} = 10\log\left(\frac{4h^2E_p^2}{\rho^2 c\pi R^5\omega^3}\right) \tag{2.18}$$

where E_p is the elastic modulus, h is the thickness, and R is the radius of the ducting. This formula suggests that the breakout transmission loss should decrease by 9 dB per doubling of frequency. The high transmission loss predicted by Equation (2.18) is not realized in practice. Cummings (1983) noted a couple possible explanations that had been suggested earlier in the literature. The first is that there are non-axisymmetric pressure distributions near the source and termination and also due to bends in the duct. These non-axisymmetric pressure distributions possibly excite the bending modes in the duct. The second explanation is that long seam and spiral wound ducts are not truly circular and any distortion leads to higher order structural modes being excited by the plane acoustic mode. This effect has been termed a mode coupling effect. This is supported by the fact that the breakout transmission loss is much higher for a spiral wound duct than for the more distorted circular duct of the long seam variety. However, perhaps the most likely explanation is that flanking noise paths prevent accurate measurement of high transmission loss at low frequencies.

There will be two minima in the breakout transmission loss at the ring and critical frequencies. The ring frequency, which is usually lower than the critical frequency, occurs when the restoring force due to the tangential stresses and the mass of the walls interact in a resonant motion similar to the kind observed in metal rings (Cummings, 1983). The ring frequency (f_R) can be expressed as

$$f_R = \sqrt{\frac{E_p}{\rho_p}} \frac{1}{2\pi R} \tag{2.19}$$

where ρ_p is the mass density of the ductwork. The critical frequency (f_{cr}) occurs when the structural and acoustic wavelengths are equal to one another and is expressed as

$$f_{cr} = \frac{c^2}{2\pi} \sqrt{\frac{12\rho_p(1-\nu^2)}{E_p h^2}} \tag{2.20}$$

where ν is the Poisson's ratio.

2.7 Concluding Comments

Prior ASHRAE research on characterizing the insertion loss and breakout transmission loss of HVAC ducts has been reviewed and important assumptions have been noted. This review has primarily focused on measurement work. It was demonstrated that the ASHRAE Handbook includes a great deal of useful information. However, some important limitations are noted. These include:

a) Insufficient resolution due to results being reported in octave bands instead of 1/3 octave bands.

b) Empirical equations for plenums are lacking in both resolution and accuracy at low frequencies.

c) Only a sampling of the wide range of duct cross-sections and especially plenum sizes is included.

d) Typical glass fiber is the only sound absorbing liner included and is in no way representative of the wide range of sound absorbing materials used.

The research in this thesis details finite element simulation and scale modeling measurement approaches which may be used to determine the important acoustic metrics for ducts and plenums.

Chapter 3 A SIMULATION APPROACH TO DETERMINE THE INSERTION AND TRANSMISSION LOSS OF UNLINED AND LINED DUCTS

(Note: Most of the research in this chapter has been previously documented in Ruan and Herrin (2016a).)

One of the primary noise transmission paths in buildings is from HVAC equipment through ventilation ducts. The ASHRAE Handbook provides tables for estimating the attenuation of lined and unlined ducts up to 10 ft (3.05 m) in length. The aim of this research is to suggest and validate a finite element approach which can be used to determine the attenuation of ducts of any length and dimension. The approach detailed simulates the standard measurement approaches for assessing duct attenuation. The duct air space, including the source and termination, is modeled using acoustic finite elements. Poroelastic finite elements are used to simulate the fiber lining, and the metal ductwork is modeled using structural finite elements. The model is used to determine the insertion and transmission loss of unlined and lined ducts. Predicted results are compared to measurement with good agreement.

3.1 Introduction

Noise is one of many design concerns that must be attended to in building. If unaddressed, mitigation measures are costly after the building is in place and the effectiveness of measures taken is reduced. Likely, the most important sources of noise are from HVAC equipment, and the dominant path is airborne transmission through ducts. Often, the most effective treatment is to add fiber lining which adds thermal insulation and has little effect on the pressure drop.

Not surprisingly, ASHRAE had devoted a number of research projects to better understanding noise attenuation in ducts and lined ducts in particular. Vér (1978) reviewed a number of prior experimental studies on duct attenuation and compared results to the 1973 and 1976 ASHRAE Handbooks. At the time, Vér (1978) pointed out 1) the need for more careful experimentation, 2) that sound

absorption properties for common linings were not well known, and 3) that effects of flanking and transmission through duct walls were not well understood.

In the next decade, Machen and Haines (1983) and Kuntz and Hoover (1987) performed extensive measurement studies. The results of Machen and Haines, though now hard to find, appear to form the basis for the rectangular duct insertion loss data in the *ASHRAE Handbook – HVAC Applications* (2015). Kuntz and Hoover measured the insertion loss and in-duct attenuation for 18 unlined and lined ducts of varying rectangular cross-section. Each of the tested ducts was 10 ft (3.05 m) in length. Their results are consistent with though not identical to the tables in the Handbook.

In follow on work, Reynolds and Bledsoe (1989a, 1989b) used regression analysis to determine equations for the sound attenuation of lined and unlined rectangular and circular ducts. The latter paper provided results for the insertion loss of 20 ft (6.10 m) circular ducts and may be the basis for the circular duct information in the *ASHRAE Handbook – HVAC Applications* (2015). To the author's knowledge, the regression equations have not been widely used by the ASHRAE community.

At this juncture, the *ASHRAE Handbook – HVAC Applications* (2015) provides tables for the attenuation of lined and unlined ducts having a variety of cross-section sizes. However, Kuntz and Hoover limited their studies to ducts that are 10 ft (3.05 m) in length, and their suitability for longer ducts is suspect. Recently, Reynolds (2015) in RP-1408 has performed a far more extensive measurement campaign than had previously been undertaken considering different duct lengths, and circular and rectangular cross-sections. This data will likely form the basis for future ASHRAE Handbook editions.

Though the empirical data and ASHRAE Handbook tables are useful for design purposes, a numerical simulation approach to predict HVAC duct attenuation is desirable and is the subject of this chapter. Simulation models may be used to evaluate duct systems of arbitrary length or cross-section, and may also

incorporate sound absorptive lining of any type and thickness. Moreover, the vibration of the ductwork may also be considered.

Astley has published widely (Astley and Cummings, 1984; Astley et al., 1991; Cummings and Astley, 1995) on the use of FEA to assess duct attenuation without and with sound absorbing lining. The current effort utilizes Astley's work as a foundation. The commercial software Siemens Virtual.Lab (2015) was used for all analyses though other commercial packages could be used with minor modifications. The duct airspace and ductwork were modeled using acoustic and structural finite elements respectively. A diffuse acoustic field was simulated at the source side and the end was modeled as a baffled termination. The transmission loss, insertion loss, and noise reduction were determined and compared to experimental data from RP-1408 and the ASHRAE Handbook. The procedure developed is general and can be applied to a wide variety or HVAC duct configurations

3.2 Finite Element Analysis Approach

The approach used follows the experimental approach laid out in ASTM E477 (2006). The source room is modeled using 20 monopole sources having equal strength located on a hemisphere as shown in Figure 3.1. Different numbers of monopoles were tested and insertion loss results converged to less than 1 dB if over 15 sources were used.

The surface of the hemisphere is modeled to be reflection free. Accordingly, there are no acoustic modes in the hemispherical space on the source side while the impedance condition at the entrance is correctly modeled. The reflection free boundary is modeled using a perfectly matched layer boundary condition (Berenger, 1994; Tam et al., 1998; Bermudez et al., 2007; Casalino and Genito, 2008). This approach permits the sound absorption of waves having high angles of incidence. The approach is advantageous because the mesh can be conformal and relatively close to the surface. Other methods can be used but at higher

computational cost. For example, infinite elements are often used to simulate an unbounded domain (Astley and Coyette, 2000; Burnett and Holford, 1998). Additional schemes for dealing with the unbounded domain are detailed in Astley et al. (2000) and Givoli and Harari (1998).

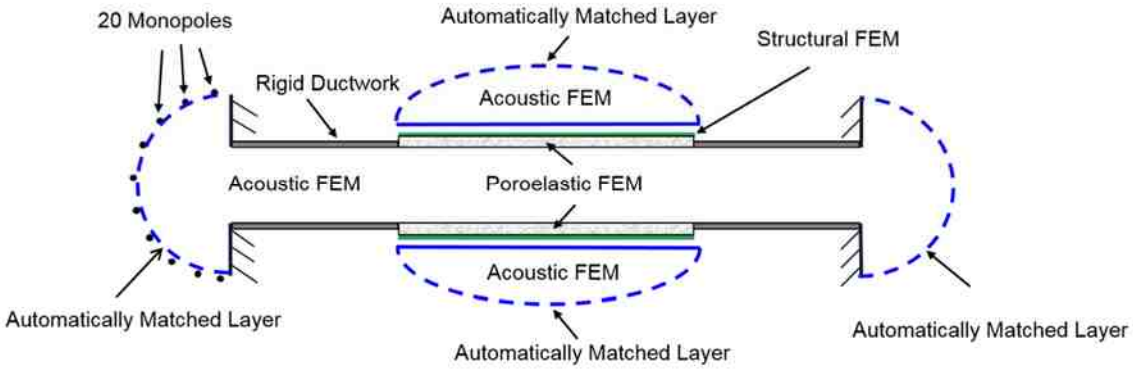

Figure 3.1 Schematic showing finite element modeling strategy.

The particular implementation in Siemens Virtual.Lab (2015) is such that the perfectly matched layer is not meshed. The software internally creates the perfectly matched layer mesh which differs in thickness and resolution at each frequency. This particular implementation has been referred to as an automatically matched layer. However, it is notionally identical to a perfectly matched layer.

The end of the duct is modeled as a baffled termination with radiation into a free space. The perfectly matched layer was utilized to simulate an unbounded domain on the hemisphere. A simple absorptive boundary condition of ρc where ρ is the mass density and c is the speed of sound was also tested and insertion loss results were found to be nearly those for a perfectly matched layer. Accordingly, several different approaches can be used to deal with the unbounded domain.

The test ductwork was modeled using shell elements for both circular and rectangular ducts. The elastic modulus and mass density were chosen for steel and were 30E6 lbf/in^2 (210 GPa) and 0.281 lbf/in^3 (7800 kg/m^3) respectively. The rectangular ducts were stiffened around the perimeter of the duct every 5 ft (1.52

m) of duct length using beam elements. The damping properties of similar ductwork were measured and average values were incorporated into the models. Damping ratios of 0.003 and 0.02 respectively were used for unlined and lined ducts. More details about the measurements and values used are included in Chapter 4.

An acoustic finite element mesh surrounded the test duct and was coupled to the structural elements representing the ductwork. The unbounded domain around the duct was also dealt with using the perfectly matched layer capability. The finite element mesh is shown in Figure 3.2 along with the structural mesh.

The sound absorbing lining was modeled using poroelastic finite elements which are also indicated in Figure 3.2. These elements include sound pressure degrees of freedom plus additional degrees of freedom for the displacement of the elastic frame (Atalla et al., 1998). Sound absorbing materials can also be modeled using a bulk reacting model where dissipative effects are integrated into the speed of sound and density by making them complex (Craggs, 1978; Craggs, 1986). Simulation results were found to agree well with measurement whether the poroelastic or bulk reacting model was used.

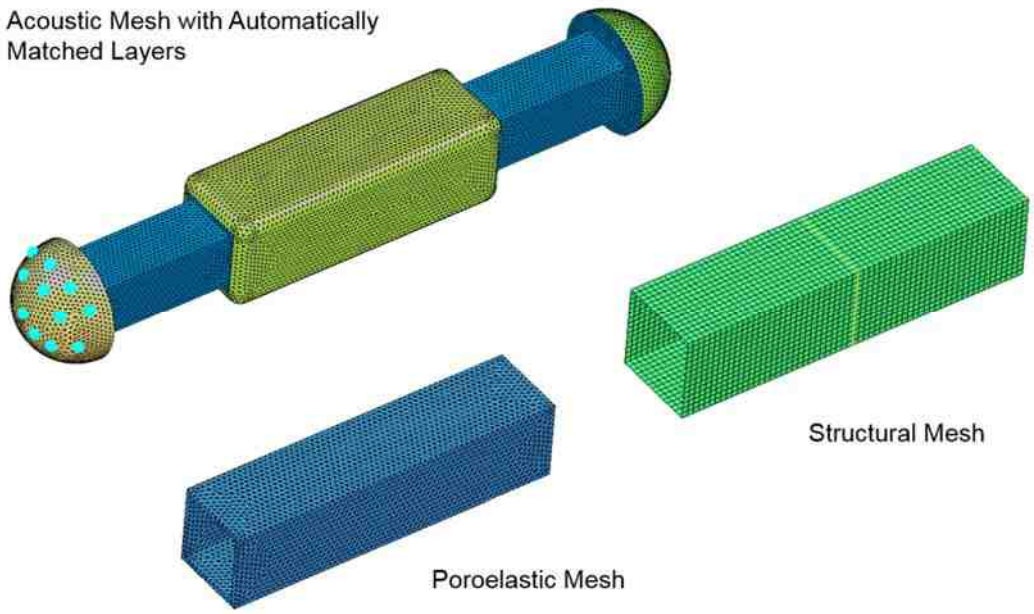

Figure 3.2 Finite element meshes for the airspace, sound absorbing lining, and ductwork for a rectangular cross-section duct.

Direct frequency response was used for the analyses since the method easily accommodates the unbounded domain and the poroelastic elements (Astley, 2007). Modal superposition analyses require solving for the modes up to 2 to 3 times the maximum frequency of interest and are not recommended due to the high mode counts for both the ductwork and the air space for solutions above 500 Hz. The vibration and forces on the structure are coupled to the respective particle velocity and sound pressure in the airspaces on both sides of the duct. For additional information, Astley (2007) well summarizes finite element theory for vibro-acoustic problems and includes an extensive list of references.

3.3 Metrics for Duct Attenuation

The *ASHRAE Handbook – Fundamentals* (2013) describes the three metrics that have been commonly used for assessing the attenuation of ducts. These are 1) insertion loss, 2) noise reduction, and 3) transmission loss. Most of the attenuation

data reported in The *ASHRAE Handbook – Applications* (2015) is based on either insertion loss or noise reduction measurements. At higher frequencies, the insertion loss and noise reduction of an element are nearly equivalent for dissipative silencer elements.

Insertion loss is defined as the decrease in sound pressure or sound intensity in dB when an attenuating element is inserted into the path between the source and receiver. Insertion loss depends on the attenuating element, source, termination, and length of duct on both sides of the attenuating element. Accordingly, it partly depends on the system that the attenuating element is placed into. Noise reduction is the difference in sound pressure level in dB measured upstream and downstream of an attenuating element. Though it does not depend on the source, it does depend on the length of duct following the attenuating element and the termination. Both insertion loss and noise reduction are attractive from a measurement standpoint. However, insertion loss is normally preferred since measurements need only be made at the end of the duct whereas noise reduction requires in duct measurements.

Insertion loss measurements have been standardized for HVAC applications in ASTM E477 (2006). A source room consisting of several loudspeakers is situated at the start of the duct so that the source is both diffuse and broadband. The duct terminates in a reverberation room where measurements are made without and with the attenuating element. For practical reasons, duct transitions must be constructed between the test duct and ductwork on both sides of the test duct. These transitions will reflect some sound and have some effect at low frequencies. The ductwork on each side of the test duct should be relatively rigid. Tests of this nature are convenient as long as the ducts entering and leaving the attenuating element are straight and in line with one another.

Transmission loss is defined as

$$TL = 10 \log\left(\frac{W_{inc}}{W_{trans}}\right) \tag{3.1}$$

where W_{inc} and W_{trans} are the incident and transmitted power respectively assuming an anechoic termination. In practice, an anechoic termination is not easily achieved and measurement is instead accomplished using the two-load method (ASTM E2611, 2010). Though this approach is widely used for small mufflers, measurement is difficult on HVAC ducts. The primary advantage of transmission loss is that it is a function of the attenuating element alone and does not depend upon the source or termination below the cutoff frequency. Above the plane wave cutoff, the nature of the acoustic source (monopole, dipole, plane wave, etc.) will affect the transmission loss and there is less advantage.

It seems that noise reduction has been the preferred metric for unlined ducts and results are normally presented in dB/ft (or dB/m). For lined ducts, insertion loss is normally used and is defined as the difference in sound power at the termination without and with lining. The total attenuation of a lined duct can be calculated as the sum of the attenuation (or noise reduction) for an unlined duct of the same length and the insertion loss due to the treatment.

Noise reduction is easily determined using analysis by comparing the sound pressure at beginning and end of the test duct. 5 ft (1.52 m) of rigid duct is included on both sides of the test duct. It was found that that the lengths of rigid duct on both sides of the test duct affected the results less than 1 dB above 150 Hz. Above the plane wave cutoff frequency of the duct, results were averaged across the cross-section on both sides of the duct.

Insertion loss was determined for lined ducts by solving separate models for the unlined and lined cases. Insertion loss was defined as the difference between sound power in dB radiated from the duct termination for unlined and lined test ducts of the same length.

Transmission loss is most easily determined using transfer matrix theory (Munjal, 2014). The method is predicated on plane wave behavior in the duct. The plane wave cutoff frequencies for rectangular and circular ducts are $c/2d$ and $c/1.71d$ respectively where c is the speed of sound and d is the respective longest cross-sectional dimension or diameter. The transfer matrix or four-pole parameters can be determined in the following manner (Herrin et al., 2007, Wu et al., 1998). Figure 3.3 shows a schematic of a straight lined duct. The four-pole parameters ($T_{11}, T_{12}, T_{21}, T_{22}$) are defined according to the matrix equation

$$\begin{Bmatrix} p_1 \\ v_1 \end{Bmatrix} = \begin{bmatrix} T_{11} & T_{12} \\ T_{21} & T_{22} \end{bmatrix} \begin{Bmatrix} p_2 \\ v_2 \end{Bmatrix} \tag{3.2}$$

where the respective sound pressures (p_1 and p_2) and particle velocities (v_1 and v_2) are identified in Figure 3.3. To determine the transfer matrix terms, two successive finite element analyses need to be completed. In the first, a unit velocity is applied on the inlet side ($v_1 = 1$) with $v_2 = 0$ on the exit. In the second, a unit velocity is applied on the exit ($v_2 = 1$) with $v_1 = 0$ on the entrance. The transfer matrix terms can be expressed as

$$\begin{aligned} T_{11} &= \frac{a_{11}}{a_{21}} \\ T_{12} &= a_{12} - \frac{a_{11}a_{22}}{a_{21}} \\ T_{21} &= \frac{1}{a_{21}} \\ T_{22} &= -\frac{a_{22}}{a_{21}} \end{aligned} \tag{3.3}$$

where

$$a_{11} = p_1|_{v_1=1,v_2=0}$$
$$a_{12} = p_2|_{v_1=0,v_2=1}$$
$$a_{21} = p_1|_{v_1=1,v_2=0} \quad (3.4)$$
$$a_{22} = p_2|_{v_1=0,v_2=1}$$

with the appropriate boundary conditions identified in the subscripts in Equation (3.4). This procedure is only valid below the plane wave cutoff frequency.

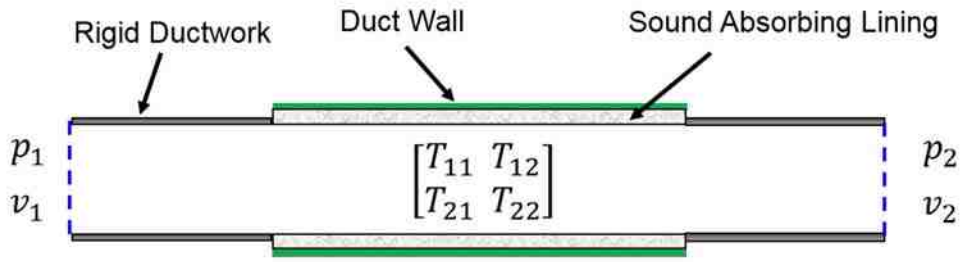

Figure 3.3 Schematic showing straight lined duct with transfer matrix variables.

The transmission loss of the silencer can be expressed in terms of the four pole parameters using (Munjal, 2014)

$$TL = 20 \cdot log_{10}\left(\frac{1}{2}\left|T_{11} + \frac{T_{12}}{\rho c} + \rho c T_{21} + T_{22}\right|\right) + 10 \cdot log_{10}\left(\frac{S_1}{S_2}\right) \quad (3.5)$$

where ρ is the density of air, c is the speed of sound, and S_1 and S_2 represent the cross-sectional area of the inlet and outlet.

Some research has been performed for predict acoustic performance above cutoff frequency in the past several decades. Munjal (1987) developed analytical solutions for dissipative ducts and included the first transverse mode. In 1990, Mechel (1990a; 1990b) derived analytical expressions for evaluating acoustic

attenuation of baffle type silencers using modal expansion. Different types of incident sound fields were investigated. Ingard (1994) developed a series of first-mode analytical solutions for prediction sound attenuation of lined ducts. Selamet (2004) included cross-modes for several types of silencers with simple configurations by assuming the acoustic pressure and velocity is continuous at the interfaces of the expansion and contraction.

Besides the above analytical solutions, numerical simulation approaches like the finite element method (FEM) and boundary element method (BEM), have been utilized to predict the sound attenuation of silencers. Cummings and Astley (1996) used the finite element method (FEM) to study the acoustical behavior of square bar silencers. Kirby et al. (2012) compared the performance of a square bar silencer to a splitter silencer. Kirby (2005) also proposed a hybrid FEM with a mode matching scheme for dissipative silencers with mean flow. Zhou et al. (2016) proposed a so-called “reciprocal identity method” that couples two different sound fields on the same muffler geometry by a simple boundary integral equation over the inlet and outlet. Wang and Wu (2016) proposed a so-called “impedance-to-scattering matrix method as an alternative method to compute the TL for large silencers at high frequencies.

3.4 Determination of Poroelastic Properties

Samples of the sound absorptive lining used in RP-1408 were procured and measured according to ASTM E1050 (2012). The two-microphone method is illustrated in Figures 3.4a and 3.4b. Figure 3.4a shows a photograph of the impedance tube with samples and 3.4b shows a schematic of the test setup. The microphone closest to the source is used as a reference and the transfer function between the two microphones (H_{12}) is measured. The determined transfer function is then used to find the reflection coefficient, which is complex, via

$$R = \frac{H_{12} - e^{-jks}}{e^{jks} - H_{12}} \tag{3.6}$$

where k is the acoustic wavenumber and s is the microphone spacing. Once the reflection coefficient is determined, the normal incidence sound absorption coefficient (α) and specific boundary impedance (z_n) can be found using

$$\alpha = 1 - |R|^2 \tag{3.7}$$

and

$$z_n = \rho c \frac{1 + R}{1 - R} \tag{3.8}$$

where ρ is the mass density and c is the speed of sound.

Sound absorptive lining can be modeled using 1) the poroelastic properties, 2) bulk properties, or 3) the specific boundary impedance from Equation (3.8). If the poroelastic or bulk properties are used, the fiber itself is modeled. If the specific boundary impedance is used, the boundary of the absorber is modeled and wave propagation through the fiber is not considered. It was found that the insertion loss found by simulation compared well with measurement when either the poroelastic or bulk properties were used. For the results that follow, the fiber is modeled using poroelastic properties.

The properties for the poroelastic model, also termed the Johnson-Champoux-Allard model (Allard and Atalla, 2009), are difficult to measure directly and were instead determined from the measured sound absorption coefficient using the ESI Foam-X software (ESI, 2014). The algorithm used breaks the sound absorption into different frequency regimes and uses a curve fit to identify the poroelastic properties from the measured absorption. Using this procedure, the flow resistivity, characteristic viscous length, characteristic thermal length, and mass density for the fiber were determined to be 0.001652 lbf-s/in^4 (17,700 N-s/m^4), 0.0099 in (0.25

mm), 0.020 in (0.504 mm), and 0.00072 lbf/in^3 (20 kg/m^3) respectively. The porosity was determined to be 0.93.

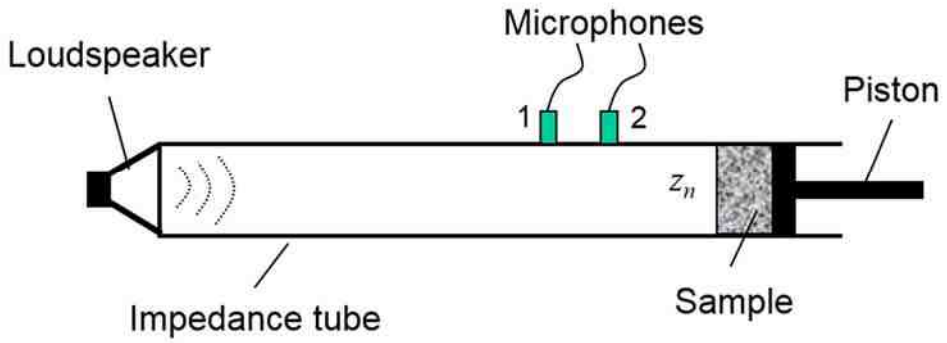

Figure 3.4a) Photograph of impedance tube showing samples and 3.4b) schematic showing microphone positions and sample in impedance tube.

10 samples each of 2 inch (5.1 cm) fiber were measured in a 1.375 inch (3.5 cm) diameter impedance tube (Spectronics impedance tube) according to ASTM E1050 (2012) and averaged. Figure 3.5 compares the sound absorption coefficient using the poroelastic model to the measured sound absorption with good agreement.

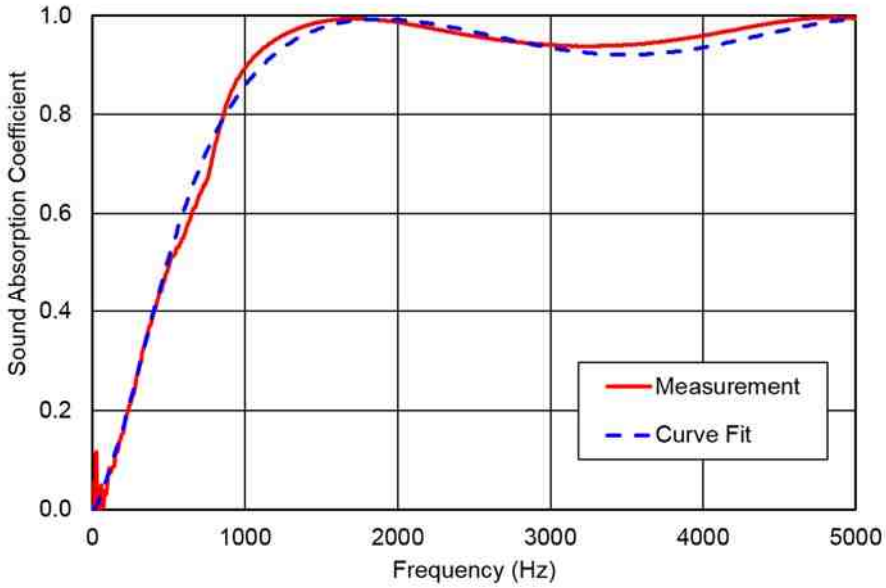

Figure 3.5 Measured and curve fitted sound absorption for 2 inch (5.1 cm) fiber.

3.5 Simulation and Measurement Comparisons

Several studies were conducted in which simulation was compared to data from the RP-1408 measurement campaign or the *ASHRAE Handbook – Applications* (2015). For unlined ducts, results were compared to the Handbook. Figure 3.6 shows the noise reduction for 2 ft x 2 ft (0.61 m x 0.61 m) cross-section, 10 ft (3.05 m) length unlined duct. Finite element results in 1/3-octave bands are compared to octave band results from the *ASHRAE Handbook – Applications* (2015). Results agree within 2 dB at frequencies above 200 Hz. Figure 3.6 also includes a similar curve for an unlined 20 ft (3.05 m) length, 24 inch (60.1 cm) diameter circular duct. Results agree well with the Handbook and are lower than the rectangular duct even for a circular duct that is twice the length. The results agree with Vér's (1978) assertion that breakout noise from the duct leads to higher attenuation at low frequencies. Below 100 Hz, results are questionable since the total length of duct is on the same order as the acoustic wavelength (i.e., the duct functions similar to

an organ pipe). Results should be more reliable when the total length of duct includes several acoustic wavelengths.

For lined ducts, simulation is compared to the RP-1408 (Reynolds, 2015) measurement campaign performed at the University of Nevada Las Vegas and E. H. Price facilities. Figure 3.7 compares the insertion loss for a 2 ft x 2 ft (0.61 m x 0.61 m) cross-section, 10 ft (3.05 m) length duct with 2 inch (5.1 cm) fiber lining enveloping the airspace. The insertion loss results agree with measurement over the entire frequency range. For comparison, the ASHRAE Handbook results are also included and agree reasonably well. It should be noted that the resolution for the ASHRAE Handbook results is in octave bands and not 1/3-octave bands.

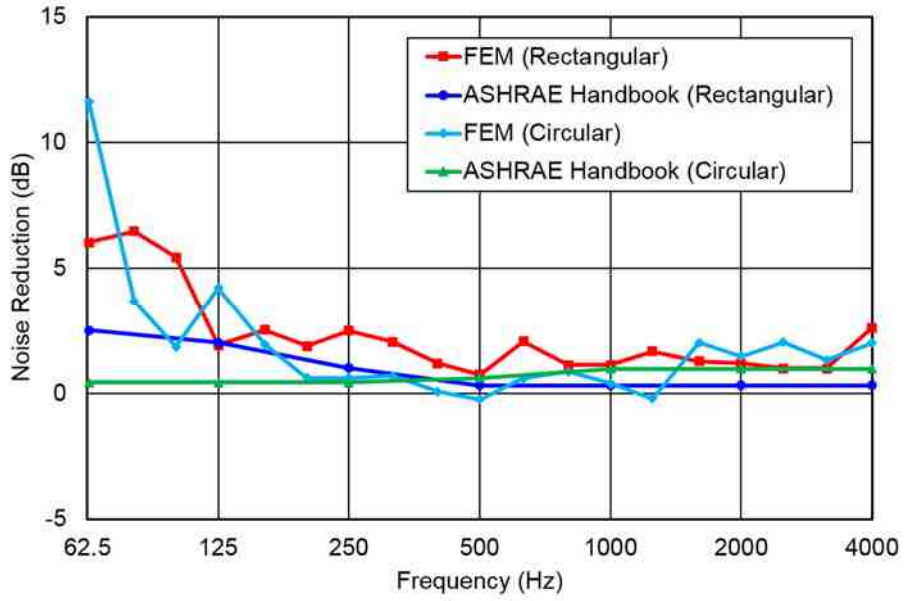

Figure 3.6 Simulated and ASHRAE Handbook comparisons of noise reduction of 24 in x 24 in (0.61 m x 0.61 m), 10 ft (3.05 m) length unlined rectangular duct and 24 in (0.61 m) diameter, 20 ft (6.10 m) length unlined circular duct.

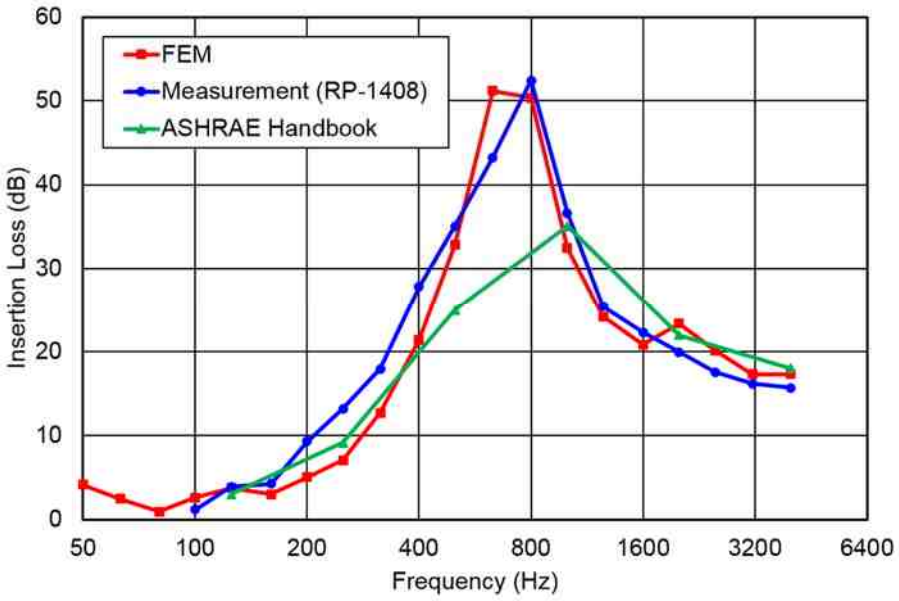

Figure 3.7 Simulated and measured (RP-1408) insertion loss of 24 in x 24 in (0.61 m x 0.61 m), 10 ft (3.05 m) length, 2 in (5.1 cm) thick fiber lined rectangular duct. *ASHRAE Handbook – HVAC Applications* (2015) are included for comparison.

Notice that the insertion loss is bell shaped with a maximum between 500 and 1000 Hz. Ingard (1994) explains this phenomenon well. Insertion loss is low at both low and high frequencies. At low frequencies, sound propagates as a plane wave and the sound absorption is ineffective because the thickness of the absorber is only a fraction of an acoustic wavelength. The acoustic wavelength is equal to c/f where c is the speed of sound and f is the frequency. In addition, sound is grazing on the sound absorber and the absorber is less effective.

At high frequencies, sound propagates longitudinally as before but also transverse to the duct since the duct cross-sectional dimension is much greater than an acoustic wavelength. The sound absorption is effective at the periphery of the duct but has a diminished effect at the center of the duct since the absorption is several wavelengths removed from the center of the duct. Accordingly, sound propagating down the center of the duct is relatively unaffected.

Insertion loss is highest in a mid-frequency range beginning at the cutoff frequency. Air pumping in the center of the duct travels to the periphery where it is absorbed. The frequency of maximum attenuation roughly corresponds to when the cross-sectional dimension of the duct is equal to an acoustic wavelength. At that frequency, sound pressure is high at both the periphery and center of the duct. Accordingly, sound absorption at the periphery will also attenuate the sound at the center of the duct since the pressure highs are part of the same transverse acoustic wave.

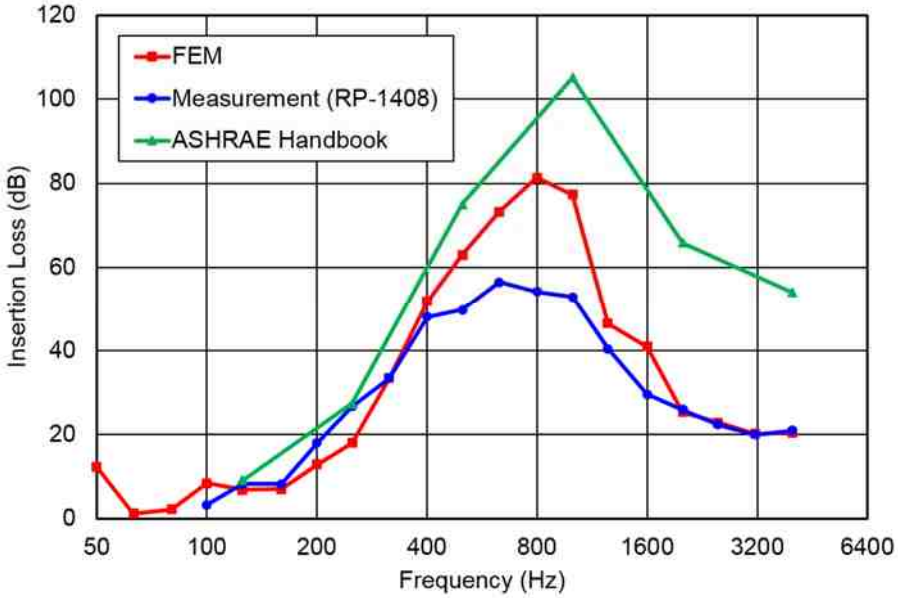

Figure 3.8 Simulated and measured (RP-1408) insertion loss of 24 in x 24 in (0.61 m x 0.61 m), 30 ft (9.14 m) length, 2 in (5.1 cm) thick fiber lined rectangular duct. *ASHRAE Handbook – HVAC Applications* (2015) are included for comparison.

Figure 3.8 compares a similar case for a 30 ft (9.15 m) length lined duct having the same cross-section. Insertion loss results compare well with measurement except between 400 and 1600 Hz. In this region, there appears to be flanking noise, which prevents measurement of attenuation that exceeds 50 or 60 dB. Flanking noise can arise due to structural excitation of the test duct from the ductwork attached on both sides, or is more likely due to external sources of noise impinging on the

exterior of the test duct or adjoining ductwork. Handbook predictions are overly high for long ducts so the Handbook should only be used for ducts up to 10 ft (3.05 m) in length.

Figure 3.9 compares the insertion loss for a 20 ft (6.10 m) length, 2 ft (0.61 m) diameter circular duct with 2 inch (5.1 cm) fiber lining. Simulation agrees well with measurement over most the frequency range though there are some differences between 500 and 1000 Hz due to flanking paths. Handbook results are comparable.

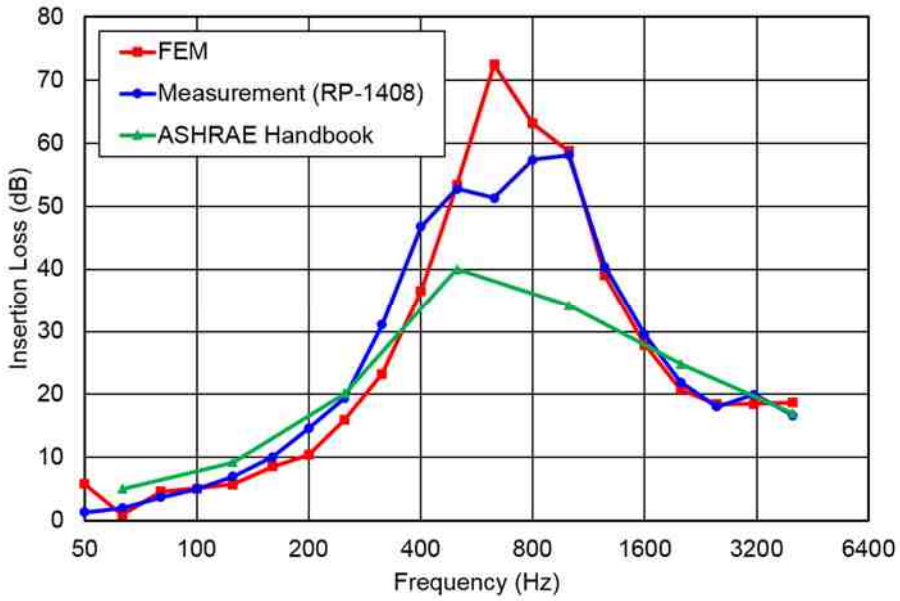

Figure 3.9 Simulated and measured (RP-1408) insertion loss of 24 in (0.61 m) diameter, 20 ft (6.10 m) length, 2 in (5.1 cm) thick fiber lined circular duct. *ASHRAE Handbook – HVAC Applications* (2015) are included for comparison.

Figure 3.10 compares insertion loss results for a 4 × 6 × 5 ft (1.2 × 1.8 × 1.5 m) (Mouratidis and Becker, 2003) unlined plenum with inlet and outlet ducts centered. It can be observed that measurement and FEM simulation results compare well. ASHRAE Handbook and Wells equation predictions are included for comparison. The Wells equation under predicts the attenuation at middle frequencies whereas

handbook results do not agree well at the lower frequencies but are acceptable at the middle and high frequencies.

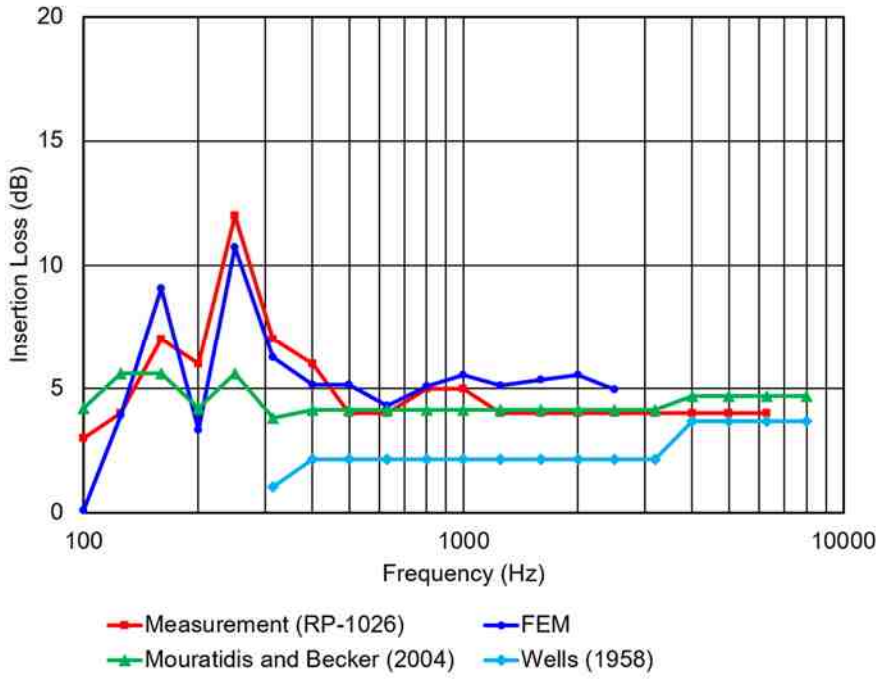

Figure 3.10 Insertion loss comparisons for a 4 ft × 6 ft × 5 ft (1.2 m × 1.8 m × 1.5 m) unlined plenum. Inlet and outlet ducts are in line. Comparison is shown between measurement, FEM simulation, Mouratidis and Becker (2004), and Wells (1958).

Similar results are shown in Figure 3.11 for a 4 × 6 × 5 ft (1.2 × 1.8 × 1.5 m) (Mouratidis and Becker, 2003) lined (2 inch or 5.1 cm fiber) plenum. Measurement and FEM simulation agree reasonably well whereas ASHRAE Handbook results are low and do not properly account for modal behavior at low frequencies.

Figure 3.12 shows similar results for a 4 × 6 × 5 ft (1.2 × 1.8 × 1.5 m) (Mouratidis and Becker, 2003) lined (8 inch or 10.2 cm fiber) plenum with a right-angle outlet. It can be seen that FEM simulation and ASHRAE Handbook results compare favorably to measurement. For this particular case, handbook results likely compare better at low frequencies because the sound absorptive lining is 8 inch (10.2 cm) thick.

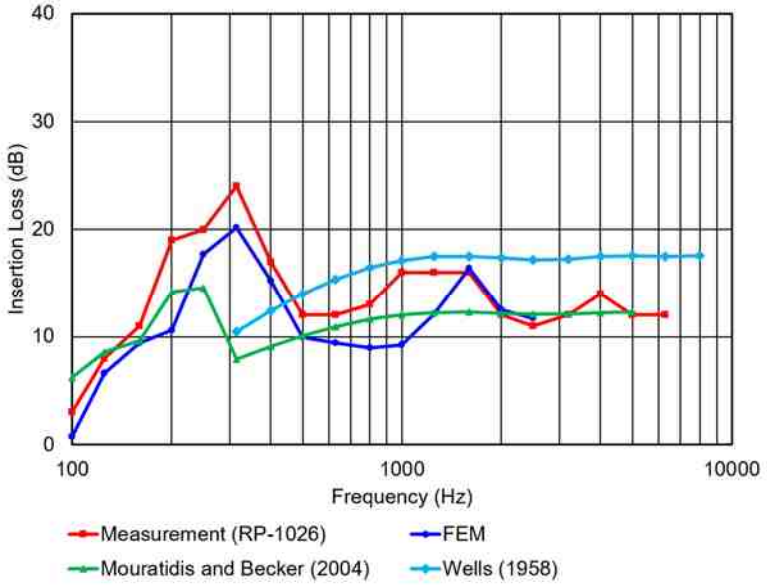

Figure 3.11 Insertion loss comparisons for a 4 ft × 6 ft × 5 ft (1.2 m × 1.8 m × 1.5 m) plenum with 2 inch (5.1 cm) glass fiber. Inlet and outlet ducts are in line. Comparison is shown between measurement, FEM simulation, Mouratidis and Becker (2004), and Wells (1958).

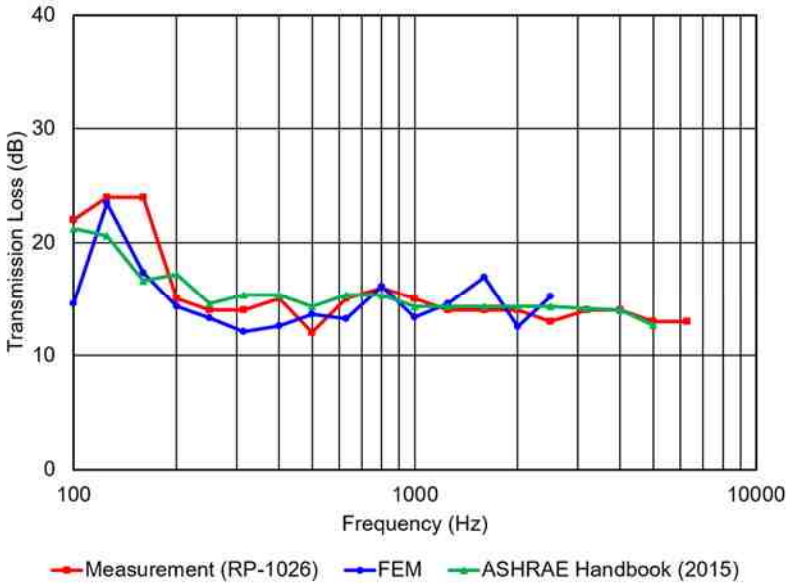

Figure 3.12 Insertion loss comparisons for a 4 ft × 6 ft × 5 ft (1.2 m × 1.8 m × 1.5 m) plenum with 2 inch (5.1 cm) glass fiber. Inlet and outlet ducts are at right angles to one another. Comparison is shown between measurement, FEM simulation, and ASHRAE Handbook (2015).

3.6 Notes Regarding Modeling and Metrics

The transmission loss below the cutoff frequency, insertion loss, and noise reduction are compared in Figure 3.13 for a 2 ft x 2 ft (0.61 m x 0.61 m) cross-section, 10 ft (3.05 m) length, 2 in (5.1 cm) thick fiber lined duct. Notice that all three metrics are similar. This is the case for most resistive silencers and suggests that the results will be similar regardless of the metric utilized.

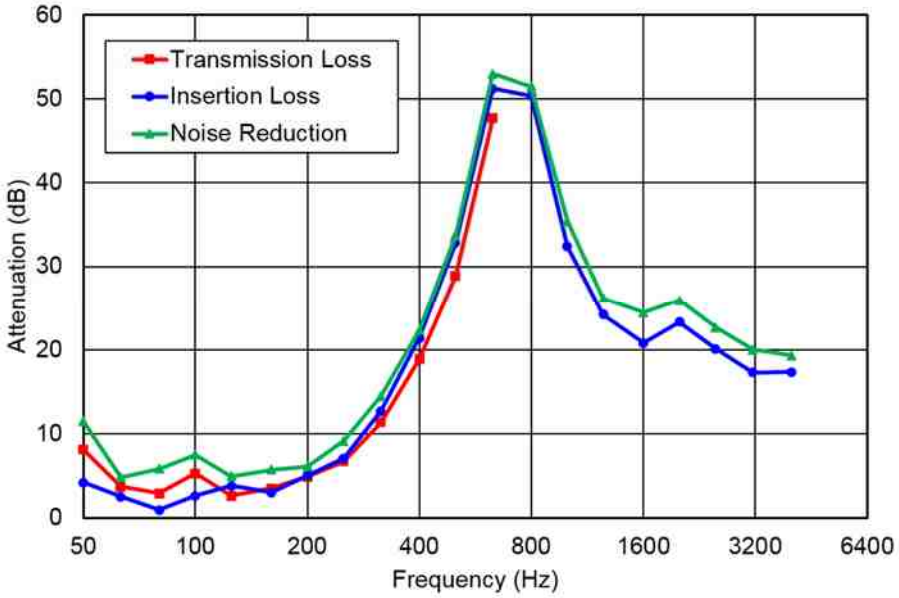

Figure 3.13 Comparison of simulated transmission loss, insertion loss, and noise reduction for a 24 in x 24 in (0.61 m x 0.61 m), 10 ft (3.05 m) length, 2 in (5.1 cm) thick fiber lined rectangular duct.

In addition, the model can be simplified significantly if the breakout noise path is ignored. In that case, the structural mesh of the ductwork and the acoustic mesh surrounding the test duct need not be included in the model. The noise reduction for the lined duct not including the breakout noise path is compared to the insertion loss for the full model in Figure 3.14. Notice that there are some differences but the noise reduction is within 5 dB of the insertion loss at most frequencies. Accuracy should be sufficient for most engineering purposes.

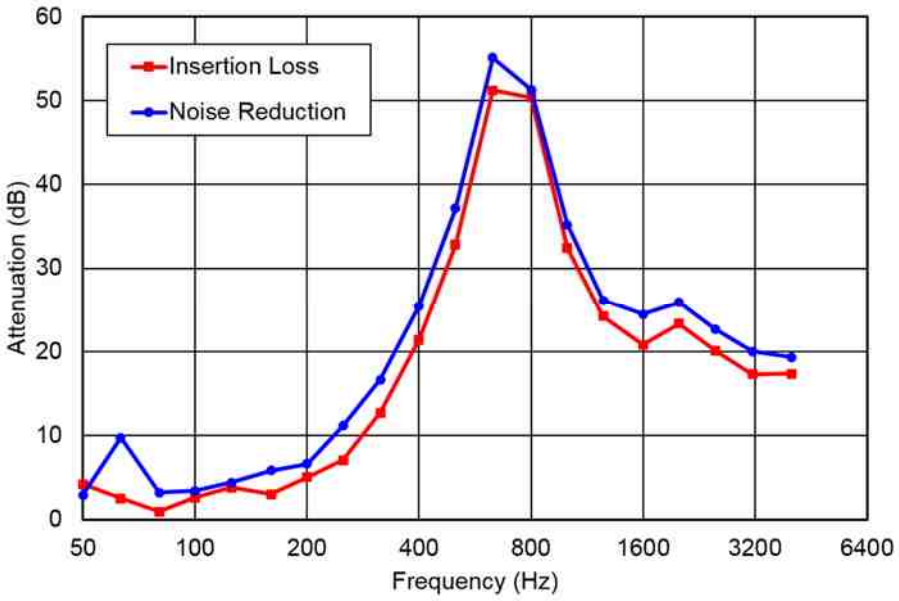

Figure 3.14 Comparison of insertion loss and noise reduction (neglecting breakout transmission path) for a 24 in x 24 in (0.61 m x 0.61 m), 10 ft (3.05 m) length, 2 in (5.1 cm) thick fiber lined rectangular duct.

Figure 3.15 shows attenuation in the duct versus the number of acoustic wavelengths from the start of the treatment at different frequencies. It can be observed that the attenuation is relatively linear for the first 5 acoustic wavelengths. Additionally, results are roughly linear above 10 wavelengths. Results are similar for both a 10 ft (3.05 m) and 30 ft (9.15 m) duct up to the number of total wavelengths for the treated portion. These results suggest that simple relationships for duct attenuation can be developed for the standard duct sizes that are summarized in the *ASHRAE Handbook – HVAC Applications* (2015). Accordingly, the Handbook can be enhanced using the developed FEM models.

It is also notable that the results in the *ASHRAE Handbook – HVAC Applications* (2015) were determined based on measurements of 10 ft (3.05 m) ducts. The Handbook tables assume that the duct attenuation is linear. This seems like an appropriate approximation if the total length of duct is below 5 acoustic wavelengths. In that case, it can be seen that the attenuation as a function of

length in wavelengths is relatively linear (Figure 3.15). However, the attenuation curves are nonlinear if the lined duct length exceeds 5 acoustic wavelengths especially for the 630 and 800 Hz 1/3-octave band curves. Hence, the results in the Handbook are suspect and can greatly over predict the attenuation for duct lengths exceeding 10 ft (3.05 m).

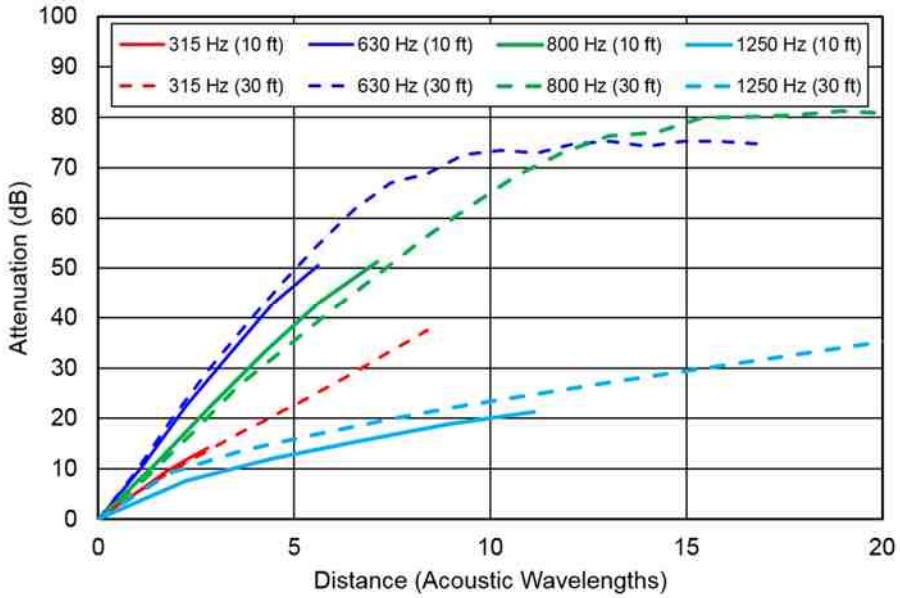

Figure 3.15 Attenuation as a function of wavelength at different frequencies for a 24 in x 24 in (0.61 m x 0.61 m), 2 in (5.1 cm) thick fiber lined rectangular duct. Results are shown for 10 ft (3.05 m) and 30 ft (9.15 m) lengths.

Flanking transmission path would be dominant at middle frequency range for a lined duct longer than 10 ft (3 m). As the results shown in Figure 3.8, Both HVAC and FEM predictions are higher than measurement. Some cases have been studied via FEM simulation to investigate the structural flanking path. Figure 3.16 compares FEM results with and without flanking to measurement results. It can be seen that including flanking drastically reduces the insertion loss in the mid-frequency range.

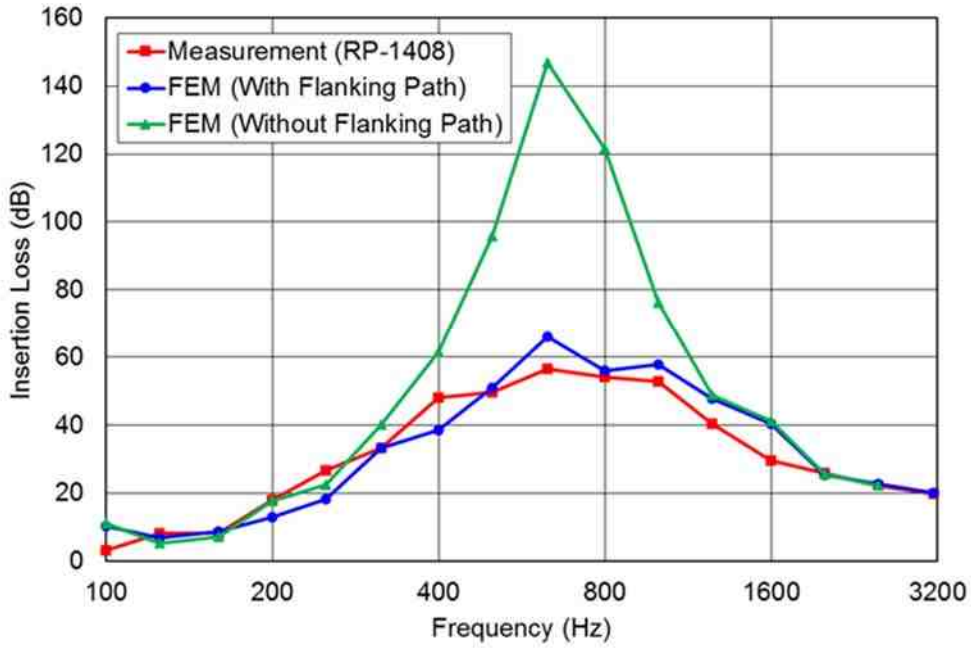

Figure 3.16 Insertion loss results for a 2 ft × 2 ft cross-section, 30 ft length lined (2 inch fiber) duct noting effect of including and excluding the flanking path.

3.7 Conclusions

A FEM approach was developed for the modeling of unlined and lined HVAC ducts. The analysis approach replicates ASTM E477 (2006). The source is modeled as a diffuse acoustic field and terminates in a rigid baffle. The structural response of the ductwork and the associated breakout noise transmission path were included. Boundaries at the source and termination were simulated using a reflection free boundary called a perfectly matched layer. Results were compared to experimental results with good agreement.

It was also shown that the model could be simplified and the breakout path could be neglected as an approximation. Results were shown to be similar but the predicted attenuation was a few dB too high at most frequencies. Since the attenuation of a lined duct is very high, an error of a few dB is not that critical.

The developed model can be used for ducts of any cross-section or length. Since the approach is now validated, future efforts can utilize the model to revise and

supplement the information that is currently in the *ASHRAE Handbook – HVAC Applications* (2015).

Chapter 4 SIMULATION OF ATTENUATION DUE TO ELBOWS AND SIDE BRANCHES AND BREAKOUT TRANSMISSION LOSS

(Note: Most of the research in this chapter has been previously documented in Ruan and Herrin (2016b).)

The primary path of noise propagation in buildings is airborne transmission from building equipment through ducts. Attenuation is increased if elbows or side branches are introduced into a duct. In Chapter 3, finite element analysis was used to predict the insertion loss of straight lined and unlined ducts and results were validated with measurement. In this work, finite element analysis is used to predict the attenuation of elbows and side branches. Results for elbows and branches are compared to the ASHRAE Handbook with good agreement. In addition, an important secondary noise transmission path is through duct walls into rooms. This path, which is often termed breakout noise, is also investigated using the finite element approach and results are correlated with an analytical solution and the ASHRAE Handbook with good agreement. Of note, it is demonstrated that the breakout transmission loss is much less than the insertion loss through lined rectangular ducts at some frequencies. This suggests that breakout noise is the dominant noise path at these frequencies.

4.1 Introduction

Noise from equipment propagates through a building via the HVAC duct network. The primary noise pathway, termed the airborne path, is directly through the ducts into the rooms. The most effective way to reduce the airborne noise is to use sound absorptive lining in the ducts. However, there is also modest attenuation at elbows or when other ducts branch off the main duct. Sound is reflected back towards the source at a bend due to the slight changing cross-sectional area, and there will be less attenuation if turning vanes are present due to regenerated noise from the turning vanes. On the other hand, the attenuation can be greatly increased if lining is added to the elbow.

Cabelli (1980) developed analytical models for unlined mitered and curved 90° bends, and Ko and Ho (1977) looked at curved bends. Vér (1983a) summarized results presented by Mechel (1975) and from a VDI Technical Report (2001) for different bends in a form appropriate for HVAC engineers. Vér's (1983a) work forms the basis for what is currently in the ASHRAE Handbook (2011). Almost all of the prior measurement studies have assumed a 90° bend.

In a companion paper (Ruan and Herrin, 2016), the attenuation of straight lined and unlined ducts with varying cross-sections was predicted using finite element analysis (FEA) and compared with measured results with good agreement. In this paper, an identical approach is used to determine the attenuation of 90° unlined and lined elbows, and of branching. Results are compared to the *ASHRAE Handbook – HVAC Applications* (2015) in order to validate the approach. The FEA approach suggested should be applicable to other bend angles and can account for cross-sectional area changes in the bend.

Though the direct airborne path is dominant some distance away from the fan, breakout noise is an important secondary path near the fan or if the ductwork is exposed. Breakout noise occurs when internal duct noise causes the duct walls to vibrate and in turn radiate noise to their surroundings and is normally a greater concern at low frequencies (Cummings, 1985). Turbulence (non-coherent noise) may also cause ducts to rumble but this is not breakout (coherent) noise in the strict sense. Breakout noise is most commonly reduced by using spiral wound circular ducts instead of rectangular ducts or increasing the duct stiffness.

Both Vér (1983b) and Cummings (1983; 1985) investigated breakout noise in ASHRAE supported efforts. Cummings continued working in the area for the next two decades and his work and others is summarized in his comprehensive review paper (Cummings, 2001). That paper nicely synopsizes the current state-of-the-art and is written at the level of a noise control engineer working in industry. The ASHRAE Handbook relies mostly on the work by Cummings (1985) with some additional information from Lilly (1987).

In addition, ducts sometimes provide a flanking path for sound transmission between rooms. In that case, noise can break in from a source into the duct and passages through the ducting to other locations. This has been termed breakin noise in the literature. Vér (1983b) and Cummings (1985) helpfully showed that the breakout and breakin transmission loss could be related to one another via a reciprocity relationship.

Astley and Cummings (Astley and Cummings, 1984; Astley et al., 1991; Cummings and Astley, 1995) have published extensively on the use of FEA to assess breakout and flanking noise. Their work laid the foundation for current commercial codes.

In the current effort, a commercial software package, Siemens Virtual.Lab (2015), is used for all analyses and results are compared to the *ASHRAE Handbook – HVAC Applications* (2015) and an analytical model. The objective is to document and validate a simulation approach that can be used to assess the attenuation of straight ducts, elbows, and terminations as well as breakout transmission loss. The FEA approach can then be used in future efforts to make the Handbook more comprehensive and to better evaluate the wide variety of HVAC ducting schemes seen in industry.

4.2 Metrics for Elbow and Branch Attenuation

Insertion loss is defined as the decrease in sound pressure or sound power in dB when an attenuating element is inserted into the path between a source and receiver. In the case of an unlined elbow, insertion loss is normally defined as the difference between the sound pressure or power at the termination of a straight duct without the bend and that of a duct including the bend having the same total length. The bend should be located at or near the mid-length of the ducting. For lined ducts, insertion loss is defined as the difference in sound pressure at the termination between a straight duct and a lined elbow.

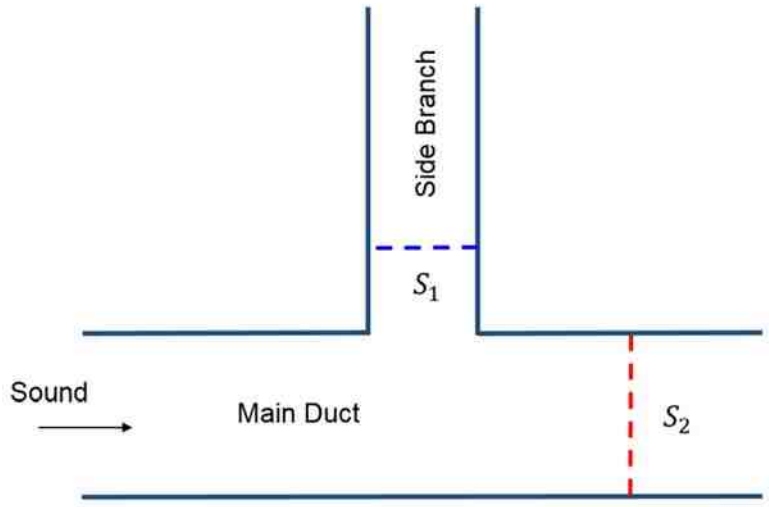

Figure 4.1 Schematic showing branch coming of main duct with respective cross-sectional areas indicated.

It is also common for several ducts to branch off of a main duct. Figure 4.1 shows a schematic of a duct branching from a main duct including the respective cross-sectional areas. Insertion loss is defined as the difference in sound pressure without and with the branch. The insertion loss for a single branching can be estimated using

$$IL = 10\log_{10}\left(\frac{S_1 + S_2}{S_2}\right) + IL_{elbow} \tag{4.1}$$

where S_1 and S_2 are the cross-sectional areas of the branch and main duct respectively. It seems that it is customary to add a term for the elbow insertion loss (IL_{elbow}) if the attenuation is desired for the side branch and not the main duct.

4.3 Simulation Model for Determination of Elbow or Branching Attenuation

The objective of the simulation approach selected is to replicate ASTM E477 (2006). In ASTM E477, a source room is connected to a receiving room through a long duct that can be assumed to be rigid. The test component is inserted into

the long duct, and insertion loss is computed as the difference in sound power in the receiving room with and without the attenuating component in place. ASTM E477 is difficult to apply to elbows and other components where the inlet and outlet ducts are at some angle because source and receiving rooms are normally in line with one another. For this reason, a simulation approach is desirable.

The source room was modeled using 20 monopole sources having equal strength and random phase positioned on a hemisphere as shown in Figure 4.2. The surface of the hemisphere is reflection free and is simulated using a perfectly matched layer boundary condition (Berenger, 1994; Tam et al., 1998; Bermudez et al., 2007; Casalino and Genito, 2008). A perfectly matched layer absorbs sound waves that have high angles of incidence. The mesh should be conformal to the surface and will not require as many degrees of freedom as alternative methods such as infinite elements (Astley and Coyette, 2001; Burnett and Holford, 1998). The exit of the duct is modeled as a baffled termination. In a similar manner, a perfectly matched layer was utilized to simulate the unbounded domain on the hemisphere. The test duct panels were modeled using shell elements. The air around the test elbow was also modeled to allow for sound radiation off the ductwork. A perfectly matched layer was again used to model the unbounded domain around the elbow.

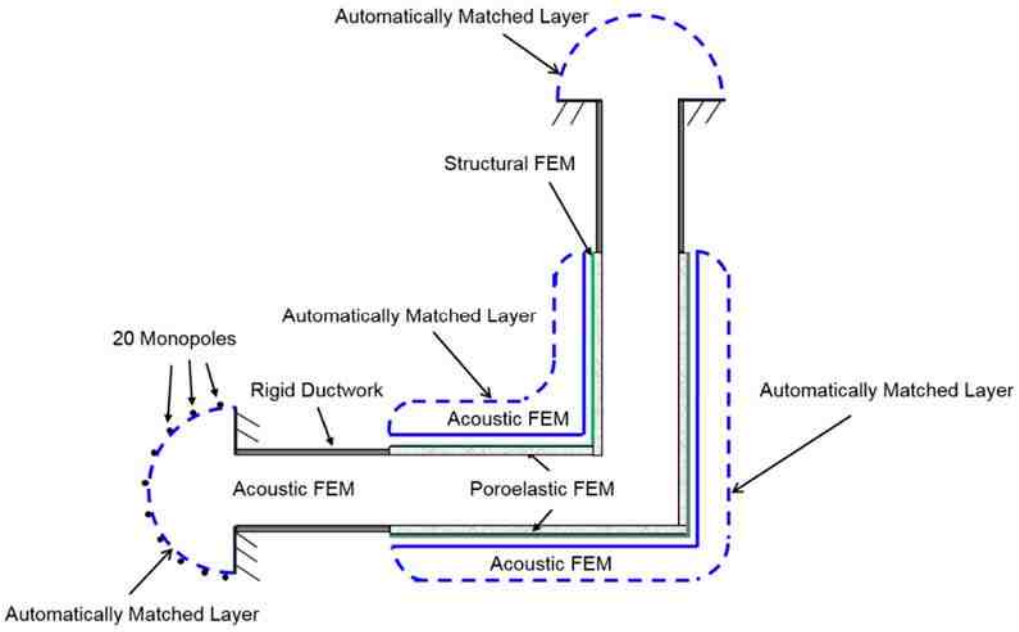

Figure 4.2 Schematic showing finite element modeling strategy.

The Siemens Virtual.Lab (2015) software was used. Their particular implementation of the perfectly matched layer is termed an automatically matched layer. Normally, a perfectly matched layer must be meshed and consists of several layers of elements. In the Siemens Virtual.Lab implementation, the perfectly matched layers are generated internally. The resolution and thickness of the layer is frequency dependent.

Figure 4.3 illustrates the manner in which sound absorbing lining was included in the model. The lining was simulated using poroelastic finite elements which include sound pressure degrees of freedom plus additional degrees of freedom for the motion of the elastic frame of the fiber (Atalla et al., 1998). Chapter 3 includes information regarding the measurement of the sound absorption and the determination of the poroelastic properties. Table 4.1 lists the poroelastic properties in both English and metric units.

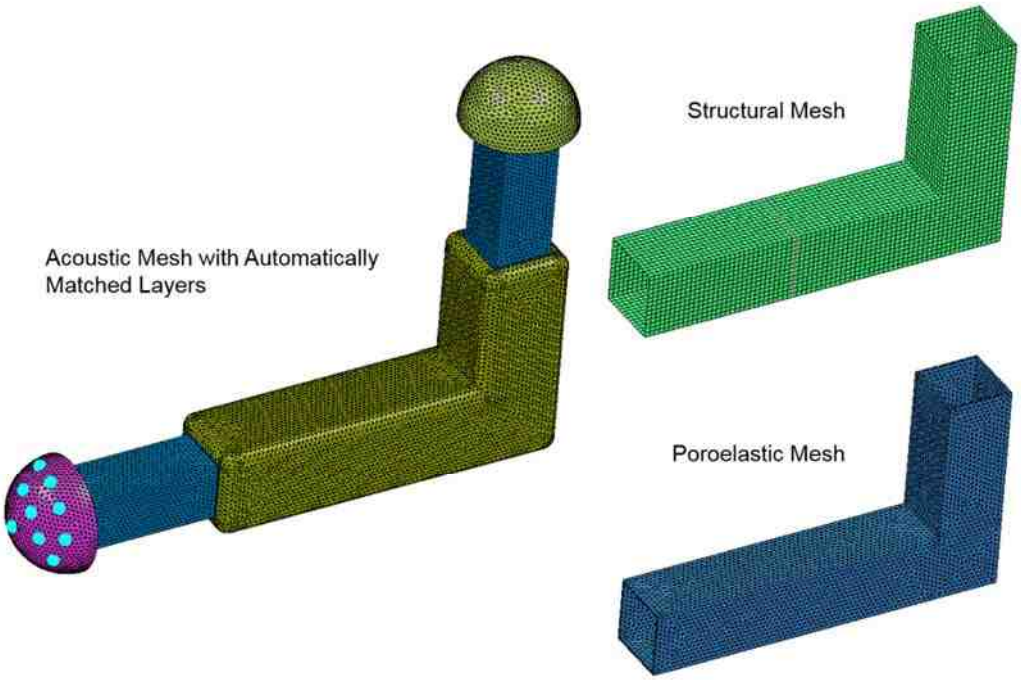

Figure 4.3 Schematic showing finite element model, structural FEM, and poroelastic FEM.

Table 4.1 Poroelastic Properties of Fiber

Poroelastic Properties	Value
Flow Resistivity	17,700 N-s/m^4 (0.001652 lbf-s/in^4)
Porosity	0.93
Tortuosity	1
Characteristic Viscous Length	0.252 mm (0.0099 in)
Characteristic Thermal Length	0.504 mm (0.020 in)
Mass Density	20 kg/m^3 “(0.00072 lbf/in^3)

A direct frequency response was used because it readily accounts for the unbounded domain and the poroelastic elements (Astley, 2007). Modal superposition analyses is not recommended due to the high mode counts for both the structure and the air space. Structural acoustic coupling effects are included between the ductwork and the air space around the elbow

4.4 Elbow and Branching Insertion Loss Results

Insertion loss is the difference in dB at the termination between a straight duct and a duct with unlined or lined elbow. Simulation is compared to the *ASHRAE Handbook – HVAC Applications* (2015) in Figure 4.4 for an unlined elbow. The cross-sectional area of the ductwork is 2 ft x 2 ft (0.61 m x 0.61 m). Figure 4.5 compares a similar case for an elbow with 1 inch (2.5 cm) fiber lining. There is good agreement with the Handbook for both the unlined and lined cases.

The insertion loss results for a branch are shown in Figure 4.6 and are compared to the *ASHRAE Handbook – HVAC Applications* (2015). At low frequencies, the model is suspect because the ducts are shorter or on the same order as an acoustic wavelength and reflections from the source and termination will affect the results. ASHRAE Handbook results are calculated not including the elbow insertion loss term in Equation (4.1). If attenuation is found for the duct which is in line with the inlet duct, it appears that elbow insertion loss term should not be included.

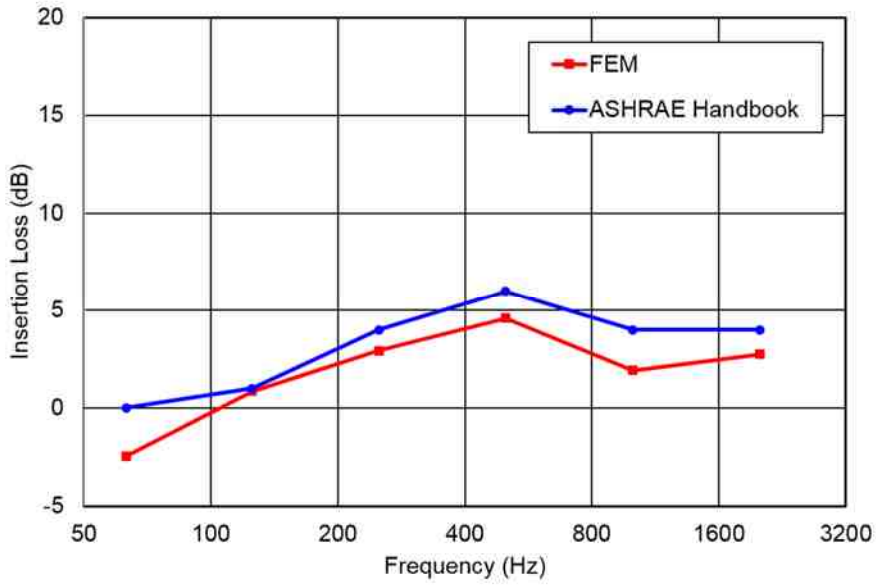

Figure 4.4 Comparison of FEM and ASHRAE Handbook insertion loss for an unlined elbow. The rectangular duct is 24 in x 24 in (0.61 m x 0.61 m).

Results in Figures 4.4 through 4.6 validate that the finite element approach can be used to determine the insertion loss of elbows and branches. Moreover, the model can be used to evaluate additional branches and to assess the best positions for sound absorbing lining in a duct system.

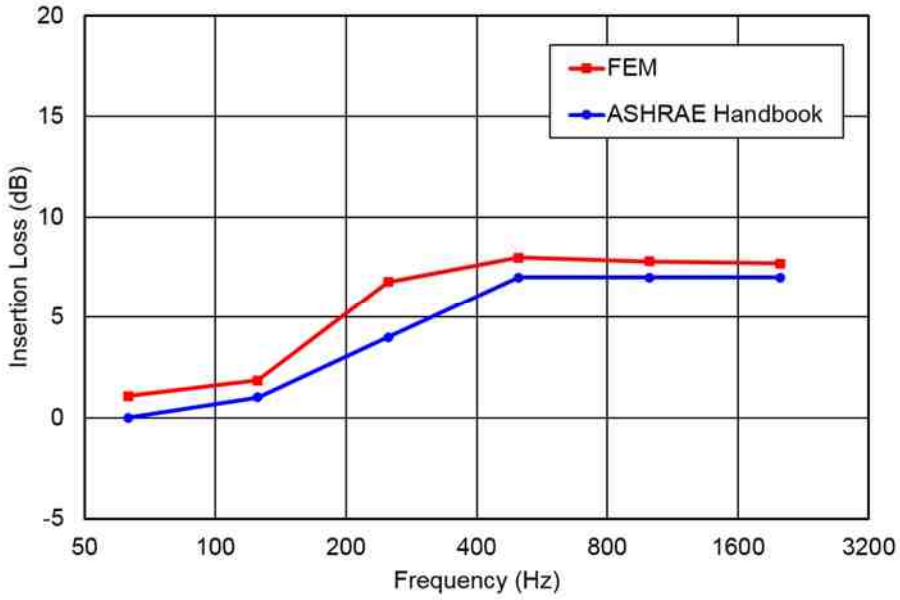

Figure 4.5 Comparison of FEM and ASHRAE Handbook insertion loss for a 2 in (5.1 cm) thick fiber lined elbow. The rectangular duct is 24 in x 24 in (0.61 m x 0.61 m).

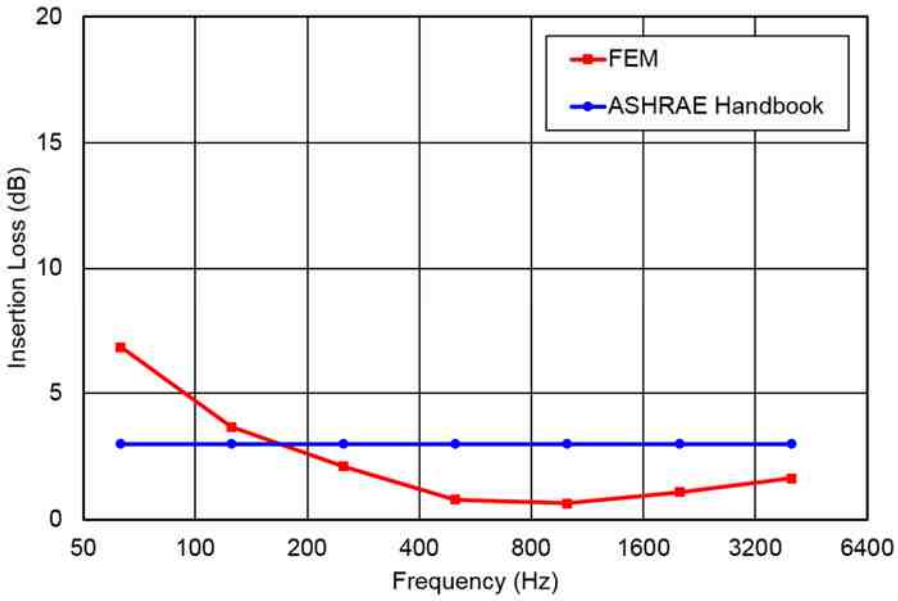

Figure 4.6 Comparison of FEM and ASHRAE Handbook insertion loss for a 24 in x 24 in (0.61 m x 0.61 m) rectangular duct with side branch of the same size.

4.5 Determination of Damping Loss Factors

The damping loss factor is defined as the ratio of energy dissipated per cycle of oscillation to the total dynamic energy in a subsystem and can be related to other commonly used damping parameters like the critical damping ratio (Lyon and DeJong, 1998). Ducts of various sizes were measured at a school that was under construction. Though the duct sizes may not exactly match those measured for the ASHRAE Handbook, the sizes were similar and lined and unlined ducts were considered. The damping loss factor was determined using the decay rate method. Figure 4.7a shows the measurement setup for the approach. The impulse response of a panel was measured in the time domain and then band pass filtered in octave bands. The initial slope of the transient response is called the decay rate (γ) and is the slope of the line in dB/sec shown in Figure 4.7b. The loss factor (η) can be determined via

$$\eta = \frac{\gamma}{27.3f} \tag{4.2}$$

where f is the center frequency.

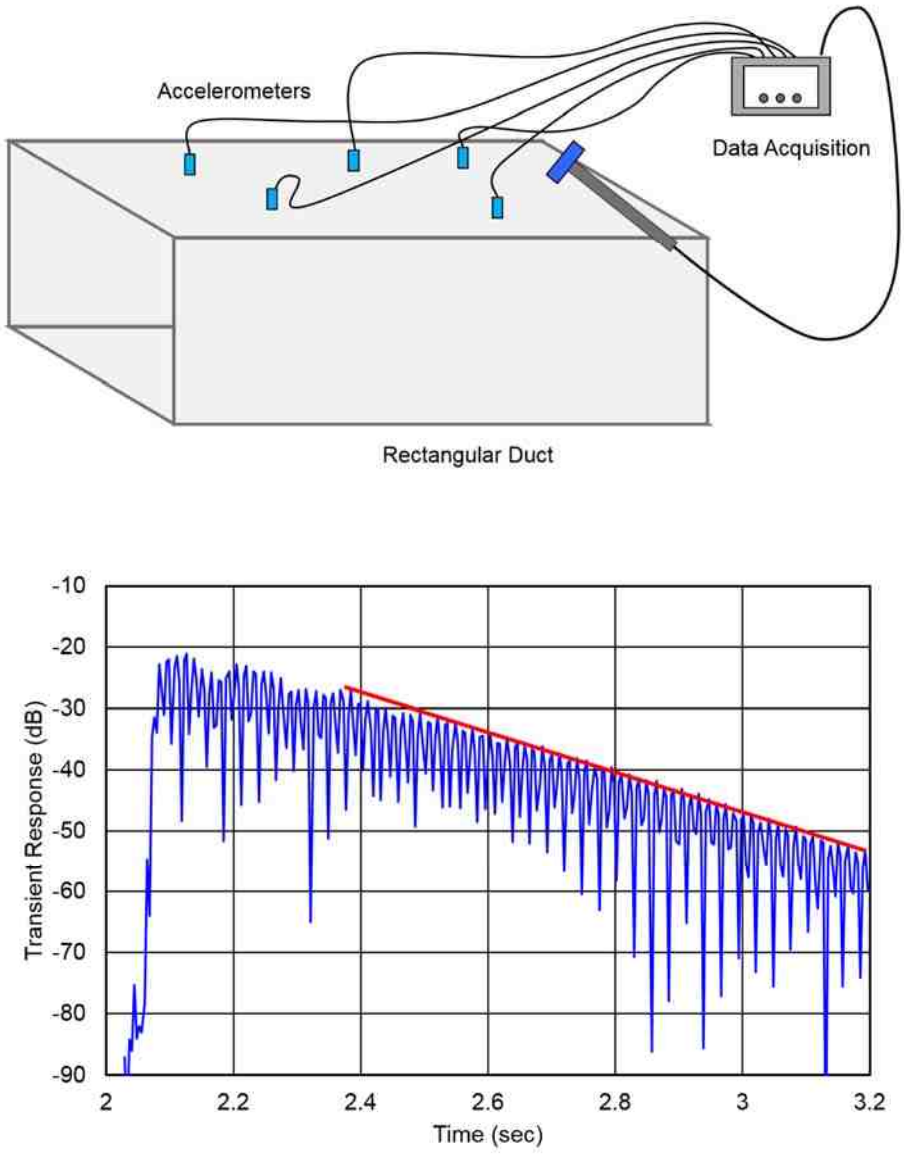

Figure 4.7a) Schematic showing procedure to determine the damping loss factor of HVAC duct panel. Impact hammer and accelerometers are shown. Data acquisition (DAQ) is not shown. b) Typical measured transient response with decay rate illustrated.

Data was acquired at 5 positions on each panel and averaged for 5 hits. The impact hammer used was a PCB 086C03 and the accelerometers used were PCB 333B32. Data was acquired using a LMS SCADAS SCM01 data acquisition. The results for the damping loss factor are tabulated in Table 4.2. Notice that the damping is higher by an order of magnitude if the duct is lined. Damping loss factor values were found to be similar for both rectangular and circular ducts. In the simulation models, the average damping ratios for the unlined and lined ducts were determined and values of 0.003 and 0.02 respectively were selected for unlined and lined ducts.

Table 4.2 Measured Damping Loss Factors

	Circular	Rectangular				
Frequency (Hz)	10 in Diameter (25.4 cm)	10 in x 10 in (25.4 cm x 25.4 cm)	16 in x 16 in (40.6 cm x 40.6 cm)		32 in x 32 in (81 cm x 81 cm)	
	Unlined	Unlined	Unlined	Lined	Unlined	Lined
63	0.016	0.011	0.012	0.014	0.012	0.021
125	0.010	0.006	0.009	0.038	0.007	0.011
250	0.007	0.004	0.006	0.036	0.004	0.030
500	0.016	0.003	0.010	0.026	0.003	0.026
1000	0.008	0.003	0.007	0.022	0.003	0.022
2000	0.004	0.003	0.004	0.012	0.002	0.014
4000	0.002	0.004	0.004	0.007	0.002	0.009
8000	0.001	0.002	0.002	0.005	0.002	0.006

4.6 Determination of Breakout Transmission Loss

The simulation modeling approach is identical to that described earlier for determining insertion loss of elbows and is shown in Figure 4.8. The air space is modeled using acoustic finite elements and any sound absorbing lining is simulated using poroelastic elements. A diffuse field at the source is approximated by 20 acoustic monopole sources having the same amplitude and random phase.

An automatically matched layer was placed on the hemispherical surface on both the source and termination sides of the duct. This boundary condition assumes that the domain is unbounded so there are no reflections even for high angles of incidence.

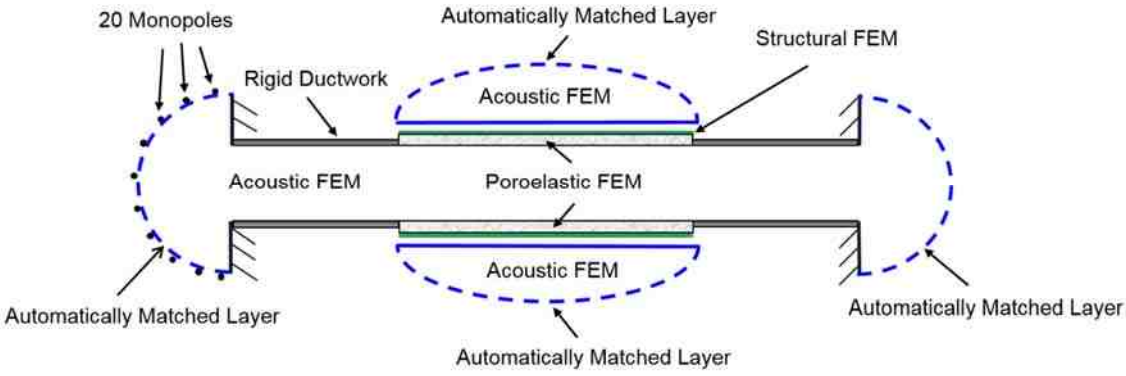

Figure 4.8 Schematic showing FEM modeling strategy for breakout noise.

The ductwork was modeled using shell elements for both rectangular and circular cross-sections. The elastic modulus and mass density were chosen for steel and were 210 GPa (30E6 lbf/in^2) and 7800 kg/m^3 (0.281 lbf/in^3) respectively. The rectangular ducts were stiffened around the perimeter of the duct every 5 ft (1.52 m) using beam elements. Circular ducts were assumed to be of the spiral wound variety with neighboring spiral lines separated by 8 inches (20 cm). Beam elements were used to model the reinforcement for rectangular ducts and the spiral winding for circular ducts. Figure 4.9 shows the finite element models for both a rectangular and circular duct.

There is an acoustic mesh surrounding the ductwork with an automatically matched layer that envelops the acoustic mesh as shown in Figure 4.9. The sound power radiating from the automatically matched layer to the acoustic domain can be assessed.

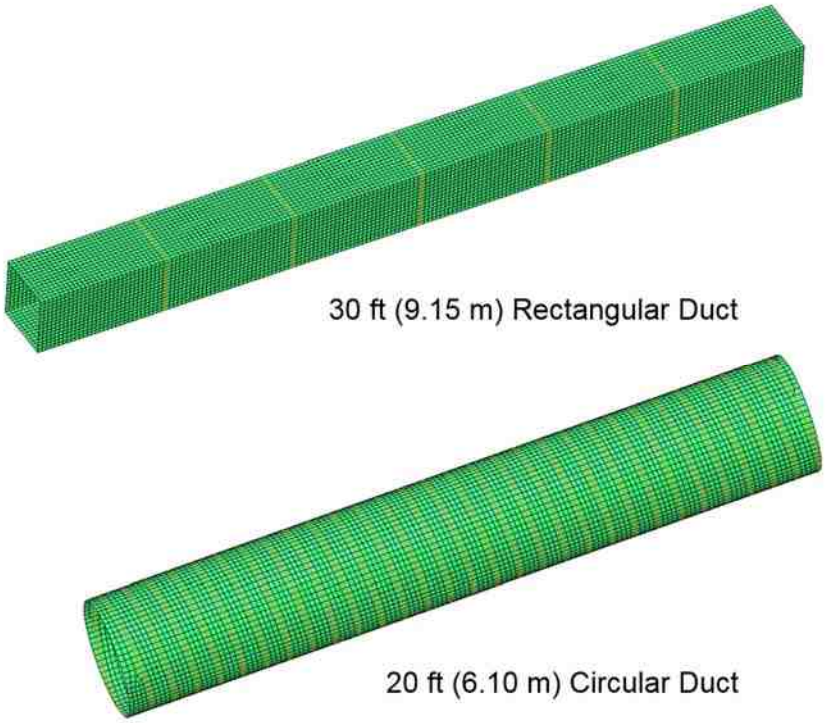

Figure 4.9 Structural FEM models for rectangular and circular ducts.

For unlined ducts, the breakout transmission loss was determined using Equation (2.11). The radiated sound power from the ductwork corresponds with $L_{w(out)}$. The incident sound power in the inlet duct was determined via

$$L_{w(in)} = 10\log\left(\frac{p_{rms}^2}{4\rho c}S\Big/W_{ref}\right) \tag{4.3}$$

where S is the cross-sectional area of the duct and W_{ref} is the reference sound power (1.0E-12 W or 7.38E-13 lbf-ft/s). Equation (4.3) assumes a diffuse field at the duct entrance. p_{rms}^2 is the spatially averaged sound pressure determined by taking the squared average for 20 sound pressures at different positions in the inlet duct.

For lined ducts, Equation (2.12) was used. The duct attenuation rate (α) was determined from the insertion loss. Insertion loss, which is the subject of Chapter 3 was determined by taking the sound power level difference in dB for the unlined and lined duct of the same length.

4.7 Breakout Transmission Loss Results

Figure 4.10 shows the breakout transmission loss for a 16 in x 48 in (41 cm x 122 cm), 0.034 in (0.85 mm) thick, 10 ft (3.05 m) length rectangular duct. Simulation results compare well with both Cummings (1983) and the *ASHRAE Handbook – HVAC Applications* (2015). Results for a 2 inch (5.1 cm) fiber lining having a density of 1.25 lbf/ft^3 (20 kg/m^3) are also included for comparison. It can be seen that the lining enhances the attenuation above 400 Hz.

Figure 4.11 shows similar results for a 24 in (61.0 cm), 20 ft (6.1 m) length circular duct. The thickness of the duct is 0.028 in (0.71 mm) and the material was galvanized steel. The ring and critical frequencies are at 2710 Hz and 16,800 Hz respectively. Notice that the breakout transmission loss is much higher for a circular duct than for a rectangular duct.

For rectangular ducts, there is good agreement over the entire frequency range. For circular ducts, there is good agreement with the analytical results at low frequencies where Equation (2.18) is valid. However, the *ASHRAE Handbook – HVAC Applications* (2015) results are from measurement and are much lower than those predicted. Cummings (1985) conjectured that the discrepancy between Equation (2.18) and measurement is due to the mode coupling effect discussed earlier. As noted earlier, this is most likely because high breakout transmission loss is difficult to measure accurately.

Figure 4.12 compares the insertion loss to the breakout transmission loss for a 24 in x 24 in (0.61 m x 0.61 m), 10 ft (3.05 m) length lined duct. In general, the breakout transmission loss will be much higher than the insertion loss or noise reduction for a lined or unlined duct. However, the insertion loss is substantially

higher than the breakout transmission loss at frequencies between roughly 600 and 1000 Hz. This suggests that breakout noise will be a dominant noise path in this frequency regime.

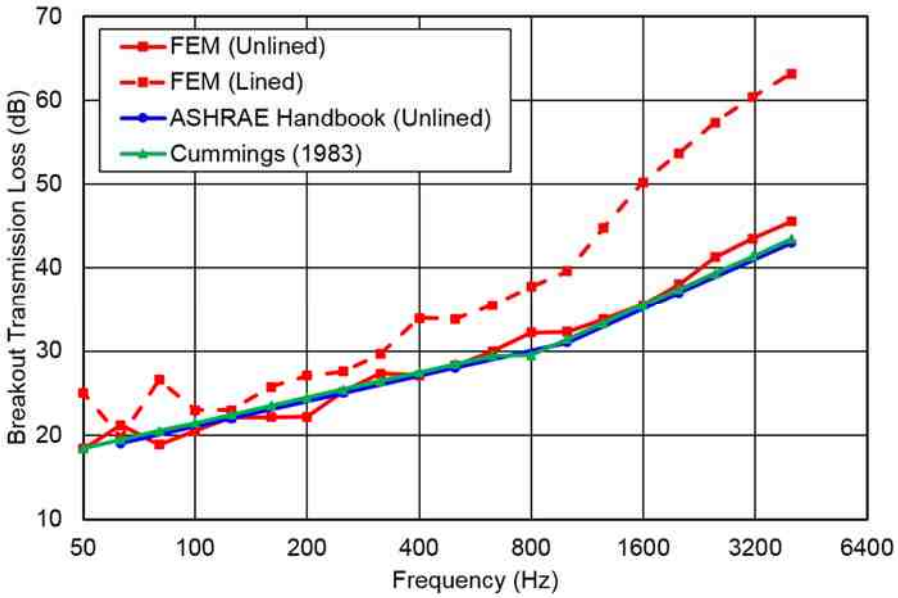

Figure 4.10 Breakout transmission loss comparing FEM unlined and lined models, Cummings (1983) equation, and ASHRAE Handbook. The rectangular duct is 16 in x 48 in (0.41 m x 1.22 m) and 10 ft (3.05 m) in length.

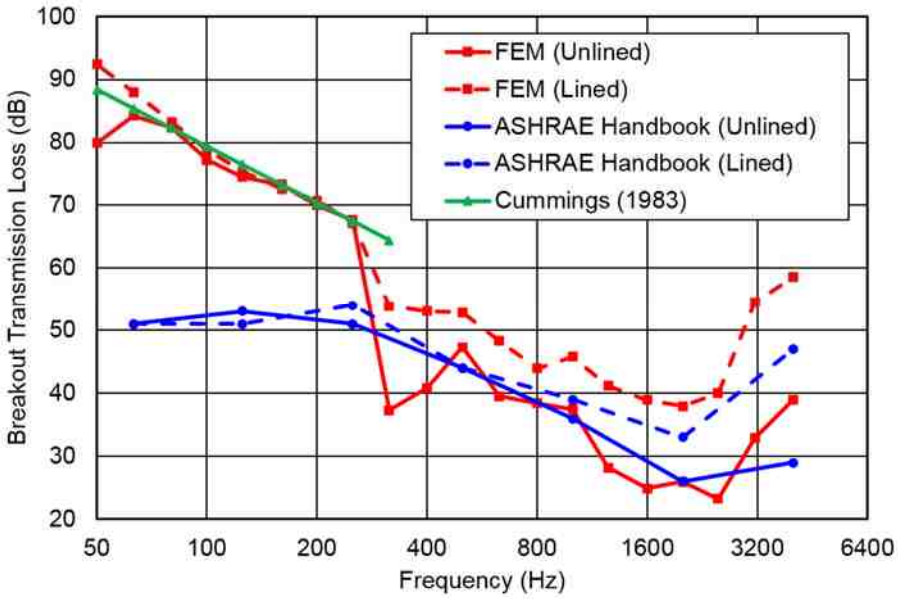

Figure 4.11 Breakout transmission loss comparing FEM unlined and lined models, Cummings (1983) equation, and ASHRAE Handbook. The circular duct is 24 in (0.61 m) and 20 ft (6.10 m) in length.

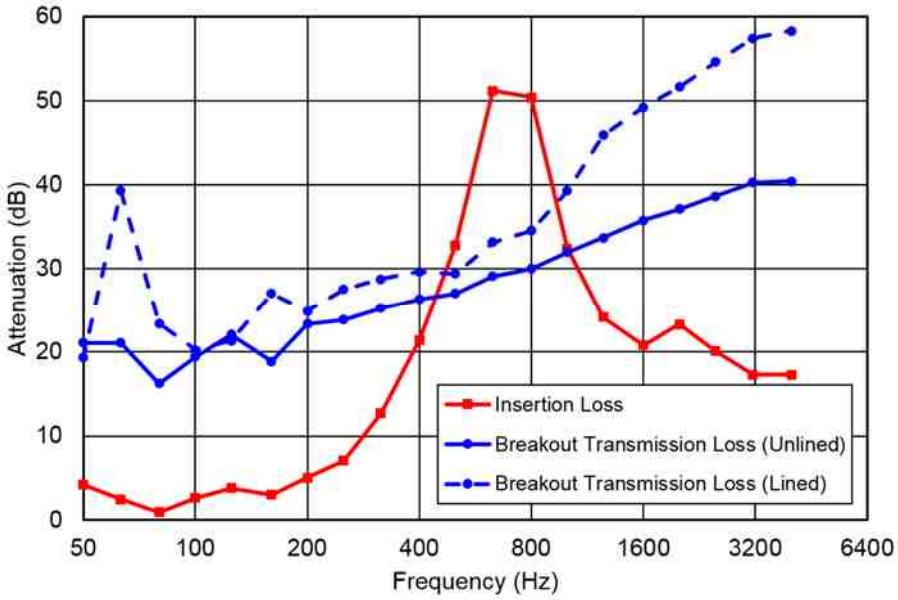

Figure 4.12 Comparison of insertion loss, and breakout transmission loss of lined and unlined 24 in x 24 in (0.61 m x 0.61 m), 10 ft (3.05 m) length, 2 in (5.1 cm) thick lined duct.

4.8 Conclusions

A FEM procedure for determining the insertion loss of elbows and branches has been detailed. The process described replicates the measurement procedure. Insertion loss is defined as the sound power difference in dB at the termination between an unlined straight duct and duct with lined or unlined elbow having the same total length. Side branch insertion loss was determined in a similar way. Simulated results compared well with the *ASHRAE Handbook – HVAC Applications* (2015).

With the procedure validated, future work can concentrate on looking at other bend configurations. For instance, published results assume a $90°$ bend whereas bends are not restricted to $90°$ in practice. Different elbow lining strategies can also be examined.

A similar FEM procedure was also developed to identify the breakout transmission loss. The ductwork was modeled using shell elements, and beam elements were used to model reinforcements or spiral winding. The airspace both inside and outside the test duct was modeled, and a reflection free boundary was modeled on the envelope FEM mesh using an automatically matched layer.

Simulation results compared well with measurement for rectangular ductwork over the entire frequency range and circular ductwork at frequencies above the plane wave cutoff frequency. Below the cutoff frequency, simulation compared well with an analytical model for circular ducts. However, lower breakout transmission loss is found in the field at low frequencies for circular ducts. This is likely due to flanking paths.

Chapter 5 USING SCALE MODELING TO ASSESS HEATING AND AIR CONDITIONING DUCT ATTENUATION

(Note: Most of the research in this chapter has been previously documented in Ruan and Herrin (2017b).)

In this chapter, scale modeling rules are summarized for assessing the attenuation of heating, ventilation, and air conditioning ducts. A standard scaling approach is applied where the frequency ratio is inversely proportional to the size ratio. Scaling rules for sound absorption and breakout noise transmission are also developed. The scaling approach is first tested virtually via finite element analysis to validate the concept. This is followed by some experimental cases where a small expansion chamber, similar to a plenum, and its corresponding scale model are measured. Scale model results agree with full scale measurements for insertion loss, transmission loss and breakout transmission loss.

5.1 Introduction

Scale modeling is commonly used in many engineering fields to investigate large problems that would require prohibitively expensive testing facilities. This is certainly the case in the field of noise and vibration research. In early scale modeling work for acoustics, Jordan (1970; 1975) determined the reverberation time for concert halls and auditoria. Emori and Schuring (1977) summarized the work on architectural acoustics in their text and detailed scaling rules for acoustic spaces and porous sound absorbing materials. More recently, Brown (2016) has used 3D-printing to develop scale models for architectural acoustics applications. Ivey and Russell (1977), Wadsworth and Chambers (2000), and Busch et al. (2003) used scale models to investigate the barrier attenuation.

Nonetheless, noise and vibration practitioners have rarely used scale models for other applications outside of the building and highway industries. This is likely because many other problems can be simulated via finite or boundary element analysis, and statistical energy analysis is sufficiently accurate at higher

frequencies. Nevertheless, it would seem that using scale models to investigate the attenuation of heating, ventilation, and air conditioning (HVAC) ductwork would be another natural application. Measurement studies require a source room, a receiving room, and space to run long ducts (Vér, 1977; Mouratidis, E. and Becker, 2003; Cummings, 1983). The source room is often a reverberation room whereas the receiving room may be either a reverberation or anechoic chamber. Moreover, setting up each duct is time consuming and testing requires low background noise. If breakout noise is of interest, ducts should be run through an anechoic or reverberant space (Cummings, 1983). Currently, only a handful of laboratories in the world are sufficiently equipped for insertion loss and breakout noise measurements.

In earlier chapters, finite element method (FEM) were used to accurately determine the insertion loss and breakout transmission loss of standard sized HVAC ductwork. Even so, software users need to be advanced and commercial acoustic FEM software is not widespread in the HVAC industry. Moreover, simulation should be validated via measurement. Hence, there is a great need for additional measurement studies. Given the expense and facility requirements, scale models are an attractive option.

The current work is an introductory research effort aimed at selecting appropriate scaling laws to determine the insertion loss and breakout transmission loss of HVAC ductwork and plenums. The scaling laws are first developed and validated using FEM simulation. The approach is then experimentally validated on a small silencer which has many characteristics in common with commercial HVAC plenums.

5.2 Scaling Rules Development

5.2.1 Sound Propagation in Air

The wave equation which is used to describe the propagation of sound can be developed from the linearized continuity equation, the linearized motion equation and the equation of state.

One-dimensional equations are utilized for demonstration of developing scaling rules. The linearized one-dimensional continuity equation can be expressed as

$$\frac{\partial \rho}{\partial t} = -\rho_0 \frac{\partial u_x}{\partial x} \tag{5.1}$$

where ρ and ρ_0 are ambient fluid density at different locations, u_x is the speed of fluid in x direction and t is the time. A scaling rule can be developed via continuity equation as

$$\gamma_\rho \gamma_f = \gamma_\rho \gamma_L \gamma_f \gamma_L^{-1} \tag{5.2}$$

The linearized one-dimensional motion equation can be expressed as

$$\gamma_\rho \gamma_f = \gamma_\rho \gamma_L \gamma_f \gamma_L^{-1} \tag{5.3}$$

A scaling rule can be developed then as

$$\gamma_\rho \gamma_f = \gamma_\rho \gamma_L \gamma_f \gamma_L^{-1} \tag{5.4}$$

Assume density of fluid is unchanged for both unscaled and scaled models, the scaling rule can be further simplified as

$$\gamma_f \gamma_L = 1 \tag{5.5}$$

The equation of gas state can be expressed as

$$c = \sqrt{\frac{\gamma^* p_0}{\rho_0}} \tag{5.6}$$

where c is the speed of sound, p_0 is pressure of atmosphere, ρ_0 is fluid density and γ^* is the adiabatic index. These four parameter are not scaled, so the equation of gas state is always true for both unscaled and scaled models.

5.2.2 Sound Propagation in Sound Absorbent Material

Sound absorbing materials are commonly characterized by their bulk properties: the complex wavenumber and characteristic impedance. Several similar empirical equations have been used to define the bulk properties as a function of the flow resistivity (σ) of a material (Bies and Hansen, 2009). The form of these equations is identical. The complex wavenumber (k_c') and characteristic impedance (z_c') are expressed as

$$k_c'/k_0 = (1 + C_1 X^{-C_2}) - jC_3 X^{-C_4} \tag{5.7}$$

and

$$z_c'/z_0 = (1 + C_5 X^{-C_6}) - jC_7 X^{-C_8} \tag{5.8}$$

where $X = \rho_0 f/\sigma$. ρ_0 is the mass density, k_0 is the wave number, and z_0 is the characteristic impedance of the fluid medium. Accordingly, scaling of the complex wavenumber, and characteristic impedance is valid as long as X is scaled correctly. Hence, one scaling rule for sound absorption can be expressed as

$$\gamma_f \gamma_\sigma^{-1} = 1 \tag{5.9}$$

assuming that the mass density of air is the same in both models.

Sound pressure and particle velocity at both sides of sound absorptive material can be related via the transfer matrix in terms of complex wave number and complex characteristic as

$$\begin{Bmatrix} p_1 \\ v_1 \end{Bmatrix} = \begin{bmatrix} cos(k_c^{'}d) & jz_c^{'}sin(k_c^{'}d) \\ \frac{j}{z_c^{'}} sin(k_c^{'}d) & cos(k_c^{'}d) \end{bmatrix} \begin{Bmatrix} p_2 \\ v_2 \end{Bmatrix} \tag{5.10}$$

where d is the thickness of sound absorptive material.

Another scaling rule for sound absorptive material can be developed to keep the sound absorption and the transfer matrix unchanged for both unscaled and scaled models.

$$\gamma_{k_c'}\gamma_d = 1 \tag{5.11}$$

Substituting Equations (5.9) and (5.11) into (5.7), this scaling rule can be simplified as

$$\gamma_f\gamma_d = 1 \tag{5.12}$$

5.2.3 Sound Transmission through a Panel

Cummings did extensive research to assess sound transmission through walls of rectangular ducts (Cummings, 1983; Cummings, 1985). Figure 5.1 shows the typical shape of breakout transmission loss of a rectangular duct. It can be noted there are four different frequency ranges. At very low frequencies, duct wall motion is controlled by stiffness of the wall (usually below 20 Hz). The second region is a resonance controlled region which depends on the first several modes of the duct wall. The third region, which is the most important, is the mass controlled region and begins at below 200 Hz for rectangular ducts. It affects all audible frequencies in heavy panels. It extends up the coincidence frequency where the bending wavelength of the duct is equal to the acoustic wavelength. This occurs at very high frequencies in rectangular duct systems and is usually not of concern (Cummings, 1983; Cummings, 1985).

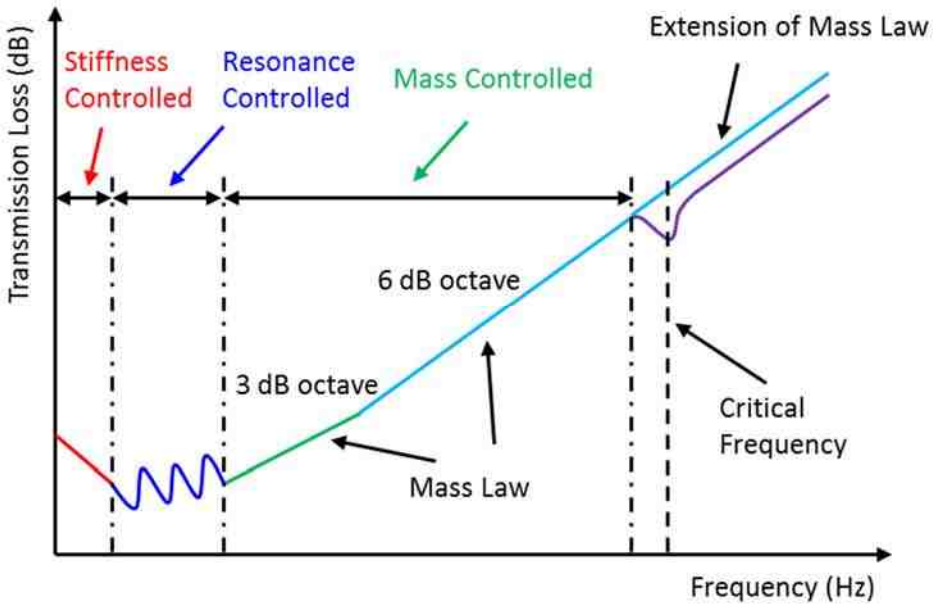

Figure 5.1 Schematic showing the typical shape of breakout transmission loss of a rectangular duct.

The normalized breakout transmission loss for unlined ducts is defined in the ASHRAE Handbook as

$$TL_{out} = 10\log_{10}\left(\frac{W_i/S_i}{W_r/S_r}\right) \tag{5.13}$$

where W_i is the incident sound power, W_r is the radiated sound power from the duct work, S_r is the surface area of the outside radiating duct, and S_i is the cross-sectional area inside the duct.

Two closed-form expression were developed to predict breakout transmission through the ductwork of a rectangular duct by Cummings (1983, 1985). The duct wall impedance Z_w (the ratio between internal sound pressure and wall vibration) is given by

$$Z_w = j\omega\rho_s \tag{5.14}$$

where ω is the angular frequency and ρ_s is the surface density of the duct wall which assumes the wall is mass controlled.

There are three different models for assessing the sound power radiated from the duct wall. On the basis of the line source model, the total radiated sound power W_r is given by

$$W_r = C_r \rho_0 L \omega V_0^2 / 8 \tag{5.15}$$

where C_r is the radiation efficiency factor which is about 0.5 in most cases of interest, ρ_0 is the density of air, L is the length of the radiating section of duct and V_0 is the volume velocity (wall vibrational velocity x duct surface area) per unit length of the duct wall.

From Equation (5.14), the volume velocity of duct wall can be identified in terms of the internal sound pressure and the impedance of wall and is expressed as

$$V_0^2 = \frac{4(a+b)^2 p_i^2}{\omega^2 \rho_s^2} \tag{5.16}$$

Equations (5.15) and (5.16) yield

$$W_r / S_r = \frac{\rho_0 (a+b) p_i^2}{8 \omega \rho_s^2} \tag{5.17}$$

where S_r is the radiating area of the duct wall.

The normalized input sound power inside of the duct is

$$W_i / S_i = \frac{p_i^2}{2 \rho_0 c_0} \tag{5.18}$$

where W_i is the sound power entering the duct, S_i is the internal cross-sectional area of the duct, and c_0 is the speed of sound in air.

Then, the breakout transmission loss can be expressed as

$$TL_{out} = 10 \log_{10} \left(\frac{4 \omega \rho_s^2}{\rho_0^2 c_0 (a+b)} \right) \tag{5.19}$$

Equation (5.19) indicates a 6 dB increase in transmission loss per doubling of surface density and a 3 dB increase per doubling of frequency. Note this formula is not valid at very low frequencies, where the breakout transmission loss will be dominated by transverse structural resonances of the duct work. However, even at low frequencies, Equation (5.19) still provides an accurate prediction.

If the air properties are unchanged, the scaling law can be expressed as

$$\gamma_\rho^2 \gamma_h^2 \gamma_f \gamma_L^{-1} = 1 \tag{5.20}$$

where ρ is mass density of the duct wall, h is duct wall thickness, f is frequency and L is the dimension of the duct wall.

Equation (5.19) is invalid at higher frequencies, where more than about 10 acoustic modes propagate in the duct. Cummings (1983) has developed expressions for the mass law breakout transmission loss of higher order duct modes by summing the contributions from all propagating modes at any frequency. Two fundamental assumptions are made to develop equations for high-frequency breakout transmission loss. First, many modes propagate in the duct, so that "statistical" statements about their combined effect are valid, and, secondly, that all duct modes are excited with equal sound pressure amplitude.

The incident sound power is given by

$$W_i = \sum_{m=0}^{M} \sum_{n=0}^{N} \frac{k_{z,mn} p_{mn}^2 ab}{2\omega \rho_0 \varepsilon_m \varepsilon_n} \tag{5.21}$$

where p_{mn} is the pressure amplitude for mode (m, n), $k_{z,mn}$ is the propagating wavenumber, ε_m and ε_n are integral values of eigenfunctions. $\varepsilon_0 \varepsilon_0$ equals 1, $\varepsilon_0 \varepsilon_1$, … $\varepsilon_0 \varepsilon_N$ equal 2, and the remainder equal 4.

The radiated sound power is identified as

$$W_r = \sum_{m=0}^{M} \sum_{n=0}^{N} \frac{0.3125\rho_0 L k_0 p_{mn}^2 (a+b)ab}{\pi\omega\rho_s^2} \tag{5.22}$$

From Equations (5.21) and (5.22), the breakout transmission loss can be expressed as

$$TL_{out} = 10\log_{10}\left(\frac{\omega^2\rho_s^2\left(1+\frac{9\pi}{4k_0}\left(\frac{1}{a}+\frac{1}{b}\right)\right)}{7.5\rho_0^2 c_0^2}\right) \tag{5.23}$$

At high frequencies, $\frac{9\pi}{4k_0}\left(\frac{1}{a}+\frac{1}{b}\right)$ is close to zero. Hence the TL expression can be further simplified as

$$TL_{out} = 10\log_{10}\left(\frac{\omega^2\rho_s^2}{7.5\rho_0^2 c_0^2}\right) \tag{5.24}$$

Based on equation (5.24), the scaling law can be expressed as

$$\gamma_\rho^2\gamma_h^2\gamma_f^2 = 1 \tag{5.25}$$

assuming the same fluid medium in both scale models. The scaling rules for low and high frequencies can be combined and the scaling rules can be expressed as

$$\gamma_h\gamma_f = 1 \tag{5.26}$$

and

$$\gamma_h\gamma_L^{-1} = 1 \tag{5.27}$$

The sound propagation (Equation (5.5)), acoustic material (Equation (5.9) and (5.12)), and sound transmission through panel (Equations (5.26-5.27)) scaling rules are used together in the examples which follow.

5.3 Virtual Validation

Two finite element method (FEM) simulation cases were performed using Siemens Virtual.Lab (Siemens, 2017) to validate the scaling rules. The first is an expansion chamber with non-symmetric inlet and outlet pipes. Figure 5.2 shows a schematic of the expansion chamber with associated dimensions. Simulation models were created for both the full-scale and half-scale models. For the full-scale model, the flow resistivity is 10,000 Rayls/m. The frequency range investigated was from 10 Hz to 2500 Hz, and the cutoff frequency for the inlet and outlet ducts is approximately 950 Hz. The simulation model was solved above the cutoff frequency by using an automatically matched layer (AML) boundary condition at the termination (Ruan and Herrin, 2015). Transmission loss results are compared for the full-scale and half-scale model in Figure 5.3. It can be seen that the results are nearly identical with each other.

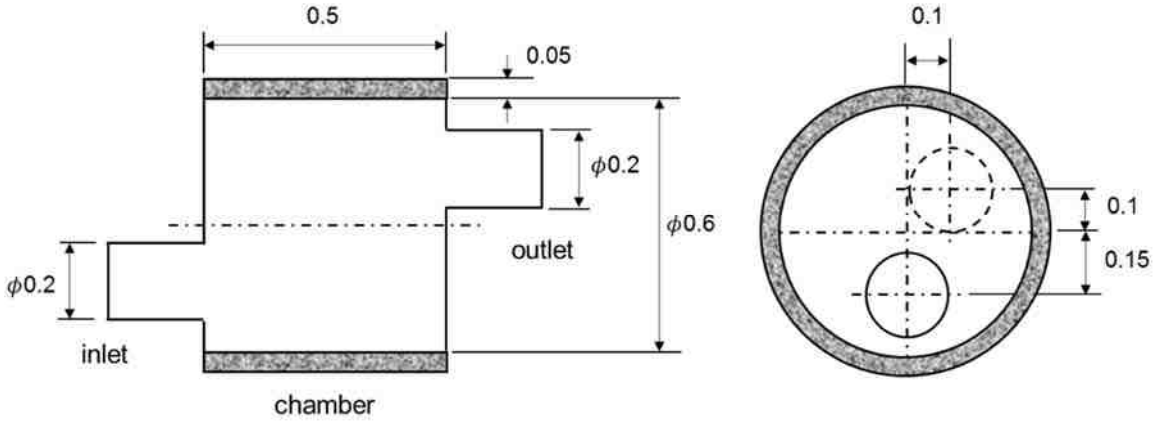

Figure 5.2 Schematic showing expansion chamber (units in m).

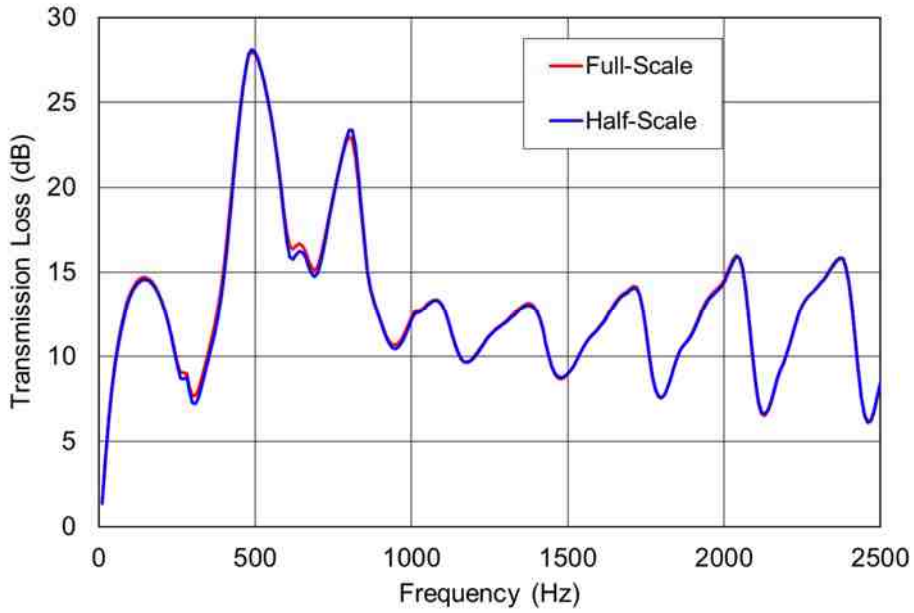

Figure 5.3 Transmission loss comparison for expansion chamber.

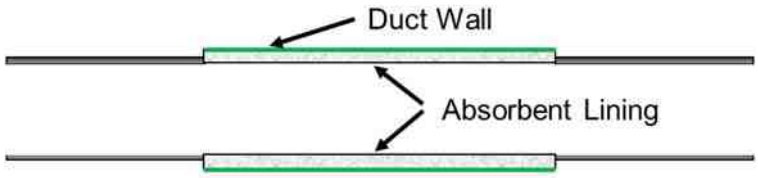

Figure 5.4 Schematic showing lined duct.

The second simulation case considered was a square HVAC duct. Figure 5.4 shows a schematic of the duct. The lined length is 3.0 m, and the unlined portions of the duct are assumed to be rigid. The cross-sectional area of the duct is 0.6 m × 0.6 m. The sound absorbing lining was 5 cm thick with a flow resistivity of 10,000 Rayls/m. Sound absorptive lining is placed around the full perimeter of the duct. The duct wall is assumed to be 0.71 mm thick steel, but the structure is only considered on the lined portion of the duct. The frequency range for the analysis was from 10 to 2000 Hz. The FEM procedure for determining the insertion loss and breakout noise is detailed and is validated in Chapter 3 and 4. Insertion loss and breakout transmission loss results are shown in Figures 5.5 and 5.6

respectively. The agreement between full-scale and half-scale results is acceptable in both cases.

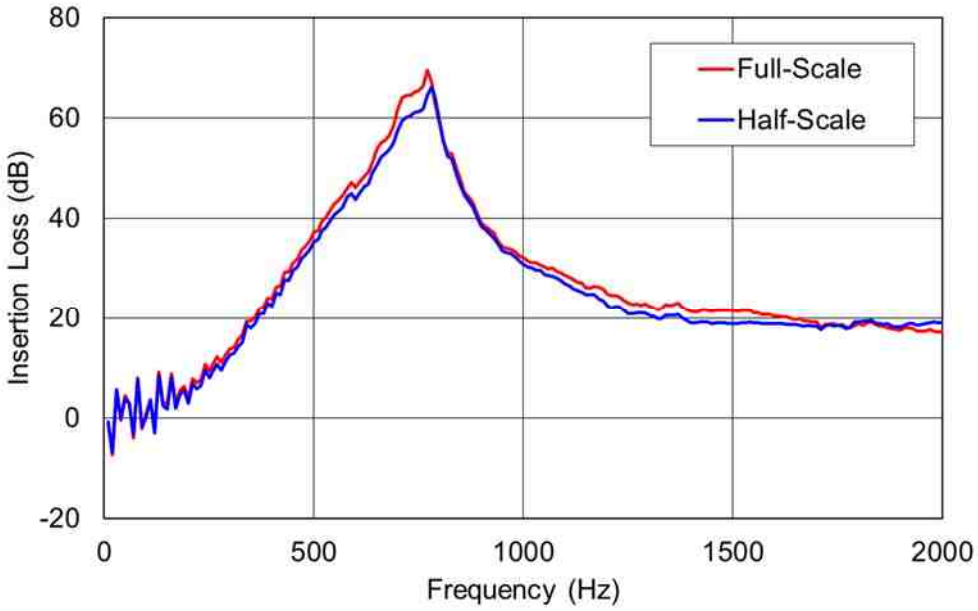

Figure 5.5 Insertion loss comparison for 0.6 m × 0.6 m HVAC duct.

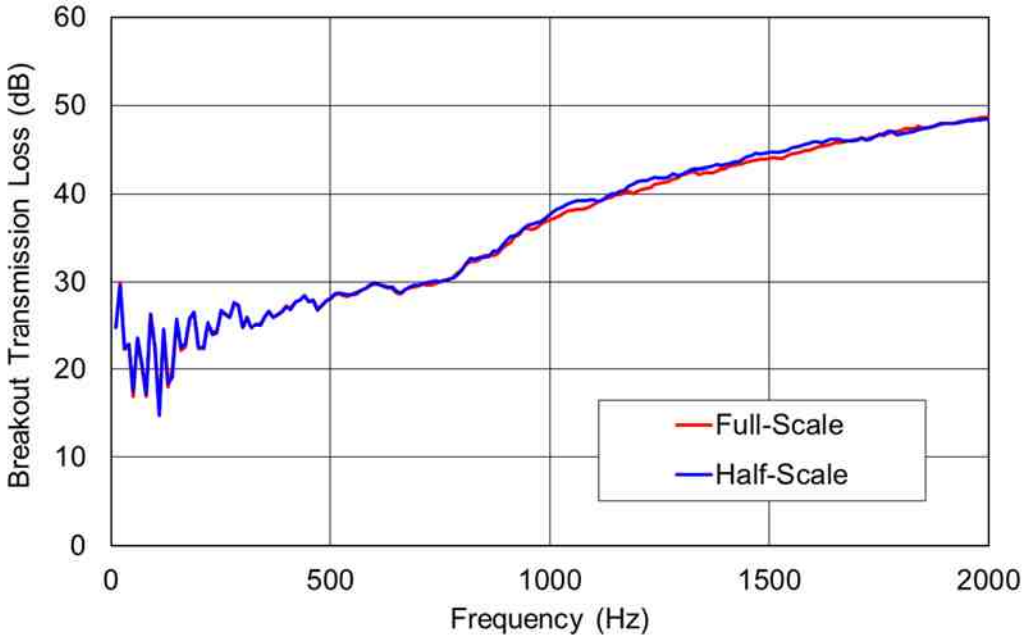

Figure 5.6 Breakout transmission loss comparison for 0.6 m × 0.6 m HVAC duct.

5.4 Experimental Validation

The scaling rules were first applied to unlined silencers shown in Figure 5.7. The 0.35× scale silencer is shown next to the full-scale silencer. The full-scale silencer is manufactured with 1.27 cm thick polycarbonate plastic and the panel on top of the silencer is 0.76 mm thick steel while the 0.35× scale silencer is manufactured with 0.48 cm thick polycarbonate plastic and 0.25 mm thick steel panel.

The transmission loss of both the full-scale and 0.35× scale silencers were measured using ASTM E2611 (ASTM E2611-09, 2009). Though plane wave behavior exists in the inlet and outlet ducts, the cutoff frequency is approximately 380 Hz in the expansion chamber. The transmission loss measurement is compared in Figure 5.8. Simulation results for the full-scale model is also included for comparison. It can be seen that the results from the full-scale and 0.35× scale models have a good agreement.

The breakout transmission loss was determined for each case by determining the incident power using wave decomposition in the inlet duct and then by measuring the radiated sound power of the upper plate using sound intensity scanning inside a hemi-anechoic chamber. The breakout transmission loss is defined as

$$TL_{Breakout} = 10\log_{10}\left(\frac{W_{inc}}{W_{rad}}\right) \tag{5.28}$$

where W_{inc} and W_{rad} are the incident and radiated sound powers respectively. Radiated sound power is measured from the thin steel panel only which is dominant. Breakout transmission loss results are compared in Figure 5.9 from the full-scale, 0.35× scale, and FEM Simulation models with good agreement.

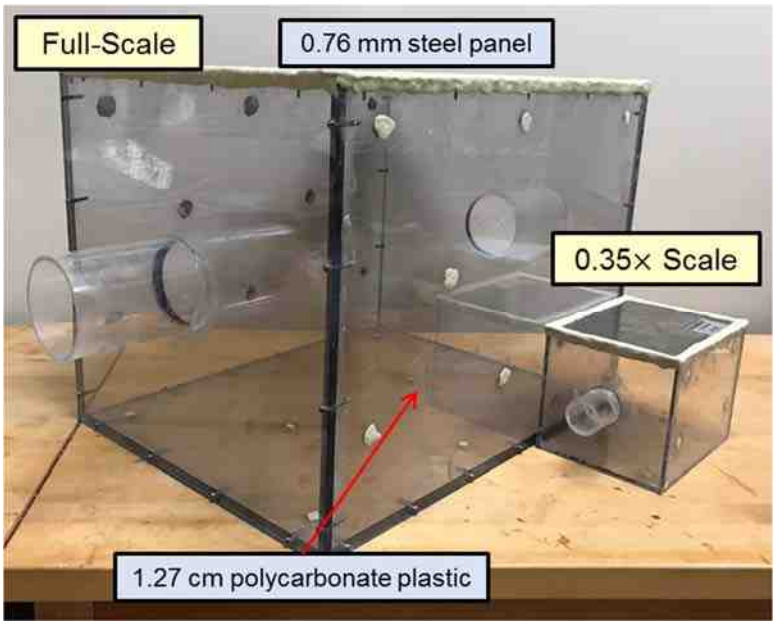

Figure 5.7 Photograph of unlined full-scale and 0.35X scale models.

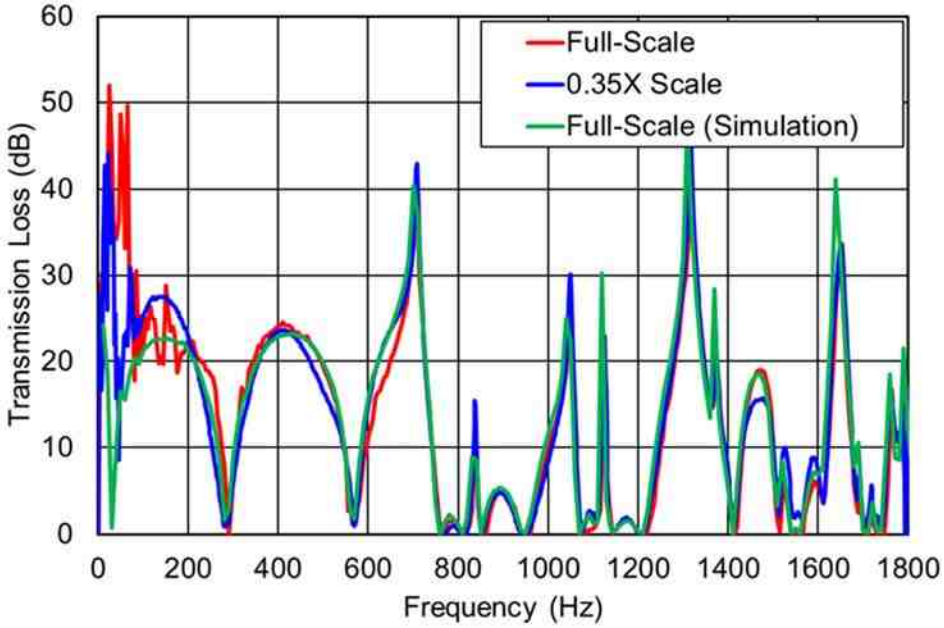

Figure 5.8 Transmission loss for unlined full-scale and 0.35X scale silencers.

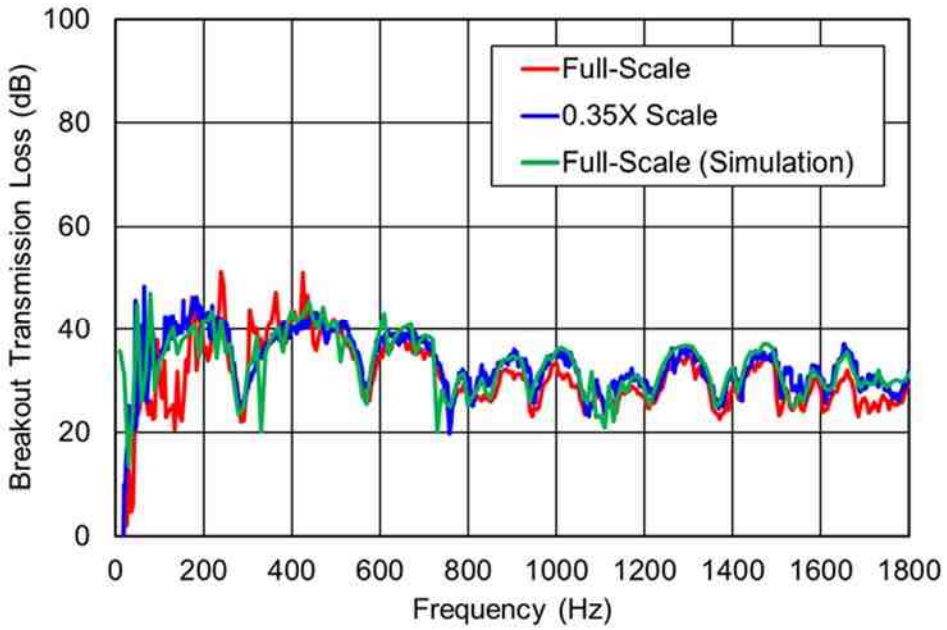

Figure 5.9 Breakout transmission loss for unlined full-scale and 0.35X scale silencers.

The second validation test case is for the lined silencers shown in Figure 5.10. Sound absorptive material is attached to 3 sides of the expansion chamber. The thin plate remains unlined. A schematic of the full-scale silencer with dimensions (in m) is shown in Figure 5.11. Notice that the bottom, left, and right sides are lined. It is difficult to precisely scale the flow resistivity in practice. In this case, flow resistivity was roughly scaled by increasing the density of the fiber by a factor of 1/0.35.

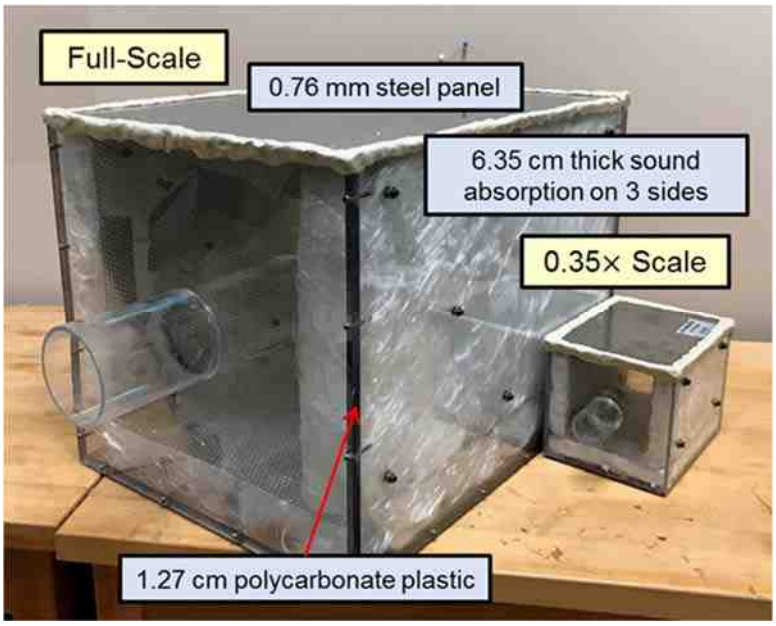

Figure 5.10 Photograph of lined full-scale and 0.35X scale models.

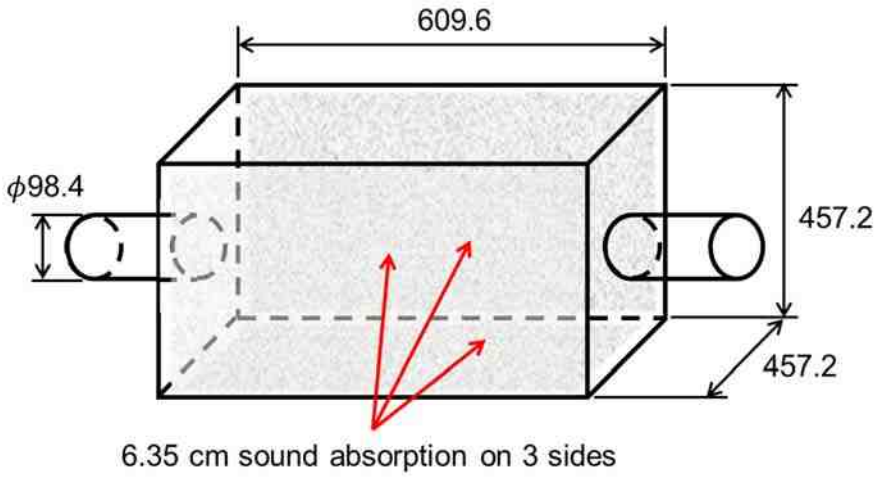

Figure 5.11 Schematic showing dimensions for full-scale model (units in mm).

A photograph of the transmission loss measurement setup for full-scale and 0.35× scale models is shown in Figure 5.12. The transmission loss measurement results comparison between full-scale and 0.35× scale models is shown in Figure 5.13. It can be seen that the results from the full-scale and 0.35× scale models compare acceptably over most of the frequency range. Breakout transmission loss results

are compared in Figure 5.14 from the full-scale, 0.35× scale, and FEM Simulation models with good agreement.

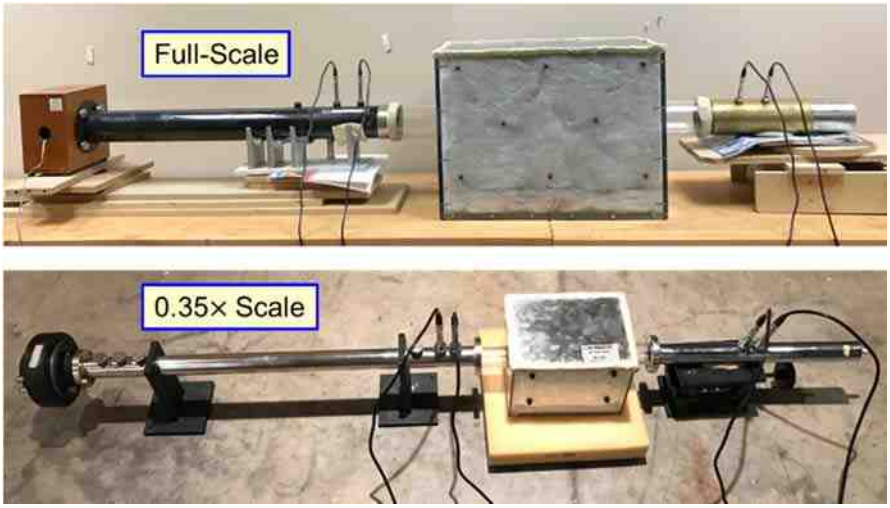

Figure 5.12 Photographs showing full-scale and 0.35X scale silencers measured using ASTM E2611.

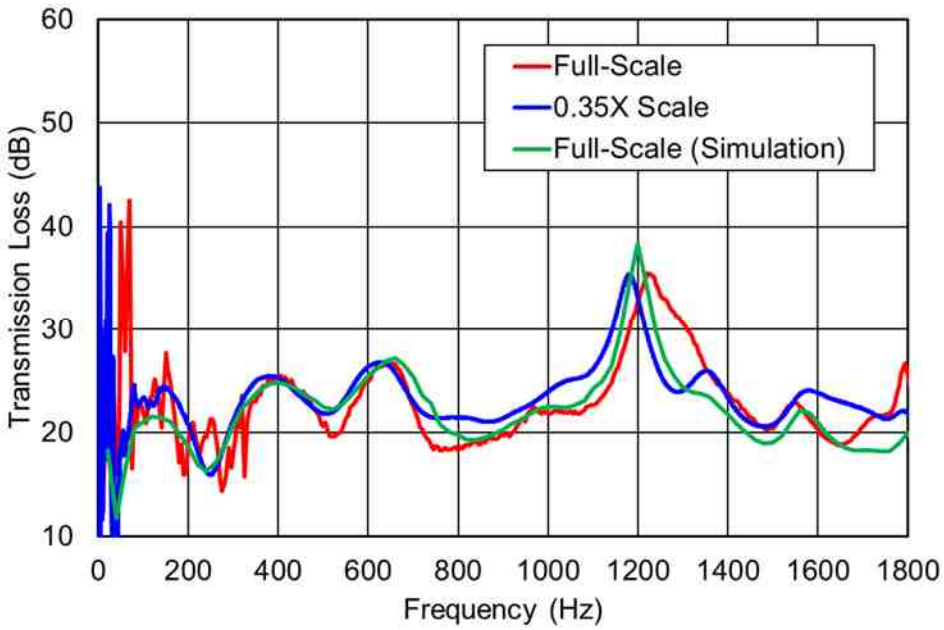

Figure 5.13 Transmission loss for lined full-scale and 0.35X scale silencers.

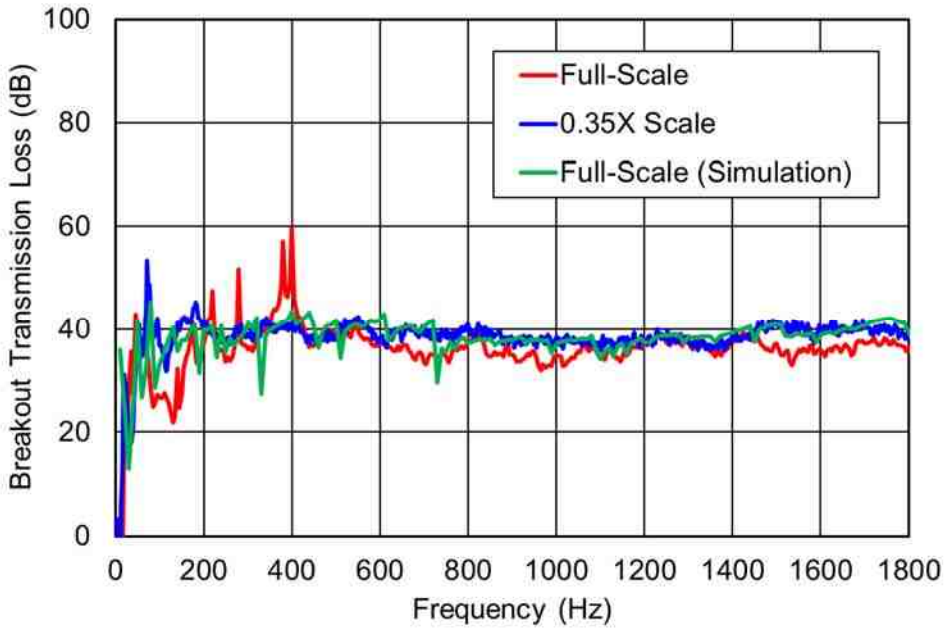

Figure 5.14 Breakout transmission loss for lined full-scale and 0.35X scale silencers.

Two more complicated silencers with two chambers were tested to validate the scaling rules. The photograph for the full-scale and 0.35× scale physical models is shown in Figure 5.15. They were developed based on the silencers used for test case 1. A baffle with two extended tubes is added to divide the single chamber into two chambers. Extended tubes would behave like quarter wavelength tubes and tend to be effective in relatively narrow frequency ranges. A schematic of the full-scale silencer with dimensions (in m) is shown in Figure 5.16.

Figure 5.17 shows the transmission loss measurement results comparison between full-scale and 0.35× scale models. It can be seen that the results from the full-scale and 0.35× scale models compare well over the whole frequency range. Simulation results are higher than measurement results between 400 and 600 Hz. As described in Chapter 3, this is almost certainly due to structureborne transmission path which should be the dominant sound path when acoustic attenuation is higher than 50 or 60 dB. However, the structureborne path was not included in the FEM simulation models. Breakout

transmission loss results are compared in Figure 5.18 from the full-scale, 0.35× scale, and FEM Simulation models with good agreement.

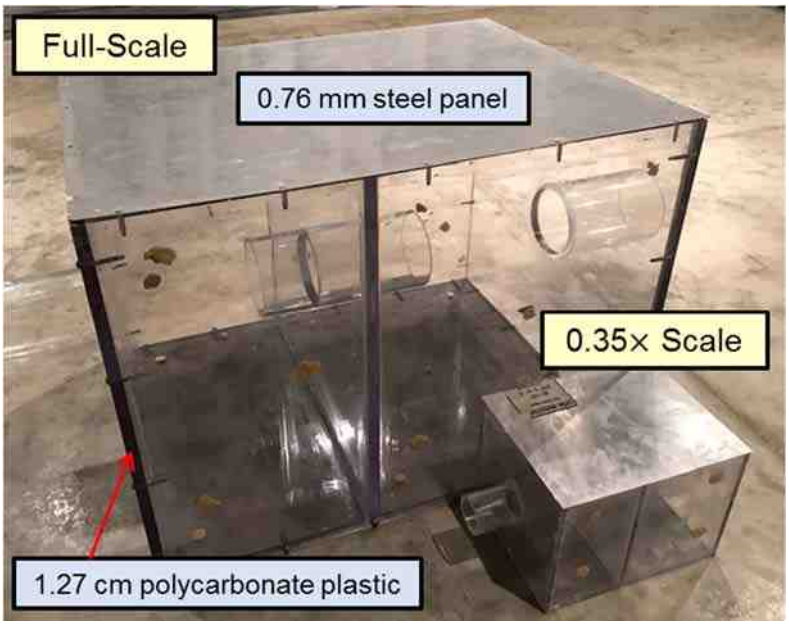

Figure 5.15 Photograph of 2-chamber reactive full-scale silencer.

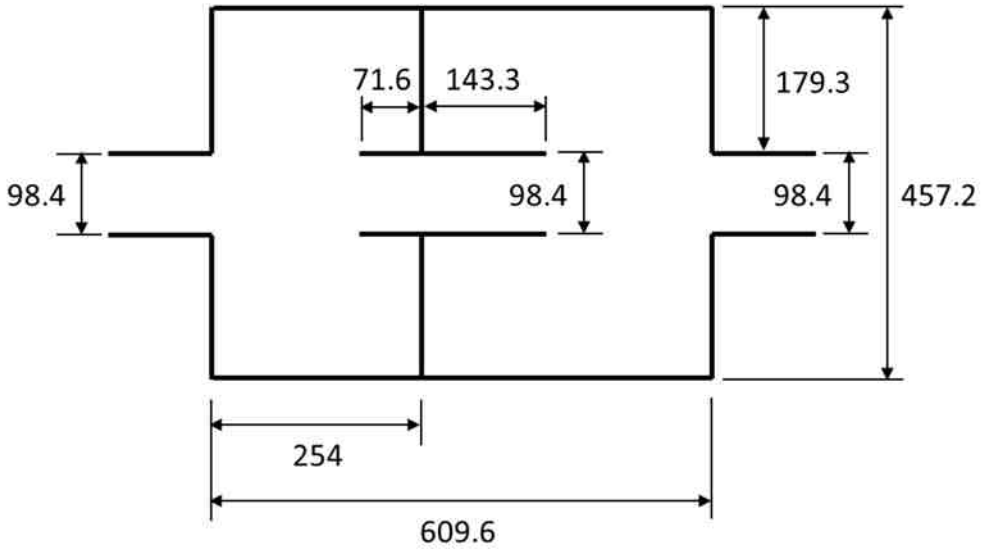

Figure 5.16 Schematic showing dimensions for 2-chamber reactive full-scale silencer (units in mm).

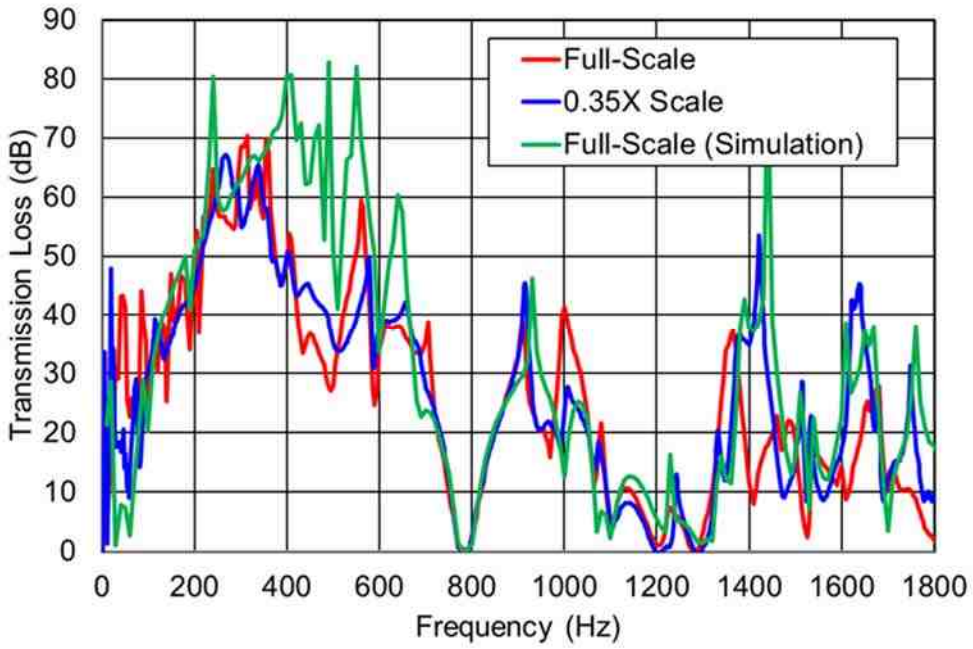

Figure 5.17 Transmission loss for 2-chamber reactive full-scale and 0.35× scale silencers.

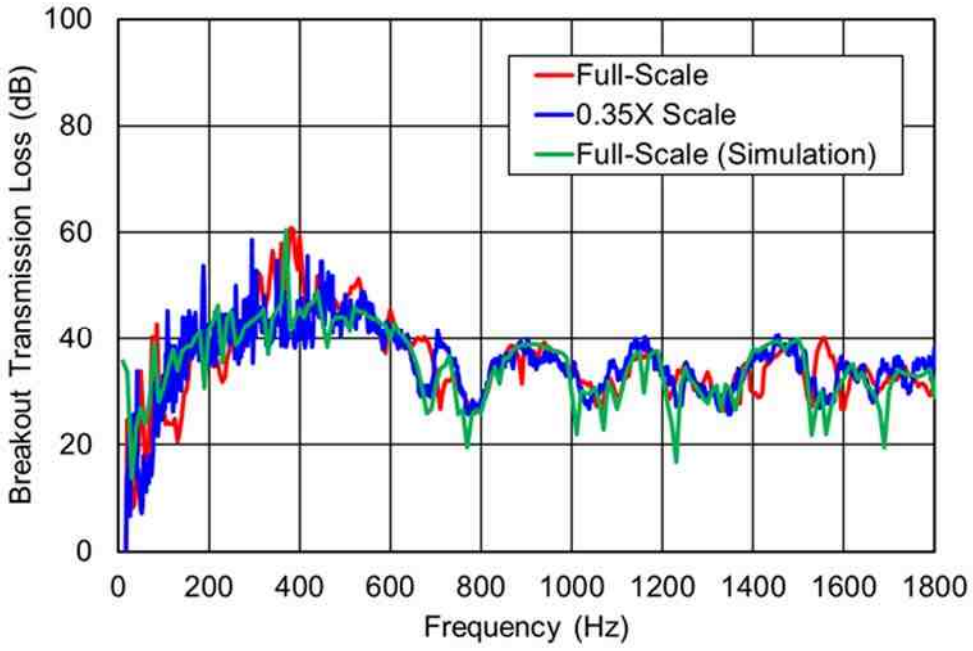

Figure 5.18 Breakout transmission loss for 2-chamber reactive full-scale and 0.35× scale silencers.

The insertion loss of both the full-scale and 0.35X scale silencers shown in Figure 5.15 were also measured. The sound intensity scanning method was used to determine the sound power radiation from the outlet of the straight pipe and silencer. The measurement setup is shown in Figure 5.19. The insertion loss results are compared in Figure 5.20. It can be seen that the results from the full-scale and 0.35X scale models are in good agreement.

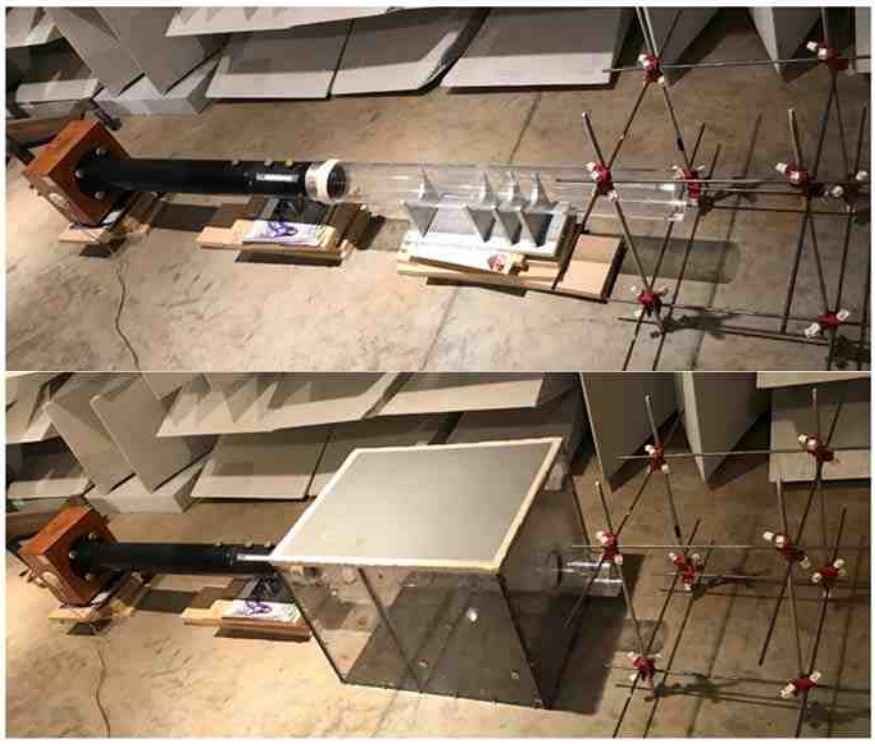

Figure 5.19 Photographs showing full-scale and 0.35X scale silencers measurement setup.

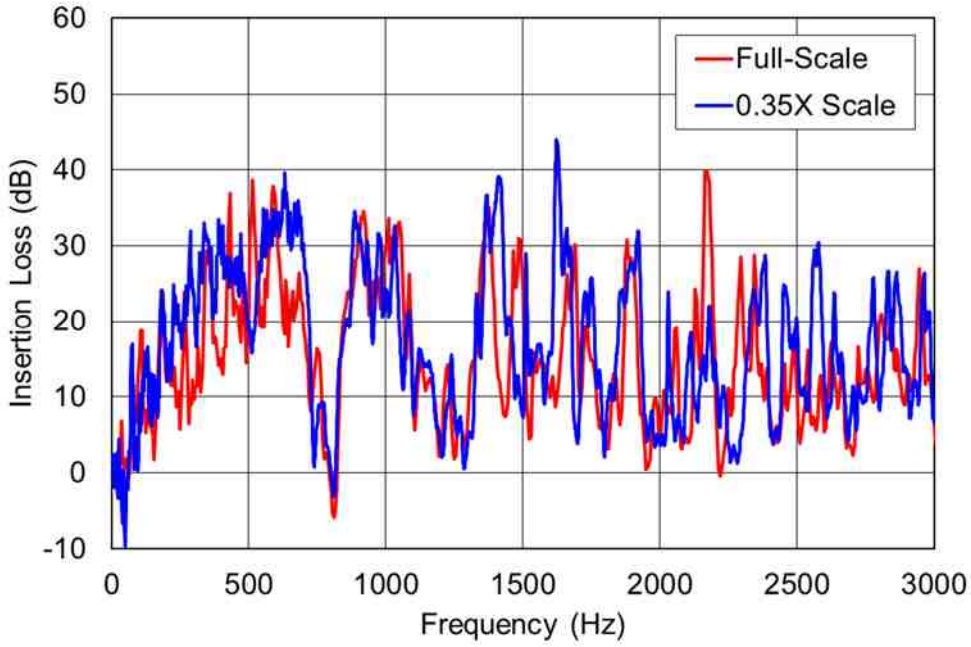

Figure 5. 20 Insertion loss comparison for 2-chamber reactive full-scale and 0.35X scale silencers.

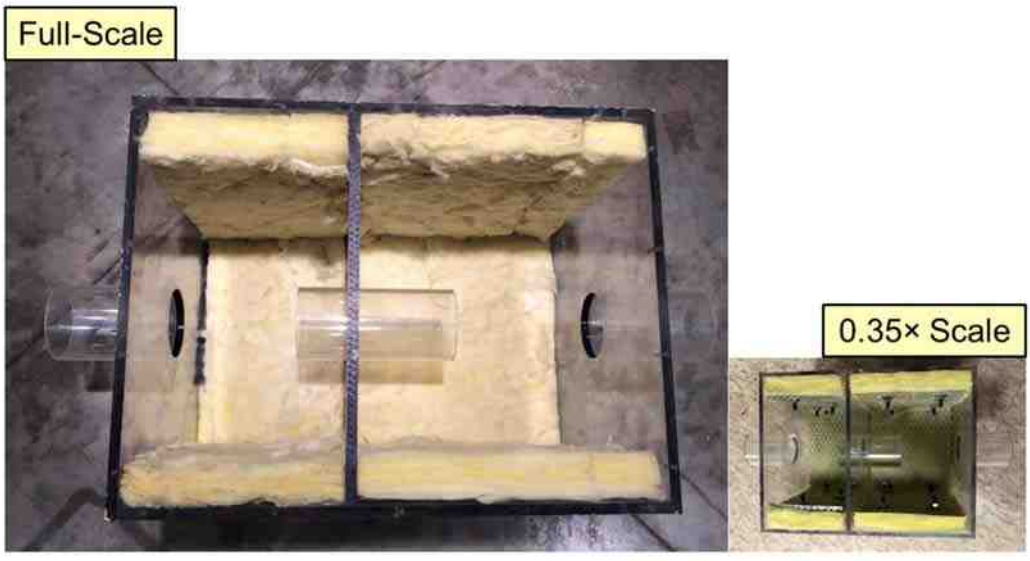

Figure 5.21 Photographs showing 2-chamber dissipative full-scale and 0.35X scale silencers.

Two dissipative, full-scale and 0.35X scale, silencers shown in Figure 5.21 were also developed to validate scaling rules for insertion loss. The insertion loss results

comparison is shown in Figure 5.22. It can be seen that the 0.35× scale model agrees well with the full-scale model.

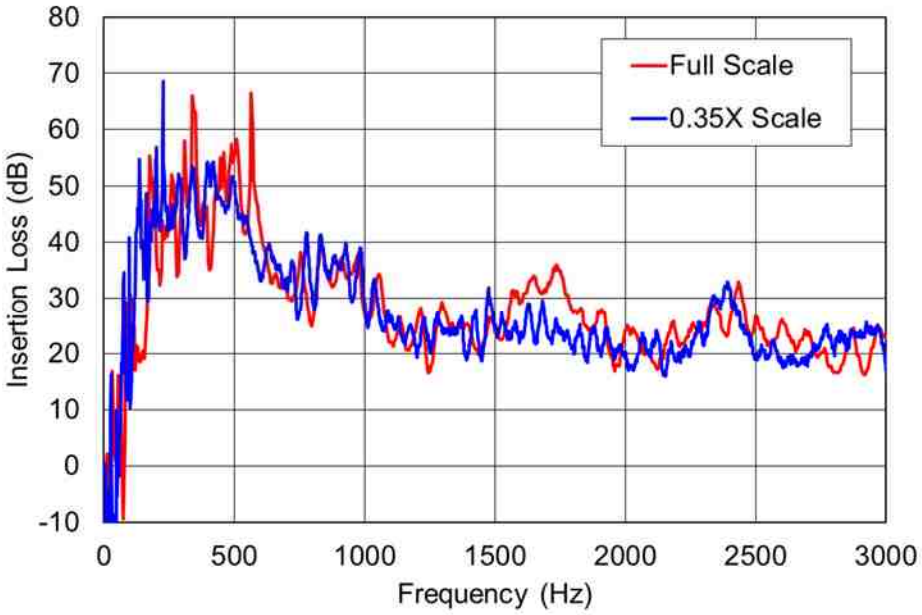

Figure 5.22 Insertion loss comparison for 2-chamber dissipative full-scale and 0.35X scale silencers.

5.5 Conclusions

Scaling rules have been recommended for HVAC ductwork that permit the determination of the insertion loss and breakout transmission loss. The scaling rules have been validated using simulation and also via a simple measurement example. It is notable that HVAC ducts including sound absorption are more difficult to scale because it may be difficult to find a suitable sound absorbing material of appropriate thickness and flow resistivity. Nevertheless, acceptable agreement was demonstrated for a lined silencer with a thin panel on one side.

Chapter 6 VALIDATION OF BEM ANALYSIS OF LARGE SILENCERS USING FEM-AML

(Note: Most of the research in this chapter has been previously documented in Ruan, Wu and Herrin (2015) and Ruan, Wu and Herrin (2018).)

Silencers in use in the power generation industry generally have large ducts entering and leaving the silencer. With large cross-sectional dimensions, the plane wave cutoff frequency will be exceeded at a low frequency so that transmission loss can no longer be evaluated by assuming constant sound pressure over a cross-section. More sophisticated calculation and processing approaches are necessary. In this research, the boundary element method is used in conjunction with a reciprocal identity method to determine the transmission loss for rectangular and circular cross-sections: the two configurations that cover most real-world designs. The boundary element method is compared to a finite element method strategy where the transmission loss is determined using a perfectly matched layer boundary condition at the inlet and outlet. This approach can be used in most commercial software. Though these two approaches have little in common, transmission loss results compare closely with one other. Validation by comparison is helpful because analytical solutions are only available for simple axisymmetric cases. Methods are compared for practical configurations like parallel-baffle silencers and reactive silencers.

6.1 Introduction

Large-scale silencers are commonly employed to reduce the noise from air moving and handling systems and power generation equipment. In commercial buildings, unlined and lined plenums are inserted into ductwork or sections of ductwork are lined with sound absorption on the periphery. Parallel-baffle silencers or splitters are placed inside air handlers to reduce noise at the source. Similar, but much larger sized, configurations are placed into the air flow after gas turbines in heat recovery steam generators for example. Sound absorptive material is arranged in

parallel baffles, bars, or other inventive configurations. In each of the aforementioned applications, resonators are often being integrated into the silencers in an effort to reduce low frequency tonal noise while not disrupting the air flow.

Noise control engineers routinely use the ASHRAE Handbook (ASHRAE, 2015) to estimate noise attenuation from plenums and baffles. As noted in Chapter 2, only select sizes are included in the Handbook tables, tabulated results for plenums are suspect, and lined duct equations are only for ducts under 3 m in length. For parallel-baffle silencers, the design curves of Vér et al. (1978) have been reproduced in several texts and are routinely used to estimate attenuation. Though very useful, results do not consider the full range of configurations seen in industry. As noted earlier, resonators are being integrated into sound absorber packages in pine tree, bar, and baffle configurations.

As stakeholders and customers become more insistent about sound quality and reduced noise levels, industry is looking to design for noise earlier in the design process. Higher fidelity models are needed and commercial finite element software is routinely being used. The most seminal work is arguably by Cummings and Astley (1996) and Kirby (2005). Cummings and Astley (1996) determined the attenuation of square bar silencers. Kirby et al. (2012) also compared the performance of bar to parallel baffle silencers. Kirby and Lawrie (2005) and Lawrie and Kirby (2006) used a hybrid finite element method (FEM) with either a point collocation approach or a mode matching scheme that used a two-dimensional FEM on a typical cross section to extract the modes and then used modal expansion for wave propagation along the axial direction: an important contribution since it permitted a computationally efficient and accurate calculation of transmission loss which did not depend on plane wave propagation in the inlet or outlet ducts leading to the silencer.

In roughly parallel work, Lou et al. (2003) developed a direct mixed body boundary element method (BEM) formulation which is especially convenient for silencer

analysis. Boundaries are meshed instead of the air itself making model preparation simple. However, it is well known that BEM methods are more computationally intensive than FEM. To reduce the computational time, Lou et al. introduced a substructure approach (Lou et al., 2003) which has the added advantage of having many standard template elements which can be assembled in series further reducing the model preparation time. For example, a very long lined duct can be broken up into a number of shorter duct elements. As demonstrated in Figure 6.1 on a bar silencer, only three short sections of a bar silencer are simulated. All the substructure impedance matrices are then combined into a resultant impedance matrix (Lou et al., 2003). Whereas, computational effort would be prohibitive for a long duct or large cross-sectional dimension, the template and consequently the entire duct can be solved in several orders of magnitude less time.

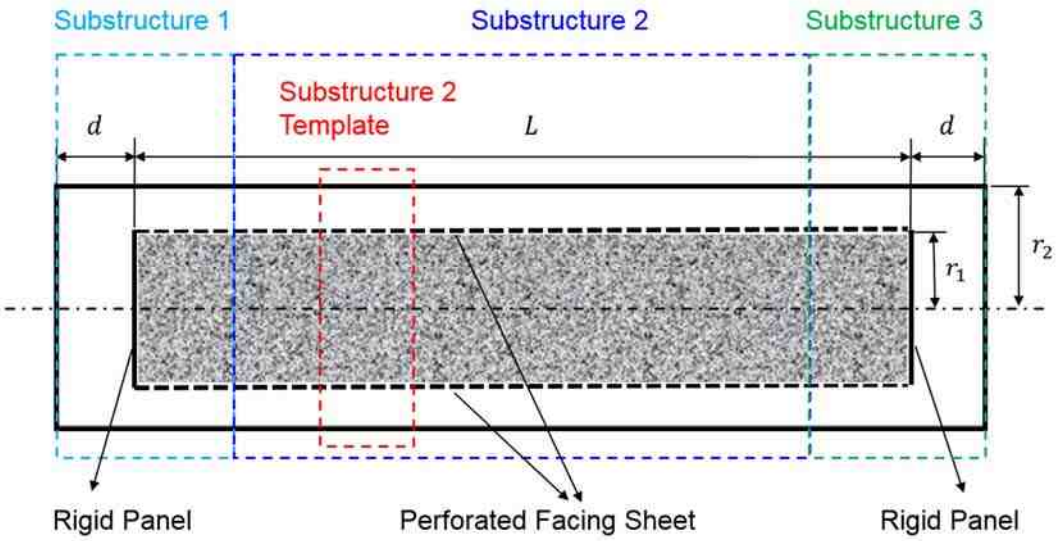

Figure 6.1 Schematic showing a bar silencer model with three substructures

Complex characteristics such as perforates, thin baffles, and sound absorbing material models (Jiang et al, 2010) can be incorporated into the model. For silencers where plane wave propagation is assured in the inlet and outlet, the resultant boundary element impedance matrix is lumped into a 2×2 transfer

matrix for transmission loss computation (Lou et al., 2003). At frequencies below the plane-wave cutoff of the inlet/outlet, the answer is exact. However, above the plane-wave cutoff, sound pressure is no longer constant across the cross-section.

To deal with this issue, Zhou et al. (2016) proposed a reciprocal identity method that couples two independent sound fields by the reciprocal identity integral. The first sound field is an analytical solution with a non-reflective condition at the outlet and a unit incident plane wave at the inlet. This is the exact sound field under which the transmission loss is defined. The second sound field can be generated from any random boundary condition set applied to the inlet and outlet. The impedance matrix computed by the boundary element solution can provide a large number of solutions based on a number of boundary condition sets. A least-squares solver is then used on the overdetermined system of equations. Zhou et al. (2016) derived the reciprocal identity formulation for axisymmetric silencers only, and validated the formulation by comparing to an analytical solution of a simple axisymmetric round bar silencer. While giving some confidence, the axisymmetric analytical solution used for comparison in Zhou et al. (2016) did not converge above 4100 Hz. Correlation is promising but hardly conclusive for a wide range of cases.

As an alternative to the reciprocal identity method, Wang and Wu (2016) proposed a so-called “impedance-to-scattering matrix method”. In contrast to the integral-based reciprocal identity method, the impedance-to-scattering method is a collocation-based method. The method directly converts the BEM impedance matrix into a so-called “scattering matrix” that relates the modal amplitudes at the inlet and outlet. The transmission loss computation will then follow after prescribing a unit incident plane wave at the inlet and making the outlet non-reflective. Though collocation based, the impedance-to-scattering matrix method does produce an almost identical transmission loss as the reciprocal identity method for the simple axisymmetric bar silencer reported in Refs. (Zhou et al., 2016; Wang and Wu, 2016).

In the paper, the axisymmetric reciprocal identity method in Zhou et al. (2016) is first re-derived for more general non-axisymmetric circular and rectangular inlet/outlet configurations which encompasses most industry applications. For validation purposes, there is little measurement data to compare to and analytical solutions are limited to simple axisymmetric silencers (Zhou et al., 2016; Wang and Wu, 2016). Although the reciprocal identity method can be compared to the impedance-to-scattering matrix method, both methods are based on the identical BEM impedance matrix (Lou et al., 2003). The comparison is useful but not as conclusive as desired. It is preferable to compare to a method that has nothing in common with the BEM.

Hence, BEM transmission loss solutions are compared to FEM in this work. The FEM approach selected is a general-purpose method and not as efficient as the hybrid method (Kirby, 2005; Kirby et al., 2012; Kirby and Lawrie, 2005; Lawrie and Kirby, 2006) but can be used in most commercial software packages including Siemens Virtual.Lab, ANSYS Acoustics, MSC ACTRAN, and other packages. It is well known that the insertion and transmission loss are equivalent if both ends of the silencer are non-reflective or anechoic. A non-reflective boundary condition can be applied using a perfectly matched layer (PML) boundary condition (Berenger, 1994; Tam et al., 1998; Vansant and Hallez, 2014). The PML requires a relatively thin mesh of the absorbing layer that should be adjusted depending on the acoustic wavelength. Siemens Virtual.Lab (2017) uses a special implementation termed an automatically matched layer (AML) (Vansant et al., 2014) that makes the mesh adjustments transparent to the user.

(a) Sound power W_1 radiated from a straight duct

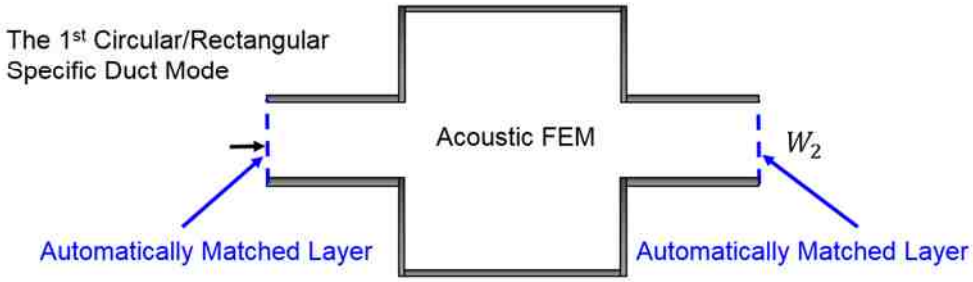

(b) Sound power W_2 radiated from the silencer

$$IL = 10log_{10}\frac{W_1}{W_2}$$

Figure 6.2 Schematic showing the equivalent TL (from IL) using FEM-AML

As shown in Figure 6.2, two configurations are needed to determine the insertion loss: one is a straight duct and the other with the silencer. By definition, the radiated sound power difference between these two configurations is the insertion loss. To determine the transmission loss, an incident plane wave is prescribed at the inlet of both configurations in Figure 6.2. While the sound power radiated from the straight duct can be easily calculated using a closed form solution, the sound power radiated from the silencer is calculated via the FEM with PML or AML boundary conditions applied. The sound source used in LMS Virtual.Lab to simulate an incident plane wave is a circular/rectangular specific duct mode boundary condition.

The primary contribution of this paper is to validate both the direct mixed body BEM and FEM using PML. A number of common large silencer configurations are considered including three different bar silencers, a lined duct, and a parallel baffle silencer. The degree of correlation is such that both computational approaches

are validated. It is noteworthy that the direct mixed body BEM is a specialized approach that is not commercially available and is customized to this application. However, the FEM insertion loss approach can be utilized in most commercial FEM packages and is expected to be of interest to a wider audience.

One example included has one inlet and two outlets. In the BEM approach with either the reciprocal identity (Zhou et al., 2016) or the impedance-to-scattering matrix (Wang and Wu, 2016), two independent modal expansions are applied to the two outlets and the total transmitted sound power is simply the sum of the two individual transmitted sound powers at the duct. Aside from that, the approach is identical to the single-inlet single-outlet case.

6.2 BEM Impedance Matrix

Equation (6.1) shows the definition of the BEM impedance matrix $[Z]$ that relates the sound pressures p at the inlet (denoted i) and outlet (denoted j) to the corresponding particle velocities v (Lou et al., 2003):

$$\begin{Bmatrix} p_{i1} \\ \vdots \\ p_{ig} \\ p_{o1} \\ \vdots \\ p_{oh} \end{Bmatrix} = \begin{bmatrix} Z_{11} & \cdots & Z_{1\,(g+h)} \\ \vdots & \ddots & \vdots \\ Z_{(g+h)1} & \cdots & Z_{(g+h)\,(g+h)} \end{bmatrix} \begin{Bmatrix} v_{i1} \\ \vdots \\ v_{ig} \\ v_{o1} \\ \vdots \\ v_{oh} \end{Bmatrix} \tag{6.1}$$

where g and h are the number of boundary elements at the inlet and outlet respectively. The impedance matrix can be obtained by application of a $v = 1$ boundary condition on each element at the inlet and outlet successively.

In Lou et al. (2003), the impedance matrix of each substructure is first obtained by the BEM, and all the substructure impedance matrices are then combined to form the resultant impedance matrix for the silencer. For the resultant impedance matrix, each column represents a unique sound field that can be used for reciprocal identity coupling (Zhou et al., 2016). In the case of the impedance-scattering

matrix method (Wang and Wu, 2016), modal expansions are directly applied at the center of each constant boundary element at the inlet and outlet.

6.3 Reciprocity Identity

Let p_A and p_B represent two different sound pressures corresponding to two distinct sound fields, A and B, respectively. Corresponding particle velocities are v_A and v_B, respectively. The two distinct sound fields are related to each other on the same muffler by the reciprocal identity (Zhou et al., 2016),

$$\int_{S_i+S_o} (p_A v_B - p_B v_A)\,\mathrm{dS} = 0 \tag{6.2}$$

where S_i is the inlet, and S_o is the outlet.

In Equation (6.2), A may be considered as a theoretical sound field with a unit incident plane wave applied to the inlet and a non-reflective boundary condition (not necessarily the characteristic impedance boundary condition, which is only valid below the cutoff) at the outlet. This is the exact condition under which the transmission loss is defined. Naturally there will be many unknown modal amplitudes in the theoretical modal expansion. On the other hand, B in Equation (6.2) may represent the BEM solution corresponding to a random boundary condition set applied to the inlet and outlet. The B solution is not related to the transmission loss definition. When a random boundary condition set is selected for B, Equation (6.2) produces a constraint equation that relates all the unknown amplitudes in A. Depending on how many unknown modal amplitudes are used in the modal expansion for A, a minimum number of random boundary condition sets must be selected for B to couple with A in Equation (6.2). The BEM impedance matrix can naturally provide a large number of such “random” BEM solutions because each column of the matrix in Equation (6.1) corresponds to a unique velocity boundary condition set. The overdetermined system is then solved by a least-squares solver.

6.4 Non-axisymmetric Circular Inlet and Outlet

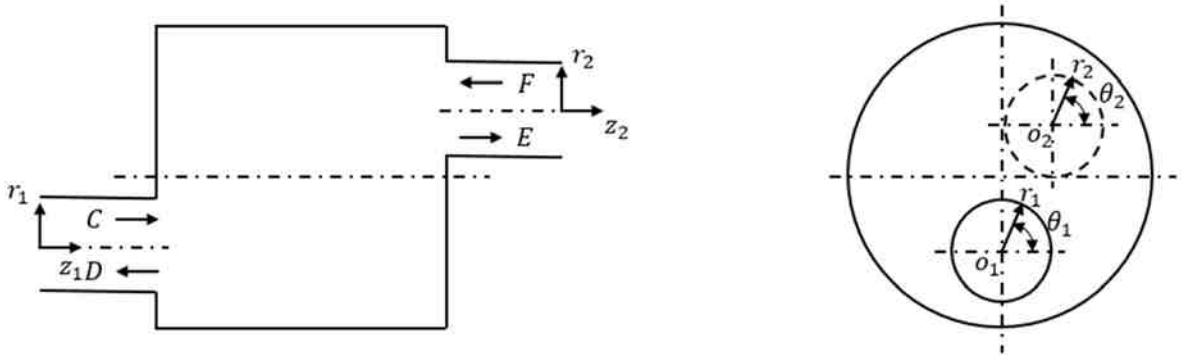

Figure 6.3 Silencer with a non-axisymmetric circular inlet/outlet

Figure 6.3 shows a generic non-axisymmetric silencer with a circular inlet and a circular outlet. The silencer chamber itself does not need to be circular, though. Instead, the chamber cross section can be rectangular, circular, elliptical, or of any arbitrary shape: most industrial silencers falling into this category.

With reference to Figure 6.3, the sound field A in the inlet duct can be written in a modal expansion in cylindrical coordinates. Let the incident wave C in Figure 6.3 be a unit plane wave. The sound pressure and particle velocity at the inlet cross section are

$$p_{A,i}(r,\theta) = 1 + \sum_{m=0}^{\infty}\sum_{n=0}^{\infty}\left(D_{mn}^{+}e^{-jm\theta} + D_{mn}^{-}e^{+jm\theta}\right)J_m\left(k_{r,mn}r\right) \tag{6.3}$$

and

$$v_{A,i}(r,\theta) = \frac{k_{z,00}}{\rho\omega} + \sum_{m=0}^{\infty}\sum_{n=0}^{\infty}\frac{-k_{z,mn}}{\rho\omega}\left(D_{mn}^{+}e^{-jm\theta} + D_{mn}^{-}e^{+jm\theta}\right)J_m\left(k_{r,mn}r\right) \tag{6.4}$$

respectively, where J_m is the Bessel function of the first kind of order m, D_{mn}^{+} and D_{mn}^{-} are the unknown modal amplitudes, $k_{r,mn}$ is the radial wavenumber, and

$k_{z,mn}$ is the axial wave number. The radial wavenumber $k_{r,mn}$ must satisfy the zero-velocity boundary condition on the rigid wall

$$J'_m\left(k_{r,mn}R_i\right) = 0 \tag{6.5}$$

where R_i is the radius of the inlet, and the prime means the derivative. The axial wavenumber $k_{z,mn}$ and the radial wavenumber $k_{r,mn}$ are related to each other by

$$k_{z,mn}^2 = k^2 - k_{r,mn}^2 \tag{6.6}$$

Similarly, the sound pressure and particle velocity at the outlet cross section with $F = 0$ due to no reflection are

$$p_{A,o}(r,\theta) = \sum_{m=0}^{\infty}\sum_{n=0}^{\infty}\left(E_{mn}^{+}e^{-jm\theta} + E_{mn}^{-}e^{+jm\theta}\right)J_m\left(k_{r,mn}r\right) \tag{6.7}$$

and

$$v_{A,o}(r,\theta) = \sum_{m=0}^{\infty}\sum_{n=0}^{\infty}\frac{k_{z,mn}}{\rho\omega}\left(E_{mn}^{+}e^{-jm\theta} + E_{mn}^{-}e^{+jm\theta}\right)J_m\left(k_{r,mn}r\right) \tag{6.8}$$

respectively. Note that the above *z*-direction velocity at the outlet needs to be flipped when used in the reciprocal identity integral since the normal in Equation (6.2) is pointing inward.

The infinite number of modes can be truncated to a finite number because most evanescent modes are nearly undetectable at the inlet and outlet. A few evanescent modes may still be included just in case. Initially, two large numbers, M and N, are selected for the numbers of modes in the θ and r directions, respectively. These initial M times N modes form a large pool and are then ranked in the order of their "cut-in frequencies". The cut-in frequency of a propagating mode is defined by the highest frequency before $k_{z,mn}$ becomes purely imaginary. The first NT modes ranked below the highest frequency of interest (for example,

8000 Hz) are then automatically selected from the pool according to their cut-in frequency rank. It is recommended that these *NT* modes should include at least one evanescent mode. As such, there are a total of $4NT$ unknowns, D_{mn}^{+}, D_{mn}^{-}, E_{mn}^{+}, E_{mn}^{-}. We then apply the reciprocal identity at least $4NT$ times: each time with the BEM solution taken straight from a column of the impedance matrix in Equation (6.1). The number of boundary elements at the inlet and outlet, $(g + h)$, should be greater than $4NT$. This yields a $(g + h) \times 4NT$ overdetermined system of equations

$$\boldsymbol{Ax} = \boldsymbol{b} \tag{6.9}$$

where $\boldsymbol{A} = \left[a_{ql}\ \ a_{q(l+NT)}\ \ a_{q(l+2NT)}\ \ a_{q(l+3NT)}\right]$ $(q = 1, 2, \dots, g + h;\ l = 1, 2, \dots, NT)$ is the system matrix, $\boldsymbol{x}$ is the unknown vector, and $\boldsymbol{b} = \left[b_q\right]^T$ is the right-hand side vector. The explicit expressions for a_{ql}, $a_{q(l+NT)}$, $a_{q(l+2NT)}$, $a_{q(l+3NT)}$ and b_q are

$$a_{ql} = \int_{S_i} \left(v_{B,i,q} + \frac{k_{z,mn}}{\rho\omega} p_{B,i,q}\right) e^{-jm\theta} J_m\left(k_{r,mn} r\right) dS \tag{6.10}$$

$$a_{q(l+N)} = \int_{S_i} \left(v_{B,i,q} + \frac{k_{z,mn}}{\rho\omega} p_{B,i,q}\right) e^{jm\theta} J_m\left(k_{r,mn} r\right) dS \tag{6.11}$$

$$a_{q(l+2N)} = \int_{S_o} \left(v_{B,o,q} - \frac{k_{z,mn}}{\rho\omega} p_{B,o,q}\right) e^{-jm\theta} J_m\left(k_{r,mn} r\right) dS \tag{6.12}$$

$$a_{q(l+3N)} = \int_{S_o} \left(v_{B,o,q} - \frac{k_{z,mn}}{\rho\omega} p_{B,o,q}\right) e^{jm\theta} J_m\left(k_{r,mn} r\right) dS \tag{6.13}$$

$$b_q = -\int_{S_i} \left(v_{B,i,q} - \frac{1}{\rho c} p_{B,i,q}\right) \mathrm{d}S \tag{6.14}$$

where the subscript B denotes the sound field B from the BEM impedance matrix, i the inlet, o the outlet, q the *q*-th boundary condition set, l the *l*-th mode, and each *l* is associated with a specific (*m*, *n*) pair when the modes are ranked according to their cut-in frequencies. After the $4NT$ unknowns are determined from Equation (6.9) by using a standard least-squares solver, the transmitted sound power W_t at the outlet can be evaluated, and the TL computation will follow.

6.5 Rectangular Inlet and Outlet

For silencers with a rectangular inlet and a rectangular outlet, the sound pressure can be expressed by a modal expansion in Cartesian coordinates with the origin placed at the lower left corner of the rectangular cross section. After specifying a unit incident plane wave, the sound pressure and particle velocity at the inlet cross section are

$$p_{A,i}(x,y) = 1 + \sum_{m=0}^{\infty}\sum_{n=0}^{\infty} p^{-}_{A,i,mn} cos\left(k_{x,m}x\right) cos\left(k_{y,n}y\right) \tag{6.15}$$

and

$$v_{A,i}(x,y) = \frac{k_{z,00}}{\rho\omega} + \frac{-1}{\rho\omega}\sum_{m=0}^{\infty}\sum_{n=0}^{\infty} k_{z,mn} p^{-}_{A,i,mn} cos\left(k_{x,m}x\right) cos\left(k_{y,n}y\right) \tag{6.16}$$

respectively, where the subscript i means the inlet, and – denotes the reflected waves, respectively. The wavenumbers in the x and y directions are

$$k_{x,m} = \frac{m\pi}{d_1} \tag{6.17}$$

and

$$k_{y,n} = \frac{n\pi}{d_2} \tag{6.18}$$

where $= 0, 1, 2, \cdots$, $n = 0, 1, 2, \cdots$, d_1 and d_2 are the dimensions of the inlet or outlet in the x and y directions, respectively. The three wavenumbers $k_{x,m}$, $k_{y,n}$ and $\mathrm{k_{z,mn}}$ are related by

$$k_{z,mn}^2 = k^2 - k_{x,m}^2 - k_{y,n}^2 \tag{6.19}$$

Similarly, the sound pressure and particle velocity at the outlet with a non-reflective boundary are

$$p_{A,o}(x,y) = \sum_{m=0}^{\infty}\sum_{n=0}^{\infty} p_{A,o,mn}^{+} cos\left(k_{x,m}x\right) cos\left(k_{y,n}y\right) \tag{6.20}$$

and

$$v_{A,o}(x,y) = \frac{1}{\rho\omega}\sum_{m=0}^{\infty}\sum_{n=0}^{\infty} k_{z,mn} p_{A,o,mn}^{+} cos\left(k_{x,m}x\right) cos\left(k_{y,n}y\right) \tag{6.21}$$

respectively, where + denotes the transmitted waves and the subscript o denotes the outlet. Note that the above *z*-direction velocity at the outlet needs to be flipped when used in the reciprocal identity integral since the normal in Equation (6.2) is pointing inward.

As in the non-axisymmetric circular case, a finite number of NT modes are selected from a large pool according to their cut-in frequency rank. There are $2NT$ unknown amplitudes. These $2NT$ unknowns can be solved by applying the reciprocal work identity at least $2NT$ times, each time with the BEM solution taken straight from a column of the impedance matrix in Equation (6.1). This yields a $(g + h) \times 2NT$ overdetermined system of equations in the same form as Equation (6.9), in which $A = \left[a_{ql}, a_{q(l+NT)}\right]$ is the system matrix with $q = 1,2, \cdots, (g + h)$ and $l = 1,2, \cdots, NT$, x is the unknown vector, and $b = \left[b_q\right]^T$ is the right-hand side vector. The explicit expressions for a_{ql}, $a_{q(l+NT)}$ and b_q are

$$a_{ql} = \int_{S_i} \left(v_{B,i,q} + \frac{k_{z,mn}}{\rho\omega} p_{B,i,q} \right) cos(k_{x,m}x) cos(k_{y,n}y) dS \tag{6.22}$$

$$a_{q(l+NT)} = \int_{S_o} \left(v_{B,o,q} - \frac{k_{z,mn}}{\rho\omega} p_{B,o,q} \right) cos(k_{x,m}x) cos(k_{y,n}y) dS \tag{6.23}$$

$$b_q = -\int_{S_i} \left(v_{B,i,q} - \frac{1}{\rho c} p_{B,i,q} \right) \mathrm{d}S \tag{6.24}$$

where B denotes sound field B taken from the BEM impedance matrix, i the inlet, o the outlet, q the q^{th} boundary condition set, l the l^{th} mode, and each l is associated with a specific (m, n) pair when the modes are ranked according their cut-in frequencies. After the $2NT$ unknown amplitudes are determined from Equation (6.9), the transmitted sound power and transmission loss can be computed through Equations (6.25) – (6.28).

$$W_t = \frac{Re\left(k_{z,(l-1))}\right)}{2\rho\omega} \sum_{l=1}^{NT} \left| p^{+}_{A,o,(l-1))} \right|^2 I_{mn} \tag{6.25}$$

where

$$I_{mn} = \int_{S_o} cos(k_{x,m}x) cos(k_{y,n}y) cos(k_{x,m}x) cos(k_{y,n}y) \, \mathrm{d}S \tag{6.26}$$

The above integral can be integrated analytically. The result is

$$I_{mn} = \begin{cases} d_1 d_2 & m = 0, n = 0 \\ \dfrac{d_1 d_2}{2} & m = 0, n \neq 0 \\ \dfrac{d_1 d_2}{2} & m \neq 0, n = 0 \\ \dfrac{d_1 d_2}{4} & m \neq 0, n \neq 0 \end{cases} \tag{6.27}$$

The incident sound power at the inlet is simply based on a unit plane wave. Finally, the TL is

$$TL = 10\log_{10}\left(\frac{1}{2\rho c W_t}\cdot\frac{S_i}{S_o}\right) \tag{6.28}$$

6.6 Test Cases and FEM-AML Validation

A simulation campaign was performed to compare direct mixed body BEM and FEM with automatically matched layer (AML) implementation of PML. The commercial software Siemens Virtual.Lab was used for the FEM simulations.

1. Circular Bar Silencer

A simple circular bar silencer reported in Zhou et al. (2016) and Wang and Wu (2016) is revisited here as the first test case. It is pointed out in Zhou et al. (2016) and Wang and Wu (2016) that the eigenvalue solver in the analytical solution fails to converge above 4100 Hz. A schematic of the silencer is shown in Figure 6.1. Key dimensions are $r_1 = 0.254\ m$, $r_2 = 0.342\ m$, $L = 6\ m$, and $d = 0.2\ m$. The bar is modeled via the fiber equation of Delaney and Baley (1970) with a flow resistivity of 16000 Rayl/m. A 30% open perforated sheet is assumed to protect the absorptive bar and is modeled by the transfer impedance approach by Sullivan and Crocker (1978). Both ends of the bar are assumed rigid (i.e., non-absorptive).

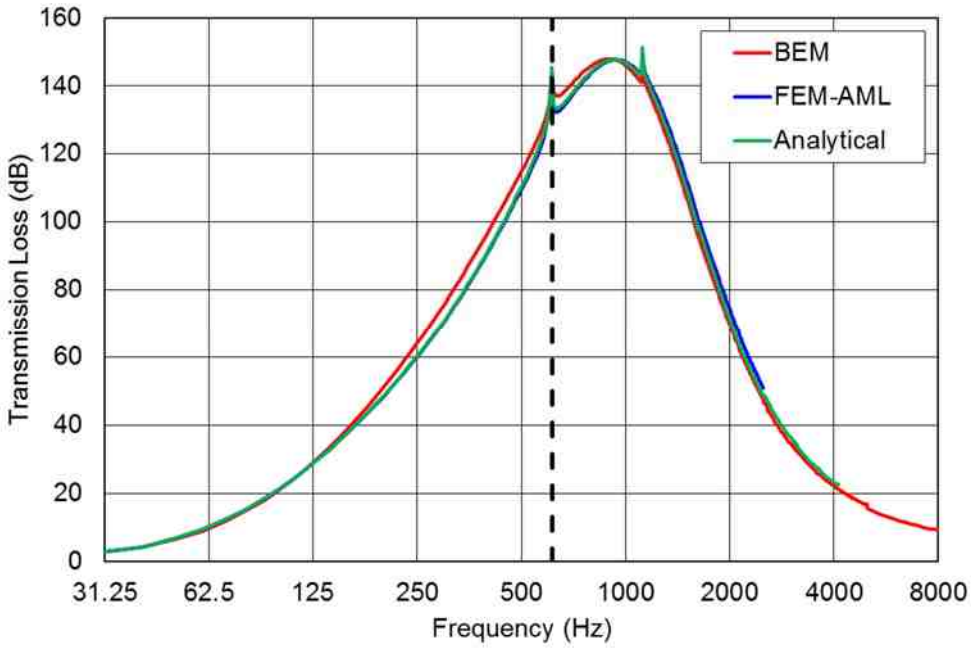

Figure 6.4 Comparison of the BEM, FEM, and the analytical solutions for the axisymmetric round bar silencer

Figure 6.4 compares the BEM, FEM, and analytical solutions. The three solutions compare well with one another. The FEM solution is presented up to 2500 Hz due to the size of the problem and the memory constraint on our available computer hardware. A commercial code is used and so it will not have the substructure capabilities that a specialized software might have. The plane-wave cutoff frequency of 612 Hz is indicated in Figure 6.4. The primary purpose of revisiting this simple axisymmetric test case is to demonstrate that both computational approaches compare well with an analytical solution.

2. Lined Expansion Chamber with Offset Inlet and Outlet Ducts

The second example is a lined cylindrical duct with offset inlet and outlet ducts shown in Figure 6.5. To our knowledge, there is not an analytical solution available at frequencies above the inlet and outlet duct plane wave cutoff. The length of the expansion chamber is relatively short at 0.5 m and permits solution up to 8000 Hz using both approaches. The thickness of the liner is 5 cm and has a flow resistivity of 16000 Rayls/m. It may be modeled using either a locally-reacting impedance

boundary condition or as a bulk-reacting absorber. In this research, it is modeled using a bulk reacting approach in both BEM and FEM.

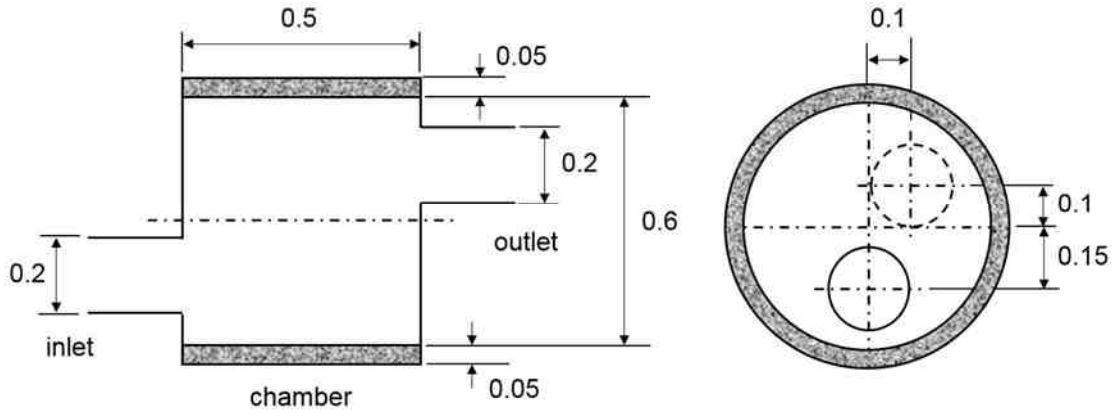

Figure 6.5 Schematic showing a lined circular expansion chamber with an offset circular inlet/outlet configuration (dimensions in m)

At room temperature, the cutoff frequency of the 0.2-m diameter inlet/outlet is 1005 Hz. Under 8000 Hz, there are 34 propagating modes, and we select $NT = 35$ in the reciprocal identity method to include one evanescent mode. Figure 6.6 compares the BEM and the FEM solutions up to 8000 Hz. It is observed that both solutions compare very well. Of particular note, the sound absorption is relatively thin and does not completely flatten out the peaks and troughs above 1000 Hz. These characteristics of the transmission loss are detected using both BEM and FEM.

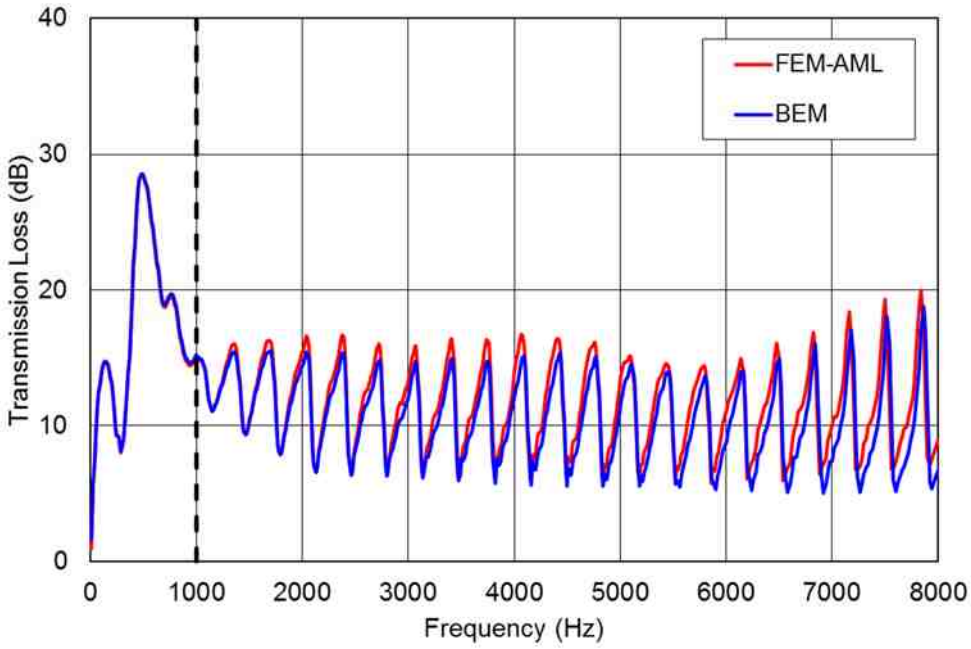

Figure 6.6 Comparison between the BEM and FEM solutions for the circular simple expansion chamber with offset inlet/outlet.

3. Two Cylindrical Bar Silencers Positioned in Duct

The third example features two circular bars housed in a circular chamber as shown in Figure 6.7. The two bars have a flow resistivity of 16000 Rayls/m and are covered by a 30% open perforated protective sheet. The cutoff frequency of the 0.8 m diameter inlet/outlet is 250 Hz.

Figure 6.8 compares the transmission loss for both BEM and FEM. There is excellent agreement. For the BEM simulation, three substructures were used: the second substructure consisting of a template repeated 28 times. Under 8000 Hz, there are 432 propagating modes, and we select $NT = 433$ to include one evanescent mode. Due to the size of the problem, FEM results are presented up to 5550 Hz due to hardware limitations. Nonetheless, both solutions compare very well with each other up to the reachable frequency.

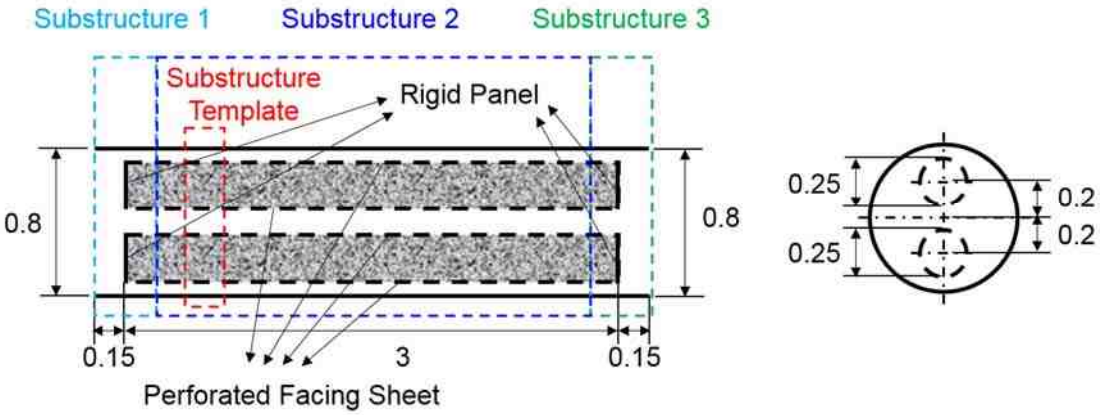

Figure 6.7 Schematic showing a non-axisymmetric bar silencer (dimensions in m)

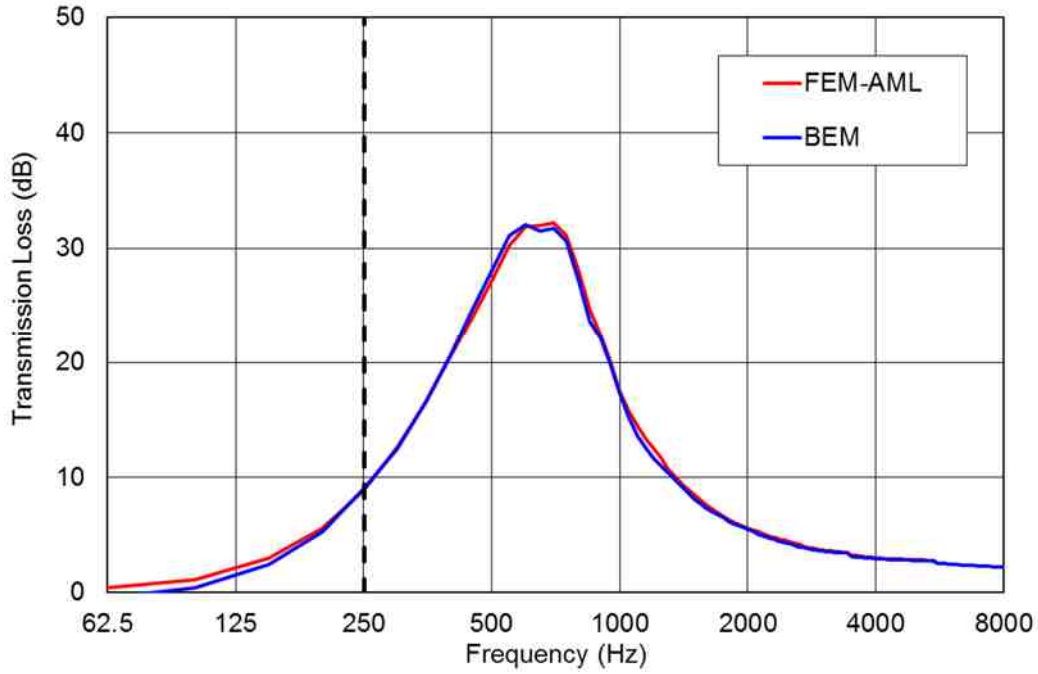

Figure 6. 8 Comparison between the BEM and FEM solutions for the non-axisymmetric bar silencer

4. Two Cylindrical Bar Silencers Positioned in Expansion Chamber

The next case is a modified design of the dual-bar silencer of the third test case. As shown in Figure 6.9, the two bars and the chamber have the same dimensions as in the third test case except that the inlet and outlet ducts now have a much smaller diameter and are offset by distance of 0.4 m from the inlet and outlet ducts

openings. This silencer is far more complicated than the prior example since it will have both dissipative and reactive features. At room temperature, the cutoff frequency of the 0.2 m diameter inlet/outlet ducts is 1005 Hz.

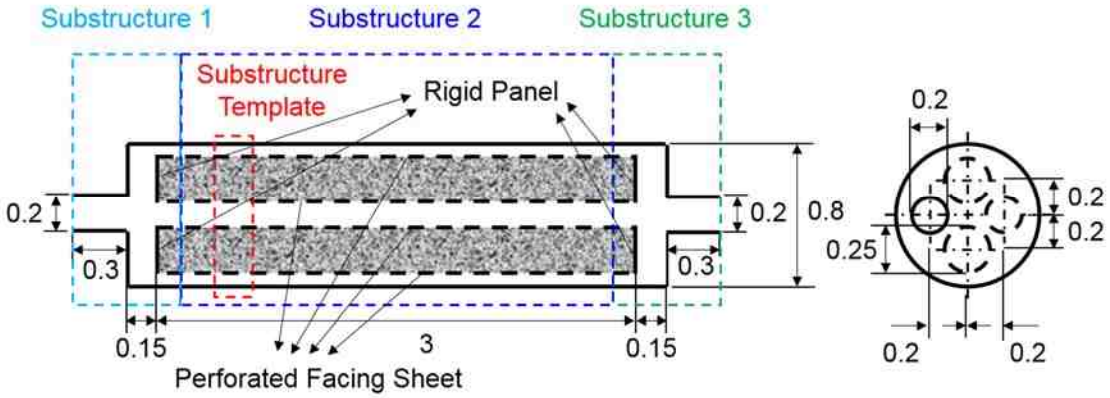

Figure 6.9 Schematic showing a dual-bar silencer (Unit: m)

Figure 6.10 compares the BEM and FEM solutions with good agreement. Under 8000 Hz, there are 34 propagating modes at the inlet and outlet, and we select $NT = 35$ to include one evanescent mode. As in the third test case, the FEM analysis stops at 5500 Hz due to the problem size whereas BEM results are presented up to 8000 Hz. Again, three substructures were used with the second substructure repeated 28 times. It is noteworthy that the impedance matrix of the central part can be taken directly from the prior test case without re-modeling in the BEM.

Both solutions compare very well but the transmission loss curve has greater variation. This silencer has reactive characteristics due to the difference in cross-sectional area between inlet/outlet ducts and the chamber. With no cross comparison between BEM and FEM, one would have much less confidence in either solution. This test case also demonstrates the value of having a second tool available to validate the first solution.

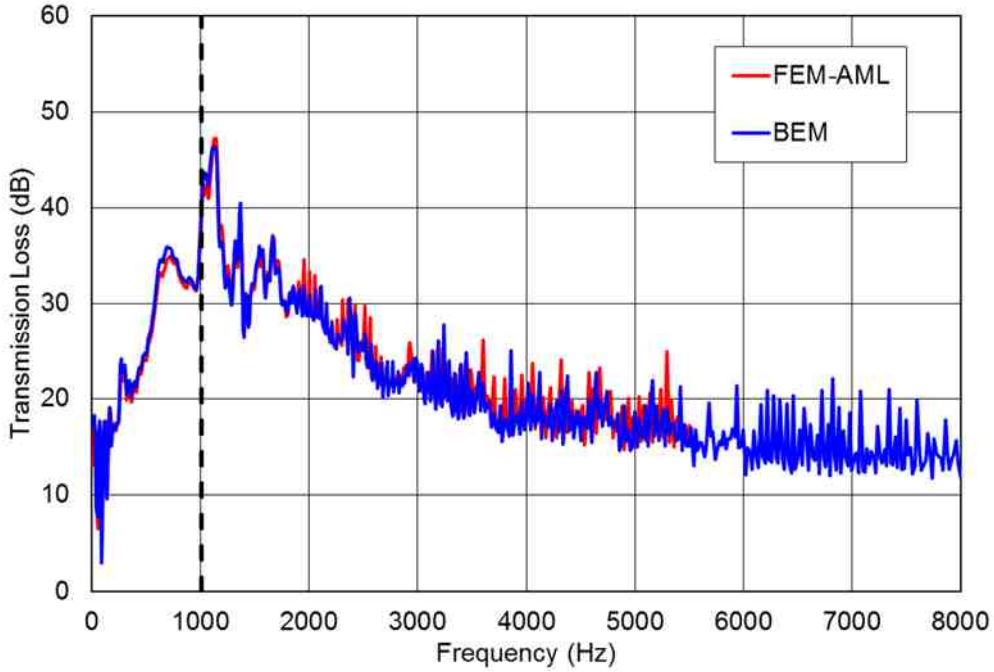

Figure 6.10 Comparison between the BEM and FEM solutions for the dual-bar silencer

5. Parallel-Baffle Silencer

Rectangular parallel-baffle silencers are commonly used in gas turbine, air handler, and power generation enclosure applications. A typical rectangular parallel-baffle silencer as shown in Figure 6.11 was simulated next. Key dimensions are $D = 0.61\ m$, $d = 0.05\ m$, $h = 0.05\ m$, $L = 0.91\ m$ and $L_1 = 0.1\ m$. The cutoff frequency is 641 Hz.

Figure 6.12 compares BEM and FEM with good agreement. Under 8000 Hz, there are 641 propagating modes, and we select $NT = 642$ to include one evanescent mode. BEM analysis extends up to 8000 Hz using three substructures with the second substructure repeated 8 times whereas FEM was used up to 6000 Hz.

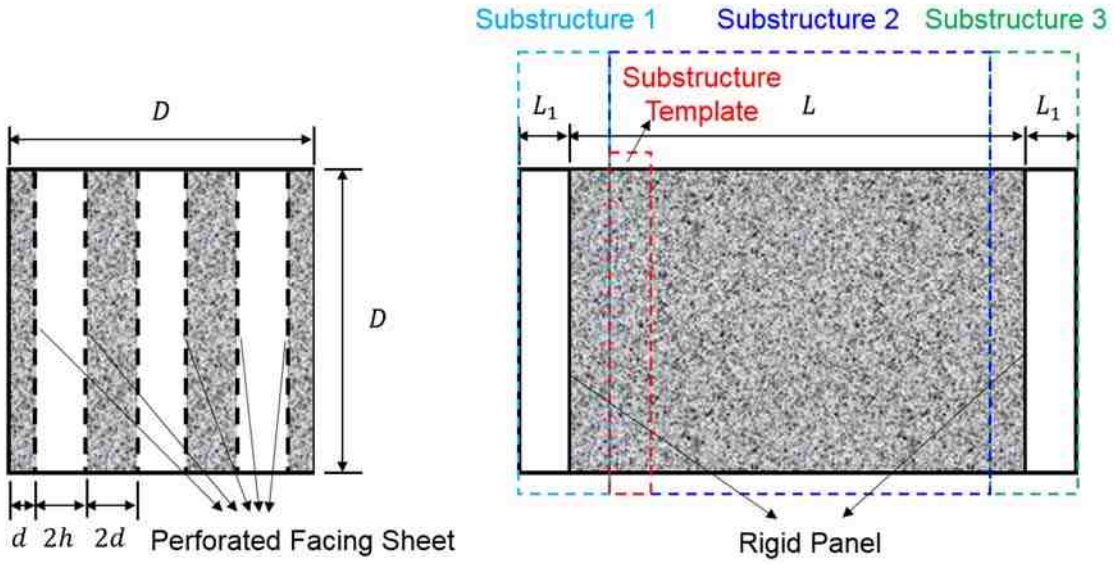

Figure 6.11 Schematic showing a rectangular parallel-baffle silencer

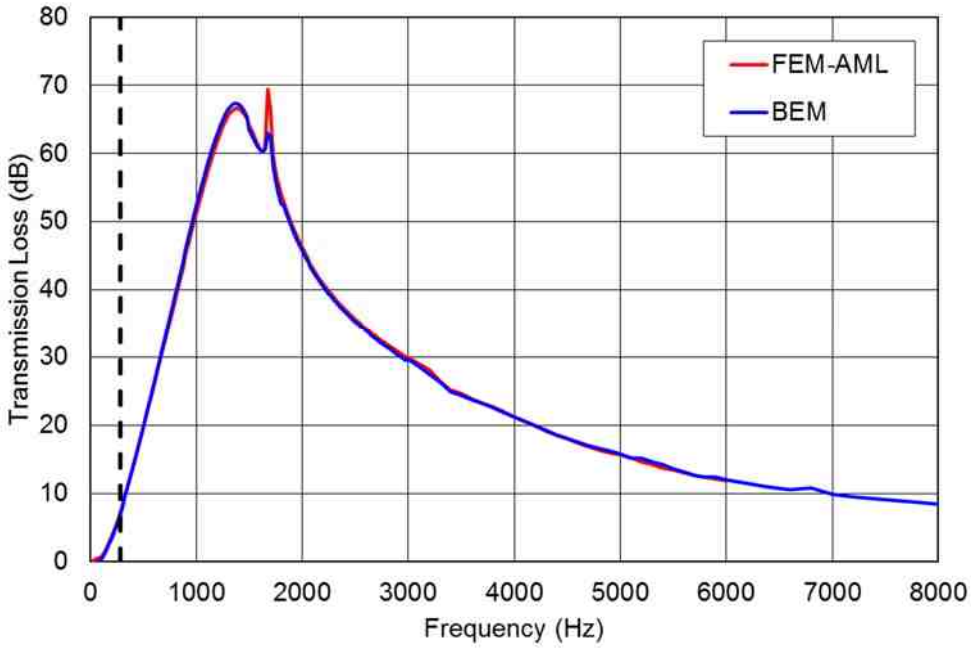

Figure 6.12 Comparison between the BEM and FEM solutions for the rectangular parallel-baffle silencer

6. Single-Inlet Two-Outlet Muffler

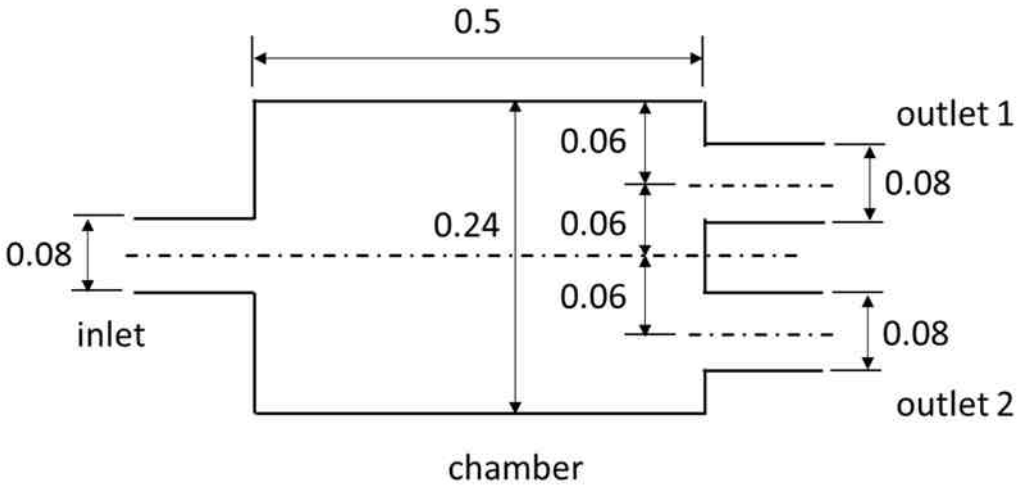

Figure 6.13 Expansion chamber with one inlet and two outlets (dimensions in m)

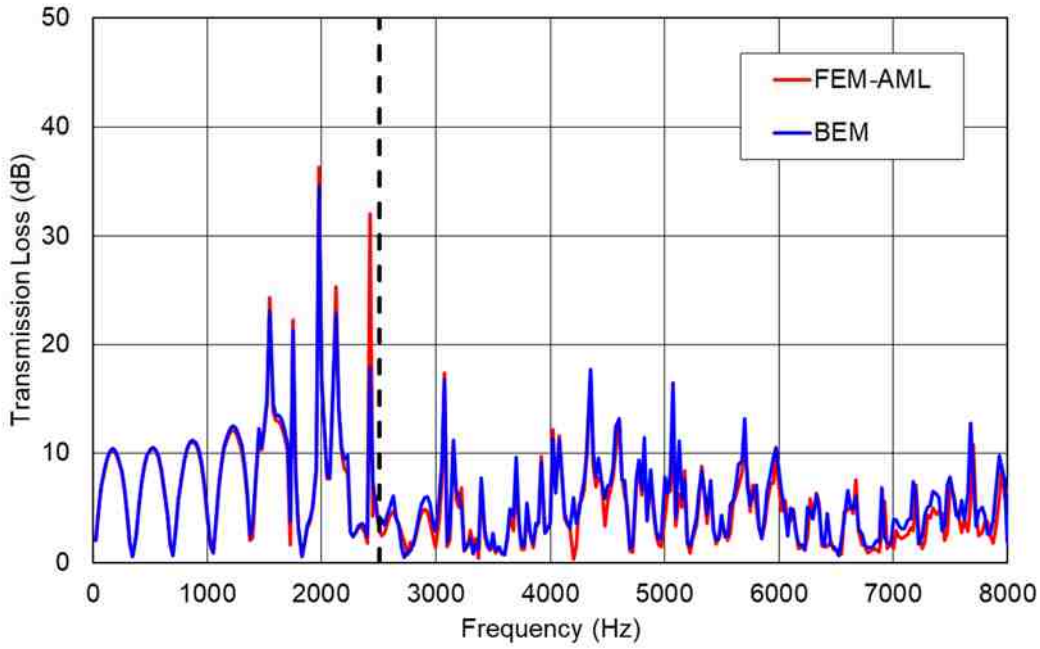

Figure 6.14 Comparison between the BEM and FEM solutions for the expansion chamber with one inlet and two outlets

The final case is single-inlet two-outlet muffler as shown in Figure 6.13. The silencer is unlined with a plane-wave cutoff frequency of 2510 Hz in the inlet and outlet ducts. To consider the higher-order modes, we select $M = 6$ and $N = 6$.

Figure 6.14 compares the BEM solution using the impedance-to-scattering matrix method (Wang and Wu, 2016) to the FEM-AML solution. It is evident that both methods compare very well up to 8000 Hz. This case validates that both the BEM and FEM-AML can be used to examine multiple-outlet silencers which are common in the HVAC industry.

6.7 Conclusions

The direct mixed body BEM and the FEM with AML were used to predict the transmission loss of several large silencers. The direct mixed body BEM is a specialized approach which has been customized for the simulation of large silencers. It includes the ability to template components of mufflers which appreciably reduces the computational time. Either the reciprocal identity method (Zhou, 2016) or the impedance-to-scattering method (Wang and Wu, 2016) can be used in BEM to assess the transmission loss above the cutoff frequency. This is compared to a less specialized FEM strategy. An AML boundary condition is applied at both the inlet and outlet so both source and termination are anechoic: transmission and insertion loss are equivalent to each other in this case. Insertion loss is determined as the difference in transmitted sound power without and with the silencer in place.

A simulation campaign was performed and excellent agreement was observed in each case. Several reactive mufflers are included which exhibit a good deal of variation of transmission loss as a function of frequency. The degree of correlation between methods serves to validate both approaches.

Though a specialized BEM or FEM approach will be more computationally efficient, it is anticipated that noise and vibration simulation specialists in industry will gravitate more towards the FEM approach since it can be applied in most commercial software packages.

Chapter 7 A POWER APPROACH TO PREDICT ACOUSTIC PERFORMANCE FOR HVAC DUCT SYSTEM

(Note: Most of the research in this chapter has been previously documented in Ruan, Herrin and Wu (2018).)

The transfer matrix approach is commonly used to simulate mufflers below the plane wave cutoff frequency. Transfer matrices have been developed for common muffler elements and models can be solved in seconds. In this paper, a similar power transfer matrix method is detailed which is applicable to systems above the cutoff frequency. To determine the 2X2 power transfer matrix, a scattering matrix calculated using the boundary element method is reduced to the power transfer matrix. The procedure for doing so is outlined. Although the reduction from the full scattering matrix to the 1-D power transfer matrix provides only an approximation, it works seamlessly with other 1-D analysis tools and first-mode analytical solutions for a cascaded exhaust design. Several examples are provided to validate and demonstrate the proposed method.

7.1 Introduction

Large and extensive duct systems are commonly employed in the HVAC and power generation industries. Deterministic models are difficult due to the large dimensions. For example, HVAC systems normally include multiple components connected in series including ducts, elbows, and plenums. At this juncture, most predictions are conducted using the tables and equations in the ASHRAE Handbook (ASHRAE, 2015). The virtue of the Handbook is that the equations are easily understood and simple to program in a spreadsheet. On the other hand, Chapter 3 reviewed the Handbook for accuracy and noted several limitations for longer lined ducts and plenums so accuracy is suspect.

At low frequencies (i.e., below the plane wave cutoff frequency of the inlet and outlet), there are several conventional approaches for evaluating the transmission loss (TL) of a silencer. The most notable of these is the transfer matrix method of

Munjal (2014). A complicated duct system is modeled as a series of 2×2 matrices that can be multiplied together to form a 2×2 matrix for the entire system. From this system matrix, the transmission loss is easily calculated. Matrices for most standard duct components are readily available in the literature. However, that is not the case above the cutoff frequency.

For HVAC components and other large silencer elements, numerical methods must be used because the cutoff frequency will be relatively low in frequency. Cummings and Astley (1996) used the finite element method (FEM) to study the acoustical behavior of square bar silencers. In similar work, Kirby and Lawrie (2005, 2006) proposed a hybrid FEM with either a point collocation approach or a mode matching scheme. Zhou et al. (2016) proposed a reciprocal identity method to be used in conjunction with the boundary element method (BEM) for large silencer analysis. In Chapter 3, the finite element method was used to determine the attenuation of standard HVAC components including structureborne flanking effects.

Although FEM and BEM simulation can be used to model a HVAC duct system without too much trouble in theory, a full 3D analysis of a duct network at high frequencies is CPU and time consuming. An approximate 1D analysis tool similar to the conventional four-pole transfer matrix approach can be beneficial for engineers in industry. In a large exhaust or HVAC network, many components may just be simple straight unlined or lined ducts and can be modeled analytically even at high frequencies. On the other hand, more complex components must be modeled by the FEM or BEM. A hybrid approach that can bridge the gap between the simple analytical solution and the more complex numerical solution will reduce the computational cost significantly.

In very recent work, Nashed et al. (2018) developed a power scattering matrix approach for the analysis of ductwork above the plane wave cutoff frequency. Scattering matrices for a number of standard components were developed based on measurement campaigns documented in the aforementioned ASHRAE

Handbook and VDI 2081 (VDI, 2001). The current effort is directly related to that work.

In this chapter, it is shown that a 2×2 power transfer matrix, which is a simple rearrangement of the scattering matrix of Nashed et al. (2018), can be reduced from the full scattering matrix obtained from BEM simulation. Although the reduction from the full scattering matrix to the 2×2 power transfer matrix provides only an approximation, the procedure can be used to develop 2×2 power transfer matrices for non-standard components. Several examples are provided to validate and demonstrate the proposed method.

7.2 Scattering Matrix

Wang and Wu (2016) developed a so-called "impedance-to-scattering matrix method" that converts the BEM impedance matrix to the scattering matrix. The scattering matrix of a large silencer relates the transmitted wave amplitudes at the outlet and the reflected wave amplitudes at the inlet to the incident wave amplitudes at the inlet and the reflected wave amplitudes at the outlet as follows:

$$\begin{Bmatrix} p_{20}^{+} \\ p_{21}^{+} \\ \vdots \\ p_{2(N-1)}^{+} \\ p_{10}^{-} \\ p_{11}^{-} \\ \vdots \\ p_{1(N-1)}^{-} \end{Bmatrix} = \begin{bmatrix} S_{1,1} & \cdots & S_{1,2N} \\ \vdots & \ddots & \vdots \\ S_{2N,1} & \cdots & S_{2N,2N} \end{bmatrix} \begin{Bmatrix} p_{10}^{+} \\ p_{11}^{+} \\ \vdots \\ p_{1(N-1)}^{+} \\ p_{20}^{-} \\ p_{21}^{-} \\ \vdots \\ p_{2(N-1)}^{-} \end{Bmatrix} \tag{7.1}$$

where N is the total number of modes used in the modal expansion at the inlet and outlet. It is noted that all propagating modes along with a few evanescent modes are included in the above relationship.

7.3 Power Transfer Matrix

If the large $2N \times 2N$ scattering matrix in Equation (7.1) has to be condensed to a small 2×2 transfer matrix, the relationship must be written in terms of sound power instead of sound pressure amplitudes. This is especially true at high frequencies. The sound power transfer matrix is defined by

$$\begin{Bmatrix} W_1^+ \\ W_1^- \end{Bmatrix} = \begin{bmatrix} T_{11} & T_{12} \\ T_{21} & T_{22} \end{bmatrix} \begin{Bmatrix} W_2^+ \\ W_2^- \end{Bmatrix} \tag{7.2}$$

With reference to Figure 7.1, W_1^+ and W_1^- are the incident and the reflected sound power at the inlet, respectively; W_2^+ and W_2^- are the transmitted and the reflected sound power at the outlet, respectively.

Figure 7.1 Schematic showing incident, reflected and transmitted sound power at the inlet and outlet.

To have a well-posed boundary-value problem, Equation (7.2) must be rearranged so that the input at the inlet and the termination condition at the outlet are placed on the right-hand side. That is,

$$\begin{Bmatrix} W_2^+ \\ W_1^- \end{Bmatrix} = \begin{bmatrix} S_{11}^* & S_{12}^* \\ S_{21}^* & S_{22}^* \end{bmatrix} \begin{Bmatrix} W_1^+ \\ W_2^- \end{Bmatrix} \tag{7.3}$$

To obtain the first column of the matrix in Equation (7.3), we assume that the incident wave at the inlet is a unit plane wave and the outlet is non-reflective. In other words, use $\boldsymbol{p_1^+} = [1,0,0,\dots,0]^T$ and $\boldsymbol{p_2^-} = [0,0,0,\dots,0]^T$ in Equation (7.1). Once

the reflected and transmitted sound pressure amplitudes are solved from Equation (7.1), the sound power of each W in Figure 7.1 can be calculated by

$$W = \frac{A}{2\rho\omega}\sum_{n=0}^{\infty} Re(k_{zn})|p_n|^2 J_0^2(k_{rn}R) \tag{7.4}$$

where A is the cross-sectional area of the inlet or outlet, and R is the radius. The first column of the matrix in Equation (7.3) then becomes

$$S_{11}^* = \frac{W_2^+}{W_1^+} \tag{7.5}$$

$$S_{21}^* = \frac{W_1^-}{W_1^+} \tag{7.6}$$

Similarly, assume $\boldsymbol{p_2^-} = [1,0,0,\dots,0]^T$ and $\boldsymbol{p_1^+} = [0,0,0,\dots,0]^T$ in Equation (7.1), and the second column of the matrix in Equation (7.3) becomes

$$S_{12}^* = \frac{W_2^+}{W_2^-} \tag{7.7}$$

$$S_{22}^* = \frac{W_1^-}{W_2^-} \tag{7.8}$$

Finally, the power transfer matrix in Equation (7.2) can be obtained from Equation (7.3) by a simple conversion:

$$T_{11} = 1/S_{11}^* \tag{7.9}$$

$$T_{12} = -S_{12}^*/S_{11}^* \tag{7.10}$$

$$T_{21} = S_{21}^*/S_{11}^* \tag{7.11}$$

$$T_{22} = S_{22}^{*} - S_{12}^{*} \cdot S_{21}^{*} / S_{11}^{*} \tag{7.12}$$

Power transfer matrices, as in Equation (7.2), can be multiplied together to obtain a total matrix for a cascaded system. From the matrix terms, the transmission loss (TL) is defined as just

$$TL = 10 \log_{10}\left(\frac{W_2^{+}}{W_1^{+}}\right) = 10 \cdot \log_{10}(T_{11}) \tag{7.13}$$

Though each power transfer matrix is “exact” to obtain the transmission loss of an individual component, the total matrix of assembled components is an approximation. This is a result of the assumed boundary condition for obtaining Equations (7.5) - (7.8) for the purpose of obtaining the matrices.

7.4 Analytical Model

Numerous researchers have developed analytical equations for standard muffler elements. Munjal (2014) summarizes much of the prior work. Once the solution is known, a power matrix can be developed. Assume that the reflected sound can be neglected: an assumption that is appropriate for most dissipative mufflers. Assuming that the sound attenuation is known, a sound attenuation factor can be defined as

$$\tau = \frac{1}{(A_{NR}/10)^{10}} \tag{7.14}$$

where A_{NR} is sound attenuation.

The power scattering matrix is expressed as

$$\begin{pmatrix} W_2^{+} \\ W_1^{-} \end{pmatrix} = \begin{bmatrix} S_{11}^{*} & S_{12}^{*} \\ S_{21}^{*} & S_{22}^{*} \end{bmatrix} \begin{pmatrix} W_1^{+} \\ W_2^{-} \end{pmatrix} \tag{7.15}$$

If the reflected sound at the inlet is neglected and termination is assumed to be anechoic, W_1^- and W_2^- equal to zero. S_{11}^* and S_{21}^* can be determined and expressed as

$$S_{11}^* = \frac{W_2^+}{W_1^+} = \tau \tag{7.16}$$

and

$$S_{21}^* = 0 \tag{7.17}$$

If the inlet and outlet are swapped, W_1^+, W_1^-, W_2^+ and W_2^- are reflected sound at outlet, transmitted sound, reflected sound at inlet, incident sound, respectively. W_1^+ and W_2^+ equal zero and

$$S_{22}^* = \frac{W_1^-}{W_2^-} = \tau \tag{7.18}$$

and

$$S_{12}^* = 0 \tag{7.19}$$

The power scattering matrix is then expressed as

$$\begin{bmatrix} S_{11}^* & S_{12}^* \\ S_{21}^* & S_{22}^* \end{bmatrix} = \begin{bmatrix} \tau & 0 \\ 0 & \tau \end{bmatrix} \tag{7.20}$$

By reorganizing the power scattering matrix, a power transfer matrix can be expressed as

$$\begin{bmatrix} T_{11} & T_{12} \\ T_{21} & T_{22} \end{bmatrix} = \begin{bmatrix} 1/\tau & 0 \\ 0 & \tau \end{bmatrix} \tag{7.21}$$

7.5 Determination of Transmission Loss

From Equation (7.6), the transmitted and incident sound powers can be related to one another using

$$W_1^+ = T_{11} \cdot W_2^+ + T_{12} \cdot W_2^- \tag{7.22}$$

Assuming the termination is anechoic, the transmission loss can be expressed as

$$TL = 10 \cdot \log_{10}(T_{11}) \tag{7.23}$$

A complicated silencer system can be divided up into a number of components as shown in Figure 7.2. The power transfer matrix of the silencer system corresponds to the product of the individual power transfer matrices. The power transfer matrix for each single subsystem can be determined by either numerical simulation (BEM or FEM) or analytical solutions. The power transfer matrix of a complicated silencer system like the one shown in Figure 7.2 can be determined via

$$[T] = [T_1] \cdot [T_2] \cdot [T_3] \tag{7.24}$$

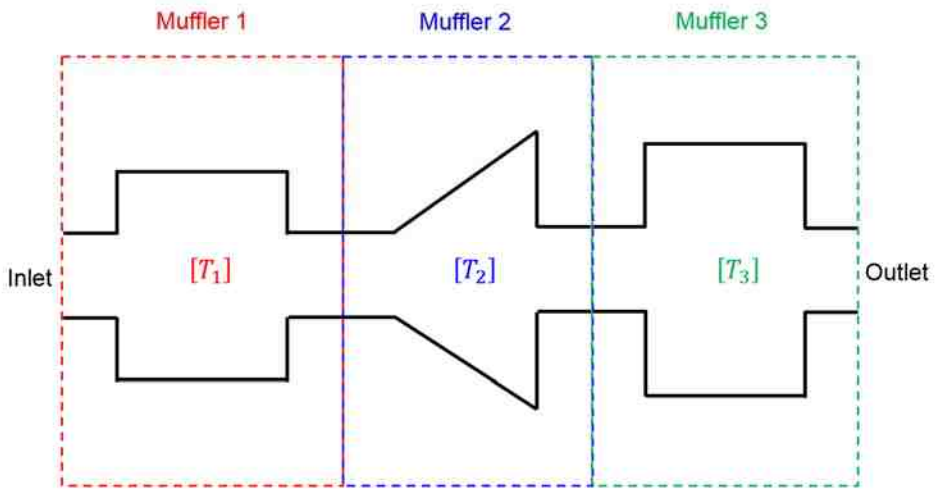

Figure 7.2 Schematic showing power transfer matrix for a complicated silencer system.

7.6 Test Cases

Several test cases are given in this section to demonstrate the power matrix method. The first test case is a lined duct which can be divided into two parts. The dimensions are given in Figure 7.3. The lining thickness is 0.0508 m. At room temperature, the plane-wave cutoff frequency is 1394 Hz. There are 4 propagating modes in the inlet and outlet ducts up to 8000 Hz. Figure 7.4 shows the comparison between the BEM solution and power transfer matrix solution in 1/3 octave bands. In the BEM solution, we model both lined ducts in one single BEM model. In the power transfer matrix method, we first obtain the 2x2 power transfer matrix for each section, and then multiply the two transfer matrices together. It is seen that the power transfer matrix method provides an acceptably accurate approximation up to 8000 Hz.

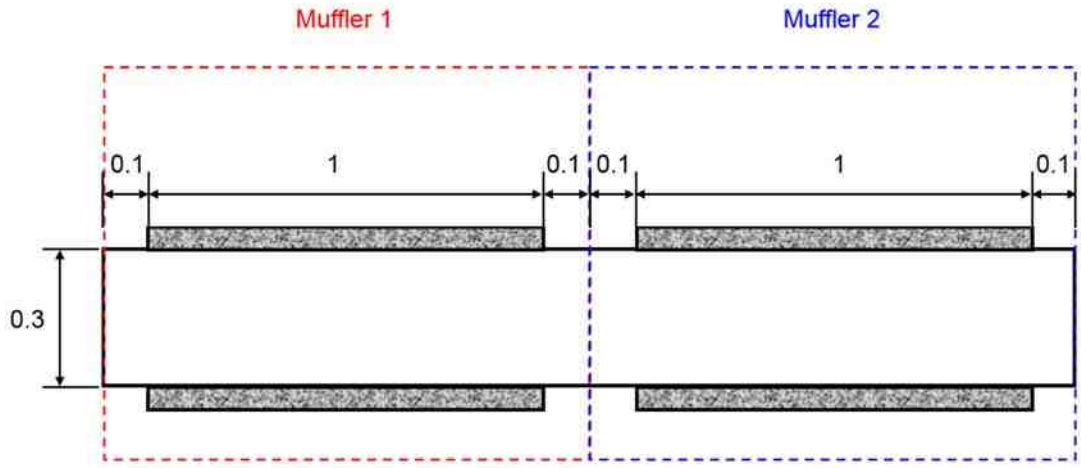

Figure 7.3 Schematic showing a dissipative silencer comprised of two lined ducts (unit: meter).

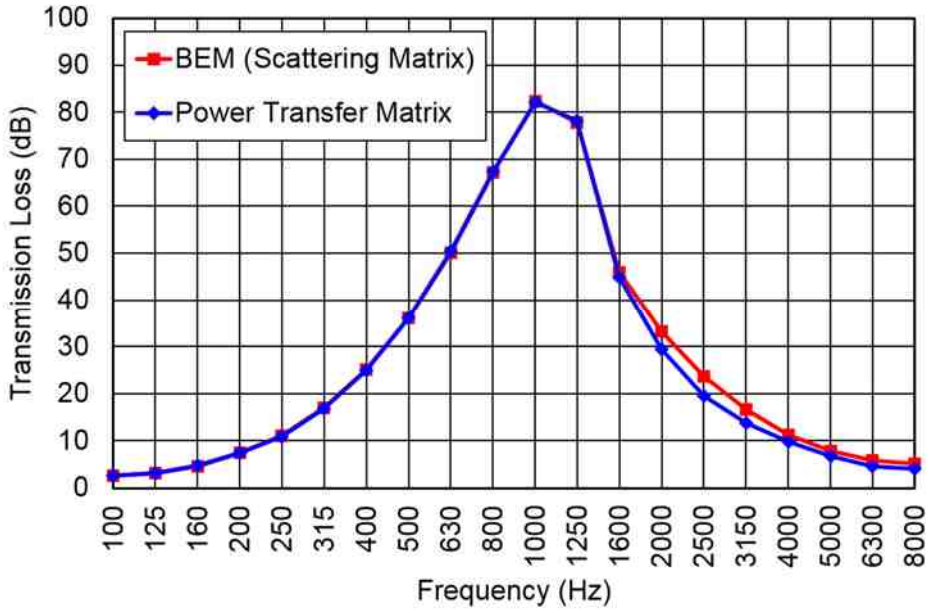

Figure 7.4 Transmission loss results comparison of power transfer matrix method and pressure scattering matrix method.

The second test case is a bar silencer as shown in Figure 7.5. Figure 7.6 shows the comparison between the BEM and the power transfer matrix solutions up to 8000 Hz in 1/3 octave bands. It is seen that and power transfer matrix solution agrees well up to 8000 Hz.

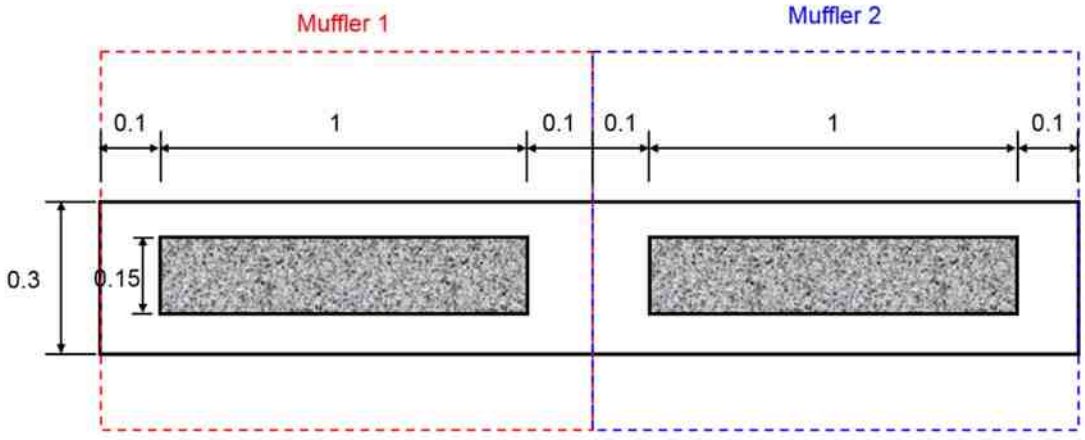

Figure 7.5 Schematic showing a dissipative silencer comprised of two bar silencers (unit: meter).

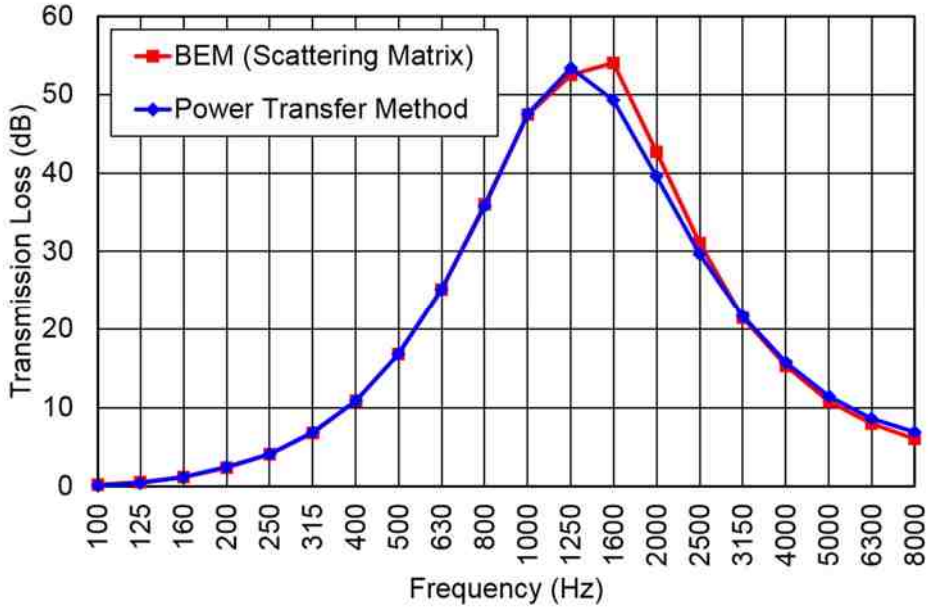

Figure 7.6 Transmission loss results comparison of power transfer matrix method and pressure scattering matrix method.

The third test case is a reactive muffler which consists of two simple expansion chambers as shown in Figure 7.7. Each expansion chamber is treated as a separate element. At very low frequencies, there will be interactions in between both components that are important. These interactions are more important in the reactive case and will not be taken into account by the power transfer matrix method. Figure 7.8 shows the comparison between the full scattering matrix and power transfer matrix methods in 1/3 octave bands. Again, agreement is quite good except at the lower frequencies.

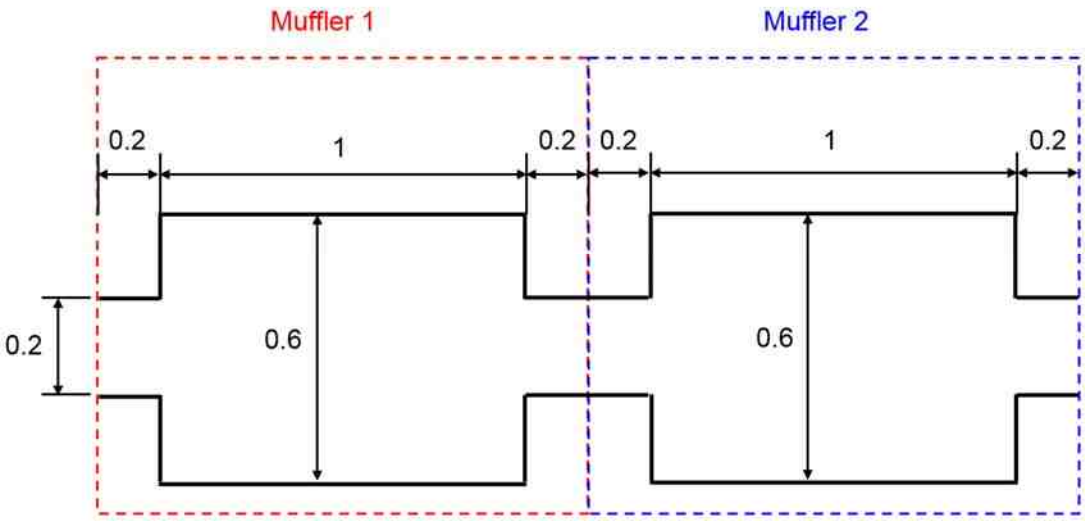

Figure 7.7 Schematic showing a reactive silencer comprised of two simple expansion chambers (unit: meter).

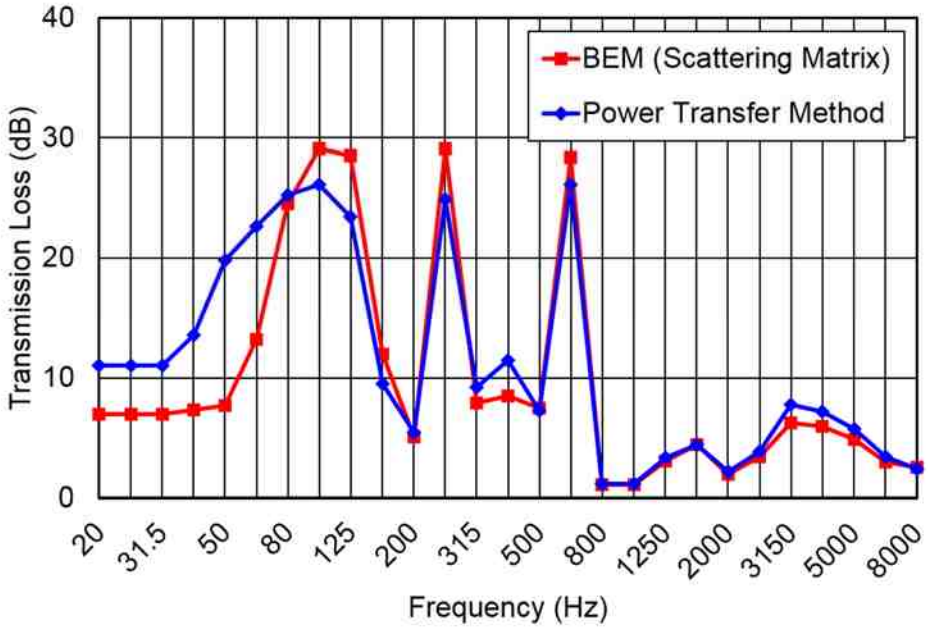

Figure 7.8 Transmission loss results comparison for test case 3 of power transfer matrix method and pressure scattering matrix method.

The last test case is a dissipative silencer which is comprised of a lined duct and a bar silencer as shown in Figure 7.9. The lining thickness is 2 inches. The power

transfer matrix of substructure 1 can be identified by either analytical model or BEM model, while the power transfer matrix of substructure 2 is identified by BEM model. The transmission loss results comparison is shown in Figure 7.10. The red line represents transmission loss computed by pressure scattering matrix directly. The green line repents transmission loss determined by combining power transfer matrix from analytical model and BEM model while the blue line is from two BEM models. It is seen that results determined by power transfer matrix from BEM models are almost the same with results assessed by the scattering matrix method. The results obtained by combining the analytical and BEM models also compare very well with the scattering matrix method.

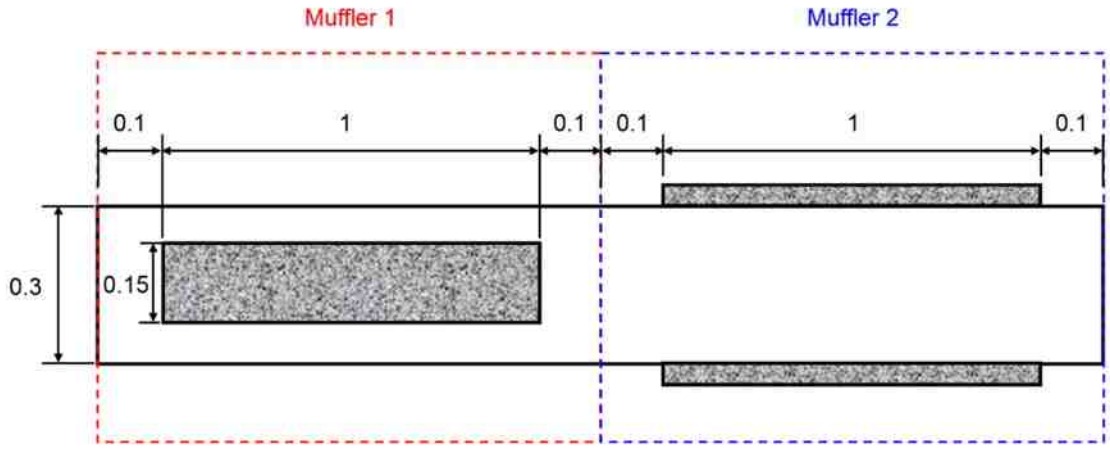

Figure 7.9 Schematic showing a dissipative silencer comprised of a lined duct and a bar silencer (unit: meter).

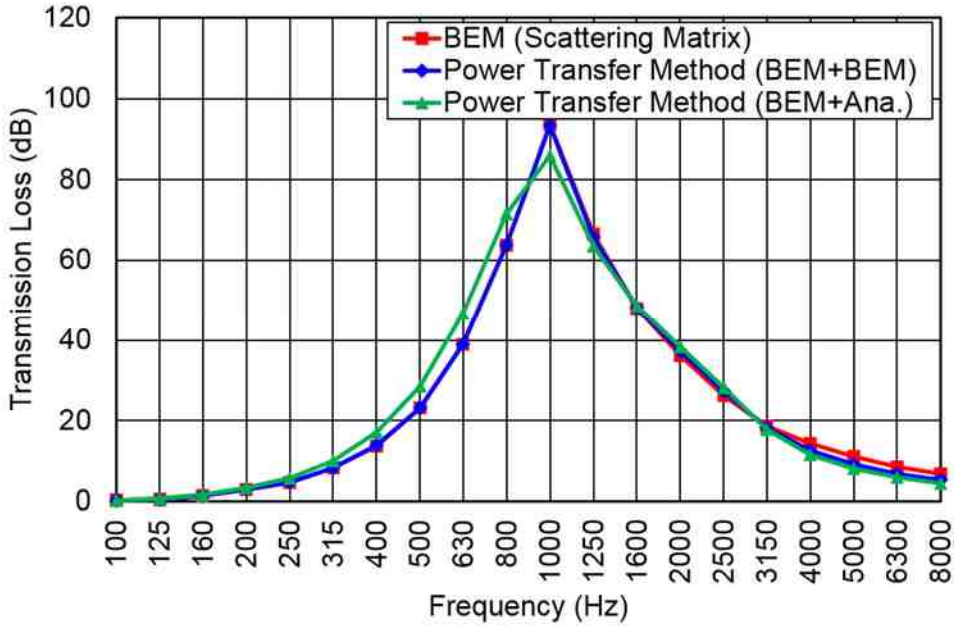

Figure 7.10 Transmission loss results comparison for test case 4 of power transfer matrix method and pressure scattering matrix method.

7.7 Conclusions

Muffler transfer matrix theory is not applicable above the plane wave cutoff frequency due to cross-modes. Yet, cross-modes occur at low frequencies in HVAC ducts and large silencers as a result of the large cross-sectional duct dimensions. An alternative power transfer matrix has been utilized in this chapter. It has been shown that the power transfer matrix can be determined using BEM analysis.

The validity of the approach has been demonstrated by applying it to several examples with muffler elements in series. The method is especially accurate for dissipative silencers that are typical in HVAC systems. However, it is reasonably accurate for large reactive elements.

Chapter 8 CONCLUSIONS AND RECOMMENDATIONS

HVAC ductwork is ubiquitous in commercial buildings. The ductwork circulates cooled or warmed air throughout the building maintaining a comfortable environment. In order to move the air, fans are positioned in large air handlers and are the primary source of noise in buildings. In order to reduce the noise annoyance, ducts are treated with sound absorbing materials and plenums are inserted into the duct system. The primary objective of this thesis is to advance the state-of-the-art in numerical prediction and scale model testing to predict acoustic attenuation through HVAC ductwork.

The major accomplishments described in this dissertation include: the development and validation of a finite element procedure to determine insertion loss and breakout transmission loss, the description and validation of a procedure for developing scale models, the validation of a finite element procedure to determine acoustic transmission loss, and the development of a procedure to determine the power transfer matrix for HVAC components.

8.1 FEM Simulation Approach to Predict Acoustic Performance of HVAC Components

A FEM approach was developed for the modeling of unlined and lined HVAC ducts. The analysis approach replicates *ASTM E477* (2006). The source is modeled as a diffuse acoustic field and terminates in a rigid baffle. The structural response of the ductwork and the associated breakout noise transmission path were included. Boundaries at the source and termination were simulated using a reflection free boundary called a perfectly matched layer. Insertion loss results were compared to experimental results with good agreement.

Additionally, breakout transmission loss results compared well with the *ASHRAE Handbook – HVAC Applications* (2015) for rectangular ductwork over the entire frequency range. For circular ductwork, results compared well at frequencies above the plane wave cutoff frequency. Below the cutoff frequency, simulation

compared well with an analytical model for circular ducts but not with measurement. It is notable that the measured transmission loss exceeds 50 dB so the discrepancy is of little practical importance.

It was also shown that the model could be simplified and the breakout path could be neglected as an approximation. Results were shown to be similar but the predicted attenuation was a few dB too high at most frequencies. An error of a few dB will not be critical except at the very low frequencies.

An identical approach was also used to determine the insertion loss of elbows. Insertion loss was defined as the sound power difference in dB at the termination between an unlined straight duct and duct with lined or unlined elbow having the same total length. Side branch insertion loss was determined in a similar way. Simulated results compared well with the *ASHRAE Handbook – HVAC Applications* (2015).

The developed model can be used for ducts of any cross-section or length. Future efforts can focus on 1) further model validation for other duct cross-sections and lengths and 2) utilization of the model to revise and supplement the information that is currently in the *ASHRAE Handbook – HVAC Applications* (2015).

8.2 Scale Modeling Approach to Assess Acoustic Performance of HVAC Components

Scale modeling rules for sound propagation in HVAC ductwork were described and then validated. This scale modeling approach can be utilized to determine insertion loss and breakout transmission of HVAC components with good agreement. This scaling approach also can be applied to predict sound transmission loss of larger silencer. However, it should be notable that HVAC ducts including sound absorption are more difficult to scale because it may be difficult to find a suitable sound absorbing material of appropriate thickness and flow resistivity. It is anticipated that scale models can be used to validate future numerical simulation studies eliminating the need for more expensive full-scale testing.

8.3 Numerical Methods to Predict Transmission Loss of Large Silencer

The reciprocal identity method for predicting transmission loss of large silencers is extended to general non-axisymmetric circular and rectangular inlet/outlet configurations, which are often used in practical applications. It is well known that the IL is equivalent to the TL if both ends of the silencer are assumed non-reflective. Hence, a FEM approach using the “automatically matched layer” (AML) boundary condition was developed to validate the reciprocal identity method.

Future work should extend the method to deal with the multi-inlet case as well as measurement validation perhaps via scale modeling.

8.4 Power Approach to Predict Acoustic Performance of HVAC System

A power transfer matrix was defined to characterize the acoustic properties of HVAC components since standard muffler transfer matrix theory is not applicable above the plane wave cutoff frequency. The sound power transfer matrix can be developed by a suitable analytical model or more generally by BEM simulation. The transfer matrices of series components can be multiplied together and the performance of extended duct systems can be predicted without reliance on large simulation models. Future work should examine included structureborne noise into the model.

REFERENCES

J. F. Allard and N. Atalla, (2009). *Propagation of Sound in Porous Media - Modelling Sound Absorbing Materials*, John Wiley & Sons, Ltd., West Sussex, United Kingdom.

ASHRAE, (2013). *2013 ASHRAE Handbook—Fundamentals*, Section 4, Atlanta: ASHRAE.

ASHRAE, (2015). *2015 ASHRAE Handbook—HVAC Applications*, Chapter 48, Atlanta: ASHRAE.

R. J. Astley, (2007). *Numerical Acoustical Modeling (Finite Element Modeling)*, Chapter 7, Handbook of Noise and Vibration Control, ed. M. J. Crocker.

R. J. Astley and J. P. Coyette, (2001). “Conditioning of Infinite Element Schemes for Wave Problems”, Communications in Numerical Methods in Engineering, 17(1), 31–41.

R. J. Astley and A. Cummings. (1984). “A Finite Element Scheme for Acoustic Transmission through the Walls of Rectangular Ducts: Comparison with Experiment”, Journal of Sound and Vibration, 92(3), 387-409.

R. J. Astley, A. Cummings and N. Sormaz. (1991). “A Finite Element Scheme for Acoustic Propagation in Flexible-walled Ducts with Bulk-reacting Liners, and Comparison with Experiment”, Journal of Sound and Vibration, 150(1), 119-138.

R. J. Astley, K. Gerdes, D. Givoli and I. Harari (Eds.), (2000). “Finite Elements for Wave Problems”, Journal of Computational Acoustics, Special Issue, World Scientific, Singapore, 8(1).

ASTM E477-06a, (2006). “Standard Test Method for Measuring Acoustical and Airflow Performance of Duct Liner Materials and Prefabricated Silencers”, American Society of Testing and Materials.

ASTM E1050-12, (2012). “Standard Test Method for Impedance and Absorption of Acoustical Material Using a Tube, Two Microphones and a Digital Frequency Analysis System”, American Society of Testing and Materials.

ASTM E2611-09, (2009). “Standard Test Method for Measurement of Normal Incidence Sound Transmission of Acoustical Materials Based on the Transfer Matrix Method”, American Society of Testing and Material.

N. Atalla, R. Panneton and P. Debergue, (1998). “A Mixed Displacement–pressure Formulation for Poroelastic Materials”, J. Acoust. Soc. Am., 104(3), 1444–1452.

J. P. Berenger, (1994). “A Perfectly Matched Layer for the Absorption of Electromagnetic Waves”, Journal of Computational Physics, 114(2), 185-200.

A. Bermudez, L. Hervella-Nieto, A. Prieto and R. Rodriguez, (2007). “An Optimal Perfectly Matched Layer with Unbounded Absorbing Function for Time-harmonic

Acoustic Scattering Problems", Journal of Computational Physics, 223(2), 469–488.

D. A. Bies and C. H. Hansen, (2009). *Engineering Noise Control: Theory and Practice*, 4th Edition, CRC Press, Boca Raton.

J. Bodely, (1988). Personal Communication, The United McGill Corp, Groveport, OH.

S. Brown, (2016). "The Suitability of Additive Manufacturing Materials in A 1:10 Scale Reverberation Chamber", INTERNOISE 2016, 21-24 August 2016, Hamburg, Germany, 468-478.

D. S. Burnett and R. L. Holford, (1998). "Prolate and Oblate Spheroidal Acoustic Infinite Elements", Computer Methods in Applied Mechanics and Engineering, 158(1-2), 117–141.

T. Busch, M. Hodgson, and C. Wakefield, (2003). "Scale-model Study of the Effectiveness of Highway Noise Barriers", J. Acoust. Soc. Am., 114(4), 1947-1954.

A. Cabelli, (1980). "The Acoustics of Duct Bends", Journal of Sound and Vibration, 68, 369-380.

D. Casalino and M. Genito, (2008). "Achievements in the Numerical Modeling of Fan Noise Radiation from Aero-engines", Aerospace Science and Technology, 12(1), 105–113.

A. Craggs, (1978). "A Finite Element Model for Rigid Porous Absorbing Materials", Journal of Sound and Vibration, 61(1), 101-111.

A. Craggs, (1986). "A Finite Element Model for Acoustic Model for Acoustically Lined Small Rooms", Journal of Sound and Vibration, 108(2), 327-337.

A. Cummings, (1983). "Acoustic Noise Transmission Through The Walls of Air Conditioning Ducts (TRP-318)", ASHRAE Report (TRP-318).

A. Cummings, (1985). "Acoustic Noise Transmission through Duct Walls", ASHRAE Transactions, 91(2A), 48-61.

A. Cummings, (2001). "Sound Transmission through Duct Walls", Journal of Sound and Vibration, 239(4), 731-765.

A. Cummings and R. J. Astley, (1995). "The Effects of Flanking Transmission on Sound Attenuation in Lined Ducts", Journal of Sound and Vibration, 179(4), 617-646.

A. Cummings and R. J. Astley, (1996). "Finite Element Computation of Attenuation in Bar-silencers and Comparison with Measured Data", Journal of Sound and Vibration, 196, 351-369.

M. E. Delaney and E. N. Bazley, (1970). "Acoustical Properties of Fibrous Absorbent Materials", Applied Acoustics, 3(2), 105-116.

R. I. Emori and D. J. Schuring, (1977). *Scale Models in Engineering: Fundamentals and Applications*, Elsevier.

ESI Group, (2007). Foam-X User's Guide.

D. Givoli and I. Harari (Eds.), (1998). "Exterior Problems of Wave Propagation", Computer Methods in Applied Mechanics and Engineering, Special Issue, North Holland, Amsterdam, 164(1-2), 1-226.

D. W. Herrin and K. Ruan, (2018) "A Review of Prior ASHRAE Research Efforts to Characterize Noise Propagation in Ducts", ASHRAE Transactions, (Under Review).

D. W. Herrin, K. Ruan and T. Wu, (2016). "Full-frequency Numerical Modeling of Sound Transmission in and Radiation from Lined Ducts", ASHRAE Report (RP-1529).

D. W. Herrin and A. F. Seybert, (2006). "Numerical Methods for Low-frequency HVAC Noise Applications", ASHRAE Report (RP-1026).

D. W. Herrin, Z. Tao, E. L. Scalf, S. A. Allen and A. F. Seybert, (2007). "Using Numerical Acoustics to Predict the Attenuation of HVAC Plenums", ASHRAE Transactions, 113(1), 10-18.

U. Ingard, (1994). *Notes on Sound Absorption Technology*, Noise Control Foundation.

E. S. Ivey and G. A. Russell, (1977). "Acoustical Scale Model Study of the Attenuation of Sound by Wide Barriers", J. Acoust. Soc. Am., 62(3), 601-606.

C. Jiang, T. W. Wu and C. Y. R. Cheng, (2010), "A Single-domain Boundary Element Method for Packed Silencers with Multiple Bulk-reacting Sound Absorbing Materials", Eng. Anal. Bound. Elem., 34, 971-976.

V. L. Jordan, (1970). "Acoustical Criteria for Auditoriums and Their Relation to Model Techniques", J. Acoust. Soc. Am., 47(2A), 408-412.

V. L. Jordan, (1975). "Auditoria Acoustics: Development in Recent Years", Applied Acoustics, 8(3), 217-235.

R. Kirby, (2005). "The Influence of Baffle Fairings on the Acoustic Performance of Rectangular Splitter Silencers", Journal of the Acoustical Society of America, 118, 2302-2312.

R. Kirby and J. B. Lawrie, (2005). "A Point Collocation Approach to Modelling Large Dissipative Silencers", Journal of Sound and Vibration, 286, 313-339.

R. Kirby, P. Williams and J. Hill, (2012). "A Comparison between the Performance of Different Silencer Designs for Gas Turbine Exhaust Systems", Proceedings of the Acoustics 2012 Nantes Conference, 3199-3204.

S. H. Ko and L. T. Ho, (1977). "Sound Attenuation in Acoustically Lined Curved Ducts in Absence of Fluid Flow", Journal of Sound and Vibration, 53, 189-201.

H. L. Kuntz, (1987). “The Determination of the Inter-relationships between the Physical and Acoustical Properties of Fibrous Duct Liner Materials and Lined Duct Sound Attenuation”, ASHRAE Report (RP-478).

H. L. Kuntz and R. M. Hoover, (1987). “The Interrelationships between the Physical Properties of Fibrous Duct Lining Materials and Lined Duct Sound Attenuation”, ASHRAE Transactions, 93(2), 449-470.

J. B. Lawrie and R. Kirby, (2006). “Mode-matching without Root-finding: Application to a Dissipative Silencer”, Journal of the Acoustical Society of America, 119, 2050-2061.

X. Li, (2010). "A Scaling Approach for the Prediction of High-frequency Mean Responses of Vibrating Systems", J. Acoust. Soc. Am., 127(5).

X. Li, (2011). "A Scaling Approach for High-frequency Vibration Analysis of Built-up Systems", Proceedings of the 8th International Conference on Structural Dynamics, 3193-3197.

X. Li, (2013). "A Scaling Approach for High-frequency Vibration Analysis of Line-coupled Plates", Journal of Sound and Vibration, 332, 4054-4058.

J. G. Lilly, (1987). “Breakout in HVAC Duct Systems”, Sound and Vibration 21(10).

G. Lou, T. W. Wu, and C. Y. R. Cheng, (2003). “Boundary Element Analysis of Packed Silencers with a Substructuring Technique”, Eng. Anal. Bound. Elem., 27, 643-653.

M. Long, (2014). *Architectural Acoustics*, Academic Press, Waltham, MA, Second Edition.

R. H. Lyon and R. G. Dejong, (1998). *Theory and Application of Statistical Energy Analysis*, RH Lyon Corp, Cambridge, MA.

J. Machen and J. C. Haines, (1983). “Sound Insertion Loss Properties of Linacoustic and Competitive Duct Liners”, Report 436-T-1778, Johns-Manville Research and Development Center, Denver, CO.

McQuay, (2004). *HVAC Acoustic Fundamentals*, Application Guide, AG 31-010.

F. P. Mechel, (1975). *Mufflers*, Chapter 19, Pocket Book of Technical Acoustics, Ed. H. Heckl and M.A. Mueller, Springer (in German).

F. P. Mechel, (1990a). "Theory of Baffle-Type Silencers", Acustica, 70, 93-111.

F. P. Mechel, (1990b), "Numerical Results to the Theory of Baffle-Type Silencers", Acustica, 72, 7-20.

P. M. Morse, (1939). “The Transmission of Sound Inside Pipes”, The Journal of the Acoustical Society of America, 11(2), 205-210.

E. Mouratidis and J. Becker, (2003). “The Aero-acoustic Properties of Common HVAC Plena”, ASHRAE Report (RP-1026).

M. L. Munjal, (1987). *Acoustics of Ducts and Mufflers with Applications to Exhaust and Ventilation System Design*, New York: Wiley-Interscience.

M. L. Munjal, (2014). *Acoustics of Ducts and Mufflers*, 2nd Edition, Wiley, New York.

M. W. Nasheda, T. Elnadya and M. Åbomb, (2018). “Modeling of Duct Acoustics in the High Frequency Range using Two-ports”, Applied Acoustics, 135, 37-47.

E. H. Price. (2015). Insertion Loss Data.

D. D. Reynolds, (2014). Preliminary Reports of Results from RP-1408, University of Nevada Las Vegas.

D. D. Reynolds, (2015). Personal Communication of Results from RP-1408, University of Nevada Las Vegas.

D. D. Reynolds and J. M. Bledsoe, (1989a). “Sound Attenuation of Unlined and Acoustically Lined Rectangular Ducts”, ASHRAE Transactions, 95(1), 90-95.

D. D. Reynolds and J. M. Bledsoe, (1989b). “Sound Attenuation of Acoustically Lined Circular Ducts and Radiused Elbows”, ASHRAE Transactions, 95(1), 96-99.

D. D. Reynolds and J. M. Bledsoe, (1990). “Algorithms for HVAC Acoustics”, ASHRAE, Atlanta, Georgia.

K. Ruan and D. W. Herrin, (2016a). “A Simulation Approach to Determine the Insertion and Transmission Loss of Unlined and Lined Ducts (RP-1529)”, ASHRAE Transactions, 122(1), 3-11.

K. Ruan and D. W. Herrin, (2016b). “Using Simulation to Determine Elbow and Side Branch Attenuation and Duct Breakout Transmission Loss (RP-1529)”, ASHRAE Transactions, 122(1), 12-21.

K. Ruan and D. W. Herrin, (2017a). “A Review of Prior Research on Assessing Insertion Loss of Ductwork”, Noise-Con 2017, Grand Rapids, Michigan.

K. Ruan and D. W. Herrin, (2017b). “Using Scale Modeling to Assess Heating and Air Conditioning Duct Attenuation”, Inter-Noise 2017, Hong Kong.

K. Ruan, T. W. Wu, and D. W. Herrin, (2015). “Validation of the Reciprocal Work Identity Method with AML for Large Silencer Analysis”, Inter-Noise 2015, San Francisco, California, Paper 953.

K. Ruan, D. W. Herrin and T. W. Wu, (2018). “Determination of A Power Transfer Matrix via A Boundary Element Method Determined Scattering Matrix”, Inter-Noise 2018, Chicago, Illinois.

K. Ruan, T. W. Wu, and D. W. Herrin, (2018). “Validation of BEM Analysis of Large Silencers using FEM-AML”, Applied Acoustics, (Under Review).

A. Selamet, M. B. Xu and I. J. Lee, (2004). "Analytical Approach for Sound Atenuation in Perforated Disspative Silencers," Journal of Acoustical Society of America, 115(5), 2091-2099.

R. A. Scott, (1946). “The Propagation of Sound between Walls of Porous Material”, Proceedings of the Physical Society of London, 58, 358-368.

Siemens, (2017). LMS Virtual.Lab Online Help. Munich, Germany, Siemens Product Lifecycle Management Software Inc..

Siemens, (2017). LMS Virtual.Lab.

J. W. Sullivan and M. J. Crocker, (1978). “Analysis of Concentric-tube Resonators Having Unpartitioned Cavities”, Journal of the Acoustical Society of America, 64, 207-215.

C. K. Tam, L. Auriault, and F. Cambuli, (1998). “Perfectly Matched Layer as an Absorbing Boundary Condition for the Linearized Euler Equations in Open and Ducted Domains”, Journal of Computational Physics, 144(1), 213–234.

VDI, (2001). “Noise Generation and Noise Reduction in Air-Conditioning Systems”, VDI Technical Report 2081.

I. L. Vér, (1977). “A Review of the Attenuation of Sound in Straight Lined and Unlined Ductwork of Rectangular Cross Section”, ASHRAE Report (RP-196).

I. L. Vér, (1978). “A Review of the Attenuation of Sound in Straight Lined and Unlined Ductwork of Rectangular Cross Section”, ASHRAE Transactions, 84(1), 122-149.

I. L. Vér, (1983a). “Noise Generation and Noise Attenuation of Duct Fittings – A Review: Part II (RP-265)”, ASHRAE Transactions, 90(2A), 383-390.

I. L. Vér, (1983b). “Prediction of Sound Transmission through Duct Walls; Breakout and Pickup”, ASHRAE TRP-319.

K. Vansant and R. Hallez, (2014). “The Adaptive Order FEM Approach for Vibro-acoustic Simulations: A Report on A Newly Implemented Technology with Application Examples Demonstrating Its Superior Performance to Conventional FEM Methods”, Inter-Noise 2014, Melbourne, Australia.

K. Vansant, H. Beriot, C. Bertolini, and G. Miccoli, (2014). “An Update and Comparative Study of Acoustic Modeling and Solver Technologies in View of Pass-by Noise Simulation”, SAE Int. J. Engines 2014, 7(3).

G. J. Wadsworth and J. P. Chambers, (2000). “Scale Model Experiments on the Insertion Loss of Wide and Double Barriers”, J. Acoust. Soc. Am., 107(5), 2344-2350.

P. Wang and T. W. Wu, (2016). “Impedance-to-scattering Matrix Method for Large Silencer Analysis using Direct Collocation”, Eng. Anal. Bound. Elem., 73, 191-199.

R. J. Wells, (1958). “Acoustical Plenum Chambers”. The Journal of the Acoustical Society of America, 29(1), 9-15.

Woods Fan Division, (1973). Design for Sound. The English Electric Corp.

T. W. Wu, P. Zhang, C. Y. R. Cheng and A. F. Seybert, (1998). “Boundary Element Analysius of Mufflers with An Improved Method for Deriving the Four-pole Parameters”, Journal of Sound and Vibration, 217,767-779.

L. Zhou, T. W. Wu, K. Ruan and D. W. Herrin, (2016). “A Reciprocal Identity Method for Large Silencer Analysis”, Journal of Sound and Vibration, 364, 165-176.

VITA

Kangping Ruan was born in Jiangsu, China in 1982. He received his Bachelor's Degree of Science in Mechanical Engineering from Southeast University, Nanjing, China in 2005. Subsequently, he received his Master's Degree of Science in Mechanical Engineering from Southeast University, Nanjing, China in 2008.

In August 2012, he enrolled in the PhD program in the Department of Mechanical Engineering at University of Kentucky. His research involves engineering acoustics and noise and vibration control. During his Ph.D. study, he has published 4 journal articles and 7 conference proceeding articles. Additionally, he has 1 journal article under review and 2 journal articles to be submitted. In the year of 2017, he received Leo Beranek Student Medal for Excellence in the Study of Noise Control and Michiko So Finegold Awards from the Institute of Noise Control Engineering (INCE). He was awarded the Young Professional Congress Attendance Grants by the International Institute of Noise Control and Engineering (I-INCE) in 2018.

Kangping Ruan